UNIVERSITA' DEGLI STUDI DI NAPOLI
" FEDERICO II"

Ph.D Thesis in

INFORMATION TECHNOLOGY AND ELECTRICAL ENGINEERING

NONLINEAR MAGNETIZATION DYNAMICS IN MULTILAYERED SPINTRONIC NANODEVICES

SALVATORE PERNA

TUTOR
Prof. Claudio Serpico

COTUTOR
Prof. Massimiliano d'Aquino

XXIX Ciclo
Scuola Politecnica e delle Scienze di Base
Dipartimento di Ingegneria Elettrica e delle Tecnologie dell'Informazione

"To my parents Sebastiano and Gelsomina,
and to my brothers and sister
Mimmo, Antonella and Mariano."

Acknowledgments

During my Ph.D. I have met many people which deserve few words here. First of all, I have to thank my supervisors Prof. Claudio Serpico and Prof. Massimiliano d'Aquino. They believed in me since the beginning and made everything possible to make me a good researcher. This includes make me meet and collaborate with people like Giorgio Bertotti from the Istituto Nazionale di Ricerca Metrologica (I.N.R.I.M) in Turin and Isaak Mayergoyz from the University of Meryland. The discussions with those people have been special occasions where I learned a lot and felt really happy and fortunate to be there. I can not help but mention here Doctor Antonio Quercia. He has been a true friend and the discussions that we had have been always an occasion to learn something new.

During my 1st year of Ph.D. course I spent one week in Messina, Sicily, collaborating with the Department of Electrical engineering of the University of Messina. For such experience my thanks go to entire department which kindly welcomed and hosted me, with special regards to Prof. Bruno Azzerboni and his research team constituted by Prof. Giovanni Finocchio, Vito Puliafito and my phd collegues Anna Giordano and Riccardo Tomasello. They made me visit the city and taste the typical dishes of the place.

During the 2nd year of Ph.D. course, I spent 10 months in Salamanca (Spain) collaborating with the Department of Applied Physics of the University of Salamanca. For such experience my thanks go to entire department, with special regards to my local tutor Prof. Luis Lopez-Diaz and my phd collegues Michele Voto, Simone Moretti and Noel Perez. They introduced

me to the city and made me meet a lot of people who treated me like a true friend and making me relax when I really needed it.

During the 3rd year of Ph.D. course, despite my personal issues, my supervisors helped me a lot supporting and sustaining me in order to finish this thesis. I am really grateful to them for everything they did for me.

Special thanks go to Prof. Giovanni Miano which in these three years introduced me to quantum mechanics thanks to his illuminating seminars about the basic principles and more advanced topics, such as: Dirac equation, the von Neumann density operators and Feynmann formulation of quantum mechanics.

Last but not least, i would like to thank my phd collegues Simone Minucci, Vincenzopaolo Loschiavo, Soudeh Yaghouti, Valentino Scalera and Roberto Tricarico. We had interesting scientific discussion and when possible helped each other.

Finally, my thanks go to my istitution the Department of Electrical Engineering and Information Technology (DIETI) of the Unversity of Naples Federico II.

Salvatore Perna

Contents

Introduction

The study of magnetization dynamics in ferromagnetic materials has been of great interest in the information and communication technology (ICT) area since the realization of the first computers. In fact, due to their atomic structure, such materials exhibit, at room temperature and on micron scale, uniformly magnetized regions called domains (see fig. 1). A preliminary analysis on the magnetic behaviour of the domains reveals interesting properties. In the absence of any external excitation, one can observe that, in general, there are certain magnetization orientations which are favored due to the peculiar shape and crystalline structure of the material and remain stable over long time. These orientations can be used to encode elementary pieces of information (e.g. bits) without the need of energy supply in order to store them, namely to realize bistable non volatile memories. The typical writing mechanism of magnetic storage devices occurs by switching the domain magnetization from the initial orientation (say bit "0") to the opposite one (bit "1") by means of an appropriate external excitation, such as a magnetic field produced by suitable coils (e.g. hard drives) or a spin-polarized electric current directly injected into the ferromagnet (e.g. electrically controlled magnetic random access memories).

The general property of ferromagnetic materials lies on the fact that the relationship between domain magnetization and external excitation exhibit hysteresis. In other words, the final magnetization state of a ferromagnet depends on the past history of the external excitation. For instance, one can easily see from the typical $M - H$ hysteresis cycle depicted in fig. 1 that, when no external field is applied, the ferromagnet shows a remanent

magnetization whose orientation may represent either bit "0" or "1". Such

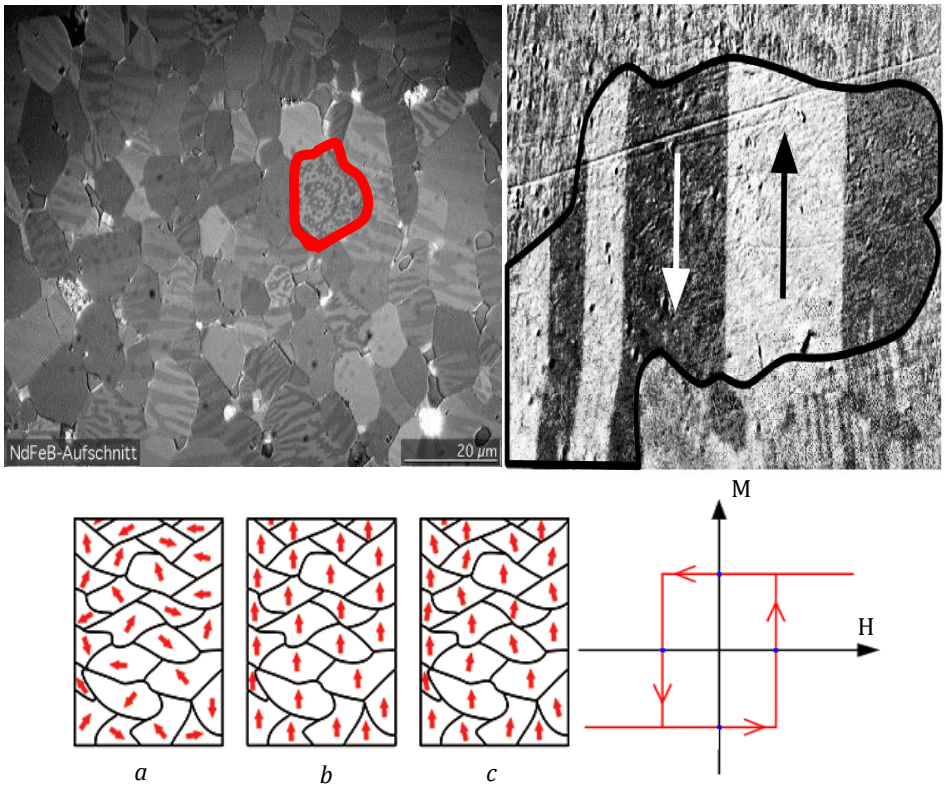

Figure 1: Upper figures: granular structure of NdFeB (left), zoom of a single grain pointing out the magnetization direction of two domains (right). Bottom figures: magnetization of a multidomain sample. (a) no applied field, (b) strong field, and (c) no field. At the same level on the right, a sketch of typical hysteretic characteristic $M - H$ for non-volatile memory applications is reported.

hysteretic nature is the key ingredient that historically motivated their use in storage devices. In fact, in 1952 the first magnetic core memory was realized

for the IBM 405 Alphabetical Accounting Machine depicted in fig.2.

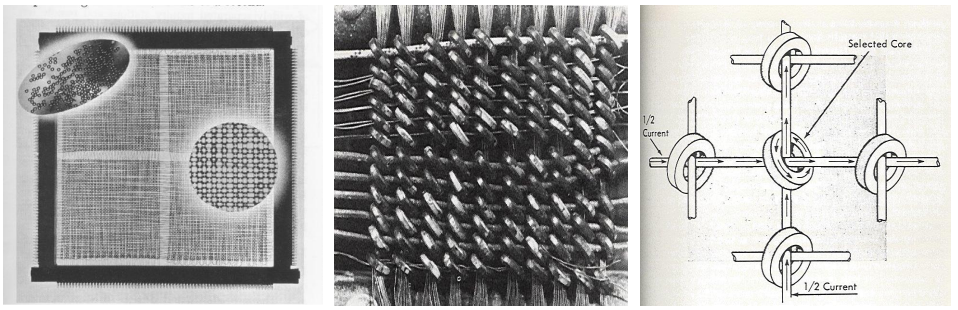

a b c

Figure 2: (a) Magnetic core plane of the IBM 405. (b) The first magnetic core memory, from the IBM 405 Alphabetical Accounting Machine. The photo shows the single drive lines through the cores in the long direction and fifty turns in the short direction. The cores are 150 mm inside diameter, 240 mm outside, 45 mm high. This experimental system was tested successfully in April 1952. (c) Sketch of the magnetic polarization of a single core selected with the direction of the electric current flowing in the long and short directions.

The working principle of that device is very simple. Each core can be magnetized in two possible configurations (clockwise and counterclockwise) corresponding to bits "0" and "1", respectively. The magnetization of a selected core can be switched by addressing it with the horizontal and vertical current lines which pass through the core. The field produced by a single current line (either horizontal or vertical) is designed in a way that is not strong enough to switch the core. Conversely, when the core is addressed by both horizontal and vertical current lines, the field is able to switch magnetization.

Since that first realization of magnetic memory, a huge research effort has been devoted for the improvement of its efficient implementation. On one hand, the need for larger and larger memory capacity has pushed the downsizing up to nanometer scale for a single stored magnetic bit. On the

other hand, the performance levels in terms of reading and writing speed arising from the exponential increase of consumer electronics market of the last decades, have stimulated considerable research activity in the study of magnetization dynamics in nanosystems.

The magnetic storage evolution starting from magnetic core memories has produced smaller in size magnetic storage supports over time, such as magnetic tapes, floppy disks and, finally, hard disk drives like those sitting in desktop PCs or those used for massive information recording by cloud storage providers.

In a modern hard disk, binary information sequences are physically coded by changing the out-of-plane magnetization orientation along circular tracks on a thin disk of ferromagnetic material. A single bit is constituted by a uniformly magnetized region (nowadays bit track widths have dimensions of tens of nm) allowing two possible orientations (up/down). The magnetic state of a selected bit is written by applying an external magnetic field produced by a pole head (basically an electromagnet with coils traversed by electric current). The positioning of the write head over the target magnetic bit is realized by means of a sophisticated electromechanical system.

The reading mechanism relies on a magnetic sensor, called spin valve, which exploits the giant magneto-resistive (GMR) effect. Basically, a spin valve is constituted by a multi-layer magnetic system where two layers are made of ferromagnetic material. The former is called free layer since magnetization change may occur. The other one, termed fixed layer, has magnetization artificially pinned to a given orientation. When suitable electric current traverses the multi-layer, significant changes in the electrical resistance of the device may occur depending on the mutual orientation of the magnetization in the free and fixed layer. In particular, the lowest (highest) resistance corresponds to parallel (anti-parallel) orientations of free and fixed layers. This behavior can be used to read magnetic bits on the recording medium. Basically, the spin valve placed in the read head is brought almost in contact with the recording medium. Then, when the head moves over it, the free layer magnetization is affected by the magnetic field created by magnetized bits. Thus, by observing the time-variation of the electrical resistance of the GMR head, the bit sequence stored on the recording

medium can be reconstructed.

The discovery of GMR effect allowed the rapid downscaling of hard disk drives technology and has been recognized as the starting point for the era of spintronics, where the close integration of magnetic and electronic devices is expected to produce an effective alternative to semiconductor electronics. The scientists Albert Fert and Peter Gruenberg who discovered this effect have been awarded with the Nobel Prize for Physics in 2007.

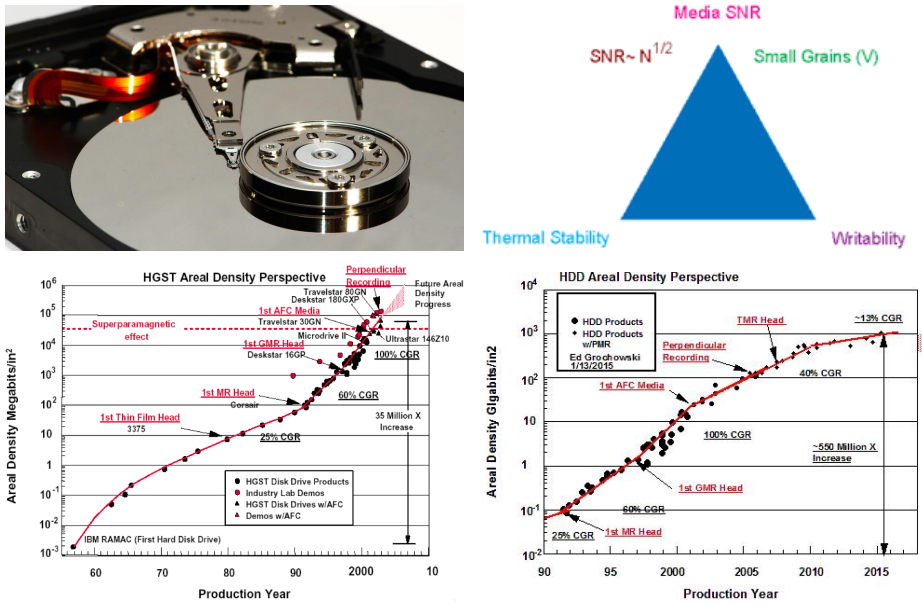

Figure 3: State-of-the-art for hard disk drive products. Upper: ferromagnetic disk layer with the read/write branch (left). Sketch of the constraints in magnetic recording (right). Bottom: historical evolution of the information density in the hard disk drives production over years.

As mentioned before, intensive research activity is devoted to increase the information density and reduce the energetic cost of the writing and reading process. The issues to deal with in order to reach the objective, can

be summarized in the so-called magnetic recording trilemma, which can be illustrated as follows. For a given device dimension, an increase of the information density would require a reduction of the bit track width. However, smaller track widths (magnetized bit volumes) are more sensitive to the effect of thermal fluctuations which tend to destroy the spatial coherence of ferromagnetic order and, consequently, to lower the signal to noise ratio (SNR) of the information reading process. Thus, in order to guarantee a sufficient durability of the stored information against thermal fluctuations (e.g. at least in the order of years), an increase in the magnetic material anisotropy which favors the stability of magnetized bit orientation would be needed. This in turn would lead to an increase of the required writing magnetic field and, consequently, of the Joule effect losses.

From the outlined framework, the design of a magnetic storage device has always to cope with the above tree issues, represented by the vertices of the triangle depicted in fig.4. This represents the current challenge for data storage engineering.

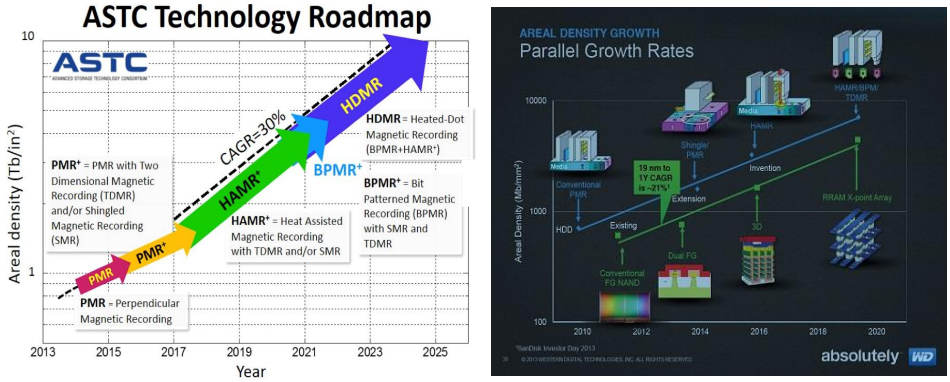

Figure 4: New technologies in hard drive storaging.

Several solutions have been proposed to overcome the constraints emerging from the magnetic recording trilemma. In fig.4, the roadmap for hard disk information density is reported for different proposed technologies.

Schematically speaking, recording schemes as heat-assisted and

microwave-assisted magnetic recording (HAMR,MAMR) aim to reduce the energy spent in the writing process, while nano-engineering of the recording medium as bit-patterned-media (BPM) allow to reduce the dimensions of single magnetized bits (magnetic islands). Furthermore, shingled magnetic recording (SMR) allows to increase the SNR by means of processing the signal coming from simultaneous reading of multiple adjacent tracks.

The hard disk drive is the most widespread magnetic storage device due to its low cost per gigabyte compared to competing solutions. However, especially in the last decade, electrically-controlled magnetic random access memories (MRAMs) are rapidly emerging to become the leading magnetic storage technology. In fact, non volatile MRAM designs are proving to be fast, scalable, energy efficient, and robust to electromagnetic interferences. This kind of memory has the typical cell-array structure (see fig.5) where each cell is a spin-valve-like structure called magnetic tunnel junction (MTJ). The free layer has a perpendicular (out-of-plane) anisotropy and its magnetic state encodes a single bit. The reading process occurs thanks to the tunnel-magneto-resistance (TMR) effect, analogous to the GMR effect described before, while the information can be written via switching of the free layer magnetization by injecting an appropriate electric current through the multi-layer. This is accomplished by the addressing current lines of the cell-array which properly select the desired cell for reading or writing. In this respect, this mechanism is similar to the original one used to write a bit in the core memory (see fig.2), but here the magnetization is switched directly by the electric current instead that by using the field produced by the current. This feature is essential for the scalability of MRAMs and is ascribed to the so-called spin-transfer-torque (STT) effect, which can be thought as dual with respect to GMR/TMR-like effects.

The spin-transfer-torque (STT), discovered in 1996 by J.C. Slonczewski and L. Berger independently, opened new possibility of realization of solid state ferromagnet-based memory devices. In fact, magnetization dynamics in this devices is excited directly by the electric current which acquires a spin polarization passing through the ferromagnetic layer with a fixed magnetization. Such a technology is really promising and pushes towards the use of STT memory devices in any context which requires data storage,

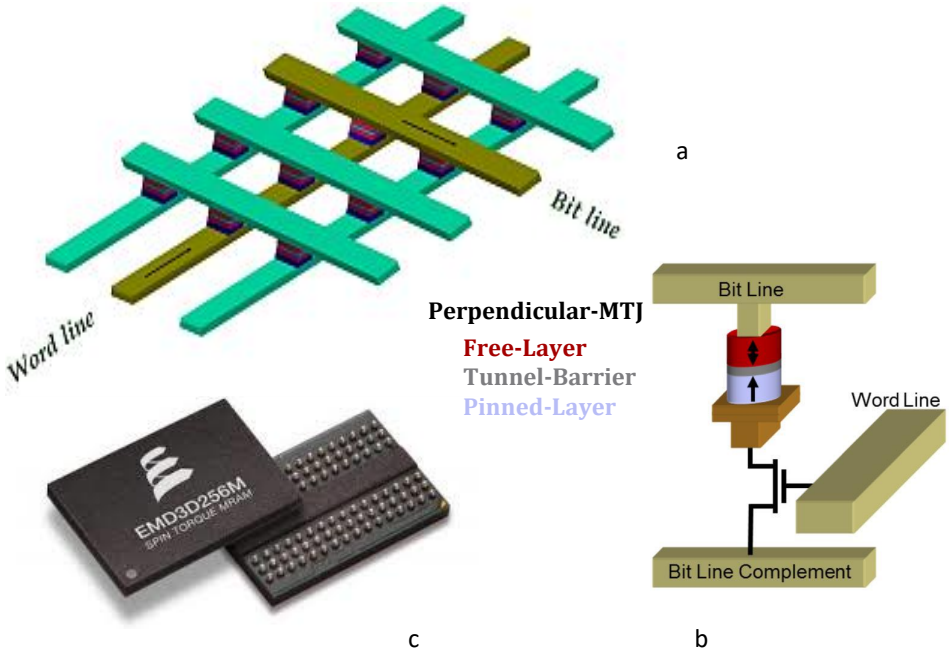

Figure 5: (a) Sketch of the cell-array structure of an MRAM device. (b) Single bit-cell of an STT-MRAM. (c) Example of STT-MRAM device commercialized

namely toward a universal memory device. At the present time, the STT-MRAMs are already present on the market and considerable research is being performed in order to optimize the performance of both materials and reading/writing processes.

The STT effect indeed opened new perspectives for the realization of spintronic devices integrable with CMOS electronics. Examples of such devices are spin-torque nano-oscillators (STNOs), which implement tunable microwave generators on nanoscale with output frequencies ranging from several hundreds of MHz to several tens of GHz. The working principle

relays on the fact that a dc electric current flowing through a magnetic multi-layer structure is able to sustain a steady-state magnetization self-oscillations regime.

The STNOs have great potential for advanced wireless applications due to their current tunability and integrability with the semiconductor technology. However the microwave power emitted by a single STNO is quite low (in the range of nW) and the oscillation linewidth is still poor compared to common LC electronic oscillators. For these reasons, considerable efforts are currently in progress in order to overcome these issues.

This is the motivation for the research activity that will be illustrated in the following chapters.

In chapter 1, the fundamental of micromagnetics are presented. First, an approach in terms of the free energy associated with the magnetic body will be presented to derive the static equilibrium conditions for magnetization vector field. Then, the dynamical effects due to the gyromagnetic precession are introduced with a Lagrangian approach. Both Landau-Lifshitz (LL) and Landau-Lifshitz-Gilbert (LLG) equation are presented. Then, the spin-transfer-torque is introduced along with the LLG equation generalized with the Slonczewski spin transfer torque term (LLGS equation). Finally, the collective variables approach to magnetization dynamics is introduced.

In chapter 2, the study of uniformly magnetized nanoparticle of ellipsoidal shape is presented. A preliminar discussion on the presence of the uniform motion of the magnetization is followed by the study of the magnetization statics. First the solution of the Brown's equations in case of zero applied field and then the Stoner-Wohlfarth theory are presented. The study of statics is followed by the introduction of the uniform magnetization dynamics. In this last part of the chapter the analytical techniques to study quantitatively and qualitatively the switching and the self-oscillation dynamics are presented.

In chapter 3, the study of magnetization dynamics in uniformly magnetized MTJ devices with perpendicular anisotropy is addressed. This study is instrumental to reduce the threshold currents which trigger magnetization dynamics. In particular, we consider a device where the second order anisotropy has measurable and determinant effects in both magnetization

switching and self-oscillatory dynamics. This system is first analyzed in the configuration where the polarizer is perpendicularly magnetized, and conditions for switching dynamics are analytically determined by using appropriate perturbation techniques. Then, the configuration with an in-plane polarizer is addressed in order to study the self-oscillations regime. The theoretical predictions are validated by full micromagnetic simulations.

Finally, in chapter 4, the oscillations regimes of a point-contact device with magnetic vortex configuration are studied. In particular, we first study the self-oscillations of the magnetic vortex around the nano-contact excited by dc spin-polarized current. To this end, a reduced order analytical model is developed by using a collective variables description of the vortex dynamics. Then, the synchronization of current-driven vortex oscillations with a circularly polarized microwave field are considered. By using bifurcation theory on the reduced order model, we are able to derive all the possible oscillation regimes as well as the transition mechanisms among them. The theoretical results, confirmed by full micromagnetic simulations, show a large hysteresis effect in synchronization which may be instrumental to enhance the synchronization of multiple nano-oscillators.

Chapter 1

Fundamentals of Micromagnetic dynamics in nanosystems

Abstract

This chapter of the thesis is devoted to explain the fundamentals of the micromagnetic theory. We start from the formulation of the magnetostatic problem of a magnetized body. We show that the problem can be formulated by following two approaches. The first and usual approach is to complement the Maxwell magnetostatic equations with the constitutive relation of the magnetic material. The second approach is to formulate the problem as the minimization of an appropriately defined free energy functional. When the constitutive relation is monotonic, the solution of the magnetostatic problem is unique. In the energy formulation, the monotonic constitutive equation corresponds to a convex free energy functional. The approach based on energy can be easily generalized to the case when the energy functional is not convex, which is the case of interest when hysteresis phenomena are important. For this reason, this is the preferred approach. By using the expression of the energy functional, the free energy density ap-

propriate for ferromagnetic materials, we arrive to the micromagnetic free energy functional. The minimization of this functional leads to the Brown's equations. Then, we focus our attention on the dynamical magnetization processes responsible of the relaxation of the magnetization toward the micromagnetic equilibria. These processes are dissipative and are described by the Landau-Lifshitz equation. Finally, we consider the generalization of the Landau-Lifshitz equation which includes the spin-transfer-torque effects.

1.1 Magnetostatics of a magnetized body

Let us consider a ferromagnetic body occupying a region Ω and subject to a constant applied field $\boldsymbol{H}_a$. This field is produced by a given current density distribution $\boldsymbol{J}_0$ distributed over the region Ω_0. In these conditions, we want to determine the distribution of the magnetization vector field $\boldsymbol{M}$ in the ferromagnetic body. The total magnetostatic field, is given by

$$\boldsymbol{H} = \boldsymbol{H}_a + \boldsymbol{H}_M \,, \tag{1.1}$$

where $\boldsymbol{H}_M$ is the field produced by the the magnetized body. The applied field $\boldsymbol{H}_a$ can be found by solving the following equations

$$\begin{aligned} \nabla \times \boldsymbol{H}_a &= \boldsymbol{J}_0 \,, \\ \nabla \cdot \boldsymbol{H}_a &= 0 \,, \end{aligned} \tag{1.2}$$

which leads to the Biot-Savart formula:

$$\boldsymbol{H}_a(\boldsymbol{r}_P) = \frac{\mu_0}{4\pi} \int_{\Omega_0} \frac{\boldsymbol{J}(\boldsymbol{r}_Q) \times \boldsymbol{r}_{PQ}}{r_{PQ}^3} dV_Q \,, \tag{1.3}$$

where $\boldsymbol{r}_{PQ} = \boldsymbol{r}_P - \boldsymbol{r}_Q$, and where $\boldsymbol{r}_P$ and $\boldsymbol{r}_Q$ are the position vectors of the points P and Q, respectively.

The field $\boldsymbol{H}_M$ is related to the magnetization $\boldsymbol{M}$ by the following system of equations:

$$\begin{aligned} \nabla \times \boldsymbol{H}_M &= \boldsymbol{0} \,, \\ \nabla \cdot \boldsymbol{H}_M &= -\nabla \cdot \boldsymbol{M} \,, \end{aligned} \tag{1.4}$$

subjected to the appropriate interface conditions at the body surface.

In order to find a solution of eqs.(1.4), these equations have to be complemented by a constitutive relation connecting the values of $\boldsymbol{H}$ and $\boldsymbol{M}$. In the case when we neglect hysteresis phenomena, and the constitutive relation is memoryless (static), the constitutive relation is of the following type

$$\boldsymbol{H} = \boldsymbol{\mathcal{H}}(\boldsymbol{M})\,,$$

where $\boldsymbol{\mathcal{H}}(\boldsymbol{M})$ is a invertible vector function of $\boldsymbol{M}$. The assumption of absence of hysteresis phenomena requires that

$$\oint \boldsymbol{H}\cdot d\boldsymbol{M} = \oint \boldsymbol{\mathcal{H}}(\boldsymbol{M})\cdot d\boldsymbol{M} = 0\,, \tag{1.5}$$

for any cyclic magnetization variation. This amounts to say that

$$\mathcal{H}(\boldsymbol{M}) = \frac{1}{\mu_0}\frac{\partial\varphi}{\partial\boldsymbol{M}}\,, \tag{1.6}$$

where $\varphi(\boldsymbol{M})$ has the physical dimension of an energy per unit volume.

By using eq.(1.1), we arrive to the following equation

$$\boldsymbol{H}_a + \boldsymbol{H}_M = \boldsymbol{\mathcal{H}}(\boldsymbol{M})\,, \tag{1.7}$$

which relates $\boldsymbol{H}_M$ and $\boldsymbol{M}$.

By solving the system of equations (1.4), we can express the field $\boldsymbol{H}_M$ is terms of $\boldsymbol{M}$ by the following integro-differential operator:

$$\boldsymbol{H}_M[\boldsymbol{M}] = -\frac{\nabla_P}{4\pi}\left[\int_\Omega \frac{\nabla_Q\cdot\boldsymbol{M}(\boldsymbol{Q})}{r_{PQ}}\,dV_Q - \int_{\partial\Omega}\frac{\boldsymbol{M}\cdot\boldsymbol{n}_Q}{r_{PQ}}\,dS_Q\right]. \tag{1.8}$$

Then, by substituting eq.(1.8) in eq.(1.7), we arrive to the following equation involving only the vector field $\boldsymbol{M}$:

$$\boldsymbol{H}_a + \boldsymbol{H}_M[\boldsymbol{M}] = \boldsymbol{\mathcal{H}}(\boldsymbol{M})\,. \tag{1.9}$$

This problem has a unique solution when the constitutive relation is monotonic. This means that the following condition is satisfied:

$$\boldsymbol{M}_2 \neq \boldsymbol{M}_1 \Rightarrow (\boldsymbol{\mathcal{H}}(\boldsymbol{M}_2) - \boldsymbol{\mathcal{H}}(\boldsymbol{M}_1))\cdot(\boldsymbol{M}_2 - \boldsymbol{M}_1) > 0\,, \tag{1.10}$$

Let us prove the above statement. We assume the existence of two distinct solutions $\boldsymbol{M}_1$ and $\boldsymbol{M}_2$ of the problem (1.9): $\boldsymbol{H}_a + \boldsymbol{H}_M[\boldsymbol{M}_1] = \boldsymbol{\mathcal{H}}(\boldsymbol{M}_1)$, $\boldsymbol{H}_a + \boldsymbol{H}_M[\boldsymbol{M}_2] = \boldsymbol{\mathcal{H}}(\boldsymbol{M}_2)$. By taking the difference of these two equation we arrive to the equality:

$$\Delta \boldsymbol{H}_M = \boldsymbol{H}_M[\Delta \boldsymbol{M}] = \boldsymbol{\mathcal{H}}(\boldsymbol{M}_2) - \boldsymbol{\mathcal{H}}(\boldsymbol{M}_1)\,, \tag{1.11}$$

where

$$\Delta \boldsymbol{M} = \boldsymbol{M}_2 - \boldsymbol{M}_1\,,$$

$$\Delta \boldsymbol{H}_{\boldsymbol{M}} = \boldsymbol{H}_M[\boldsymbol{M}_1] - \boldsymbol{H}_M[\boldsymbol{M}_2]\,.$$

We also define the field

$$\Delta \boldsymbol{B} = \mu_0 \left(\boldsymbol{\mathcal{H}}(\boldsymbol{M}_2) - \boldsymbol{\mathcal{H}}(\boldsymbol{M}_1) + \Delta \boldsymbol{M}\right) = \mu_0 \left(\Delta \boldsymbol{H}_{\boldsymbol{M}} + \Delta \boldsymbol{M}\right)\,,$$

Then, we can write:

$$\int_{\Omega_\infty} \frac{\Delta \boldsymbol{B}}{\mu_0} \cdot \Delta \boldsymbol{H}_M \, dV = \int_{\Omega} \Delta \boldsymbol{H}_M \cdot \Delta \boldsymbol{M} \, dV + \int_{\Omega_\infty} |\Delta \boldsymbol{H}_{\boldsymbol{M}}|^2 \, dV\,, \tag{1.12}$$

where Ω_∞ is the whole space. Since the vector field $\Delta \boldsymbol{B}$ is solenoidal and the vector field $\Delta \boldsymbol{H}_M$ is conservative then

$$\int_{\Omega_\infty} \Delta \boldsymbol{B} \cdot \Delta \boldsymbol{H}_M \, dV = 0\,. \tag{1.13}$$

In addition, from eq.(1.11) and the monotonicity of the function $\mathcal{H}(\boldsymbol{M})$ it turns out that

$$\int_{\Omega} \Delta \boldsymbol{H}_M \cdot \Delta \boldsymbol{M} \, dV > 0\,.$$

From the above considerations we arrive to a contradiction as in eq.(1.12) the sum two positive quantities would be equal to zero. Therefore the uniqueness of the solution of the magnetostatic problem formulated as in the eq.(1.9) is proved.

Next we formulate the above problem as a minimization problem of an appropriate functional. In order to do that, let us consider the following functional:

$$G(\boldsymbol{M}, \boldsymbol{H}_a) = \int_\Omega \left(\varphi(\boldsymbol{M}) - \frac{\mu_0}{2} \boldsymbol{H}_M \cdot \boldsymbol{M} - \mu_0 \boldsymbol{H}_a \cdot \boldsymbol{M} \right) dV \,, \tag{1.14}$$

and its first variation with respect to an arbitrary variation of the magnetization distribution $\delta\boldsymbol{M}$, keeping fixed the applied field distribution $\boldsymbol{H}_a$:

$$\delta G(\boldsymbol{M}, \boldsymbol{H}_a)|_{\boldsymbol{H}_a} = \int_\Omega \left(\frac{\partial \varphi}{\partial \boldsymbol{M}} - \mu_0 (\boldsymbol{H}_M + \boldsymbol{H}_a) \right) \cdot \delta\boldsymbol{M} \, dV \,. \tag{1.15}$$

At this point, by imposing the condition

$$\delta G(\boldsymbol{M}, \boldsymbol{H}_a)|_{\boldsymbol{H}_a} = 0 \Rightarrow \frac{1}{\mu_0} \frac{\partial \varphi}{\partial \boldsymbol{M}} = \boldsymbol{\mathcal{H}}(\boldsymbol{M}) = \boldsymbol{H}_a + \boldsymbol{H}_M[\boldsymbol{M}] \,, \tag{1.16}$$

we obtain again the eq.(1.9) of the magnetostatic problem. The monotonicity property expressed in the eq.(1.10) is a sufficient condition to prove that the functional G is convex, namely

$$\delta^2 G|_{\boldsymbol{H}_a} = \int_\Omega \left(\delta\boldsymbol{M} \cdot \frac{\partial^2 \varphi}{\partial \boldsymbol{M}^2} \cdot \delta\boldsymbol{M} - \mu_0 \boldsymbol{H}_M[\delta\boldsymbol{M}] \cdot \delta\boldsymbol{M} \right) dV \; > 0 \,, \tag{1.17}$$

where $\delta^2 G$ is the second order variation of G. This means, that the magnetization field solution of the magnetostatic problem formulated as in the eq.(1.9), is a minimum of G. In order to show that, let us consider the relation (1.9) when $\boldsymbol{M}_1 = \boldsymbol{M}$ and $\boldsymbol{M}_2 = \boldsymbol{M} + \delta\boldsymbol{M}$, where $\delta\boldsymbol{M}$ is an arbitrary small magnetization field variation ($|\delta\boldsymbol{M}| \ll |\boldsymbol{M}|$). In this framework, the equation (1.10) can be written as

$$\delta\boldsymbol{\mathcal{H}}(\boldsymbol{M}) \cdot \delta\boldsymbol{M} \approx \delta\boldsymbol{M} \cdot \frac{\partial^2 \varphi}{\partial \boldsymbol{M}^2} \cdot \delta\boldsymbol{M} > 0 \,, \tag{1.18}$$

where the right hand side of the equality is the first member in eq.(1.17). At this point, the the last step to prove the convexity of G is to show the following relation

$$\int_\Omega -\mu_0 \boldsymbol{H}_M[\delta\boldsymbol{M}] \cdot \delta\boldsymbol{M} \, dV \; > 0 \,. \tag{1.19}$$

Since it holds the decomposition: $\delta \boldsymbol{M} = \delta \boldsymbol{B}/\mu_0 - \boldsymbol{H}_M[\delta \boldsymbol{M}]$, we can write the following equation:

$$\int_\Omega -\mu_0 \boldsymbol{H}_M[\delta \boldsymbol{M}] \cdot \delta \boldsymbol{M}\, dV = -\int_{\Omega_\infty} \boldsymbol{H}_M[\delta \boldsymbol{M}] \cdot \delta \boldsymbol{B}\, dV + \int_{\Omega_\infty} \mu_0 |\boldsymbol{H}_M[\delta \boldsymbol{M}]|^2\, dV \,. \tag{1.20}$$

Since the vector field $\delta \boldsymbol{B}$ is solenoidal and the vector field $\delta \boldsymbol{H}_M$ is conservative then

$$\int_{\Omega_\infty} \delta \boldsymbol{B} \cdot \boldsymbol{H}_M[\delta \boldsymbol{M}]\, dV = 0 \,. \tag{1.21}$$

This means, that the relation (1.19) is proved. In fact, we can write:

$$\int_\Omega -\mu_0 \boldsymbol{H}_M[\delta \boldsymbol{M}] \cdot \delta \boldsymbol{M}\, dV = \int_{\Omega_\infty} \mu_0 |\boldsymbol{H}_M[\delta \boldsymbol{M}]|^2\, dV > 0 \,. \tag{1.22}$$

So with the energy representation (functional formulation) we show that the uniqueness of the solution to the magnetostatic problem corresponds to have a convex energy functional G where the solution is the magnetization field $\boldsymbol{M}$ which minimizes it. The convexity of G is ensured by giving a monotonic constitutive relation which relates the total magnetostatic field $\boldsymbol{H}$ and the magnetization field $\boldsymbol{M}$. The direct consequence of the uniqueness is the absence of hysteresis in the magnetization process. In fact, the uniqueness property ensures a one-to-one correspondence between the applied field and the magnetization field of the magnetic body. However, when the condition (1.10) is not satisfied anymore, we have that the functional G shows several minima and maxima. The set of minima represents the possible solutions of the equation (1.9) . As a consequence of the multiplicity of minima we have hysteresis in the magnetization process. To illustrate that, let us consider the following one dimensional version of the problem (1.10):

$$\frac{\partial \varphi}{\partial x} = h_a + h_M(x) \,. \tag{1.23}$$

The role of the magnetization is taken by the one dimensional variable x and the quantities $\varphi(x)$ and $h_M(x)$ are so defined:

$$\begin{aligned} \varphi(x) &= \frac{c_4}{4} x^4 + \frac{c_2}{2} x^2 \,, \\ h_M(x) &= -c_\chi x \,. \end{aligned} \tag{1.24}$$

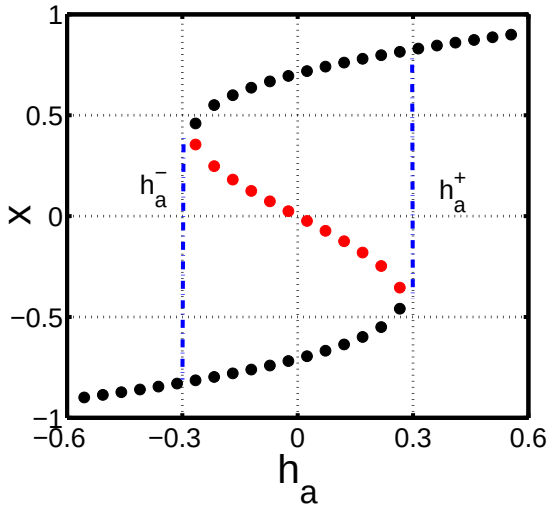

Figure 1.1: Representation of the solutions (h_a, x) of the equation (1.25). Parameters value: $c_4 = 2$ and $c_\chi + c_2 = -1$.

where the variable h_a is externally controlled. Then the solution of the prolem (1.23), (1.24) can be addressed to the solution of the following polynomial equation:

$$\frac{\partial g}{\partial x} = c_4 x^3 + (c_2 + c_\chi)x - h_a = 0\,, \tag{1.25}$$

where the function $g(x) = \varphi(x) - \frac{1}{2} h_M\, x - h_a\, x$ play the role of G. In fig.1.1 is shown the graphical solution of the equation (1.25). It is possible to see that when $h_a < h_a^-$ and $h_a > h_a^+$, there is one single solution. However, when $h_a^- < h_a < h_a^+$, the equation (1.25) admits two solutions (minima of g), represented in figure with black dots. If we imagine that x is the outcome of an experiment, for value of h_a in the interval $h_a^- < h_a < h_a^+$ which x value is observed depends on the hystory of h_a. The possibility to have different solutions x for the same value of h_a leads to a dispersive

relationship over the time between x and h_a. This remarkable fact, is the evidence of the hysteresis as a consequence of the multiplicity of possible configurations.

1.2 Thermodynamics of a magnetized body

In this section we show that the variational principle expressed in the equation (1.16), in the framework of thermodynamics, corresponds to the minimization of a properly defined Gibbs free energy.

The first step to do so is the calculation of the work necessary to magnetize the body under consideration. In order to magnetize the body, we have to change the applied magnetic field and this is achieved by changing the current distribution $\boldsymbol{J}_0$. In order to avoid dissipation of energy due to radiation, we do this process quasi statically. The current is increased by using appropriate electromotive fields $\boldsymbol{E}_g$. It balances the electric field induced by the change of the magnetic field which is given by

$$\boldsymbol{E} = -\partial_t \boldsymbol{A}\,,$$

where $\boldsymbol{A}$ is the potential vector associated to the magnetic flux density and where the Coulomb Gauge $\nabla \cdot \boldsymbol{A} = 0$ is used. The work per unit of time made by the electromotive force $\boldsymbol{E}_g = -\boldsymbol{E}$ is then given by

$$\begin{aligned}\frac{dL_{tot}}{dt} &= \int_{\Omega_\infty} \boldsymbol{E}_g \cdot \boldsymbol{J}_0 \, dV = \int_{\Omega_\infty} \partial_t \boldsymbol{A} \cdot \nabla \times \boldsymbol{H} \, dV = \\ &= \int_{\Omega_\infty} \left[-\nabla \cdot (\partial_t \boldsymbol{A} \times \boldsymbol{H}) + \boldsymbol{H} \cdot \partial_t \boldsymbol{B}\right] dV = \\ &= \int_{\Omega_\infty} \boldsymbol{H} \cdot \partial_t \boldsymbol{B} \, dV\,,\end{aligned} \tag{1.26}$$

which can be written as:

$$\frac{dL_{tot}}{dt} = \frac{d}{dt}\left(\int_{\Omega_\infty} \frac{1}{2}\,\mu_0\,\boldsymbol{H}^2\,dV\right) + \int_{\Omega} \mu_0\,\boldsymbol{H} \cdot \partial_t \boldsymbol{M}\,dV\,. \tag{1.27}$$

The last step made in the equation (1.26) can be justified by proving the following relation:

$$\int_{\Omega_\infty} \nabla \cdot (\partial_t \boldsymbol{A} \times \boldsymbol{H}_a)\, dV = 0\,. \tag{1.28}$$

To this purpose, let us consider a region of space Ω_R of spherical shape with radius R. When $R \to \infty$ the sphere cover the whole space, then $\Omega_R \to \Omega_\infty$. The first integral in the equation (1.28) can be written as

$$\begin{aligned} &\int_{\Omega_\infty} \nabla \cdot (\partial_t \boldsymbol{A} \times \boldsymbol{H}_a)\, dV = \lim_{R\to+\infty} \int_{\Omega_R} \nabla \cdot (\partial_t \boldsymbol{A} \times \boldsymbol{H}_a)\, dV = \\ &= \lim_{R\to+\infty} \int_{\partial\Omega_R} \partial_t \boldsymbol{A} \times \boldsymbol{H}_a \cdot\, d\boldsymbol{S}_{\Omega_R} = 0\,. \end{aligned} \tag{1.29}$$

since for $R \to \infty$ $|\partial_t \boldsymbol{A}| \to 0$ as $\mathcal{O}(1/R)$ and $|\boldsymbol{H}_a| \to 0$ as $\mathcal{O}(1/R^2)$.
The work per unit of time dL_{tot}/dt is necessary to both increase the energy of the field and to magnetize the material body. We postulate that the energy stored in the field is given by the following formula:

$$W_H = \int_{\Omega_\infty} \frac{1}{2}\, \mu_0\, \boldsymbol{H}^2\, dV\,. \tag{1.30}$$

Accordingly, the second term at the righ hand side of equation (1.27) is identified as the work per unit of time made to magnetize the magnetic material and it is expressed by the following relation:

$$\frac{dL}{dt} = \int_{\Omega} \mu_0\, \boldsymbol{H} \cdot \partial_t \boldsymbol{M}\, dV\,. \tag{1.31}$$

Notice that in the equation (1.31) $\boldsymbol{H}$ can be viewed as a generalized force and $\boldsymbol{M}$ as a generalized displacement conjugated with that force. Therefore, we can infer that the work done per unit volume is $\partial_t l = \mu_0\, \boldsymbol{H} \cdot \partial_t \boldsymbol{M}$.
The second step of this treatment is to write the principles of the thermodynamics for the magnetic body. Let's assume the body in contact with a thermal bath at fixed temperature T. The temperature distribution inside the body is considered uniform and equal to T. Moreover we assume

that it is possible to divide the body in small volumes which are small from macroscopic point of view but still large from molecular point of view. This means that each small volume contains a large number of elementary particles (atoms or molecules) so we can define the thermodynamic properties. Then we make the assumption of the local equilibrium: each of these elementary volumes is assumed to be in thermodynamic equilibrium so that we can apply the laws of thermodynamics locally. This means that the thermodynamic state of the generic elementary volume ΔV is characterized by assigning the following thermodynamic properties:

$$\begin{aligned} \Delta U &= u\,\Delta V\,, \\ \Delta S &= s\,\Delta V\,, \\ \Delta \boldsymbol{\mu} &= \boldsymbol{M}\,\Delta V\,. \end{aligned} \tag{1.32}$$

where ΔU, ΔS, and $\Delta \boldsymbol{\mu}$ are the internal energy, the entropy and the magnetic dipole moment, and where u, s, and $\boldsymbol{M}$, are the respective densities per unit volume (intensive thermodynamic properties). In an arbitrary transformation, the internal energy and the entropy change according to the first and the second principle of thermodynamics which can be expressed by the following relations respectively:

$$\begin{aligned} \frac{d\,\Delta U}{dt} &= \frac{d\,\Delta L}{dt} + \frac{d\,\Delta Q}{dt}\,, \\ \frac{d\,\Delta S}{dt} &= \frac{1}{T}\frac{d\,\Delta Q}{dt} + \frac{d\,\Delta S_i}{dt}\,, \end{aligned} \tag{1.33}$$

where ΔL is the work made on the elementary volume while $\Delta Q = q\,\Delta V$ is the energy absorbed by the volume from the thermal bath in form of heat and $\Delta S_i = s_i\,\Delta V$ is the entropy production. Notice that $\partial_t s_i \geq 0$. By substituting the equation (1.31) in the equations (1.33) and by writing them in terms of the intensive thermodynamic properties (u, s), we obtain the following set of equations:

$$\begin{aligned} \partial_t u &= \mu_0\,\boldsymbol{H}\cdot\partial_t \boldsymbol{M} + \partial_t q\,, \\ \partial_t s &= \frac{1}{T}\partial_t q + \partial_t s_i\,. \end{aligned} \tag{1.34}$$

Moreover, by substituting the second equation in the first one we obtain the following equation:

$$\partial_t u = \mu_0 \, \boldsymbol{H} \cdot \partial_t \boldsymbol{M} + T \partial_t (s - s_i) \, . \tag{1.35}$$

At this point, since we assume valid for the small volume at the thermodynamic equilibrium a relation like $u = u(s, \boldsymbol{M})$, it is more convenient to work with a thermodynamic potential where the independent variable is the temperature and not the entropy. Let us introduce the Helmholtz free energy density by the following Legendre transformation:

$$f = \min_s (u - Ts) = f(T, \boldsymbol{M}) \, , \tag{1.36}$$

from which follows the following differentiation relation:

$$\partial_t f = \partial_t u - T \partial_t s - s \, \partial_t T = \partial_t u - T \partial_t s \, , \tag{1.37}$$

where the last equality is a consequence of the fact that the temperature of the thermal bath is constant. The equation (1.35) written in terms of f becomes

$$\partial_t f = \mu_0 \, \boldsymbol{H} \cdot \partial_t \boldsymbol{M} - T \partial_t s_i \, , \tag{1.38}$$

which for an arbitrary reversible transformation produces the following relation:

$$\boldsymbol{H} = \boldsymbol{H}_a + \boldsymbol{H}_M = \frac{1}{\mu_0} \frac{\partial f}{\partial \boldsymbol{M}} \, . \tag{1.39}$$

Once obtained the equations governing the time evolution of the density of the thermodynamic properties, let us introduce the internal energy U, the entropy S, the entropy production S_i and the Helmholz free energy F_m for the magnetic body:

$$\begin{aligned} U &= \int_\Omega u \, dV \, , \\ S &= \int_\Omega s \, dV \, , \\ S_i &= \int_\Omega s_i \, dV \, , \\ F_m(T, \boldsymbol{M}(.)) &= \int_\Omega f(T, \boldsymbol{M}(\boldsymbol{r})) \, dV \, . \end{aligned} \tag{1.40}$$

In this respect, the equation (1.38) for the integral quantities takes the following form

$$\frac{dF_m}{dt} = \int_\Omega \mu_0 \boldsymbol{H} \cdot \partial_t \boldsymbol{M}\, dV - T\frac{dS_i}{dt}\,, \tag{1.41}$$

which introducing the energy term:

$$F = F_m - \int_\Omega \frac{\mu_0}{2} \boldsymbol{H}_M \cdot \boldsymbol{M}\, dV\,, \tag{1.42}$$

and taking into account the following

$$\frac{d}{dt}\int_\Omega \frac{\mu_0}{2}\, \boldsymbol{H}_M \cdot \boldsymbol{M}\, dV = \int_\Omega \mu_0 \boldsymbol{H}_M \cdot \partial_t \boldsymbol{M}\, dV\,, \tag{1.43}$$

is written as:

$$\frac{dF}{dt} = \int_\Omega \mu_0 \boldsymbol{H}_a \cdot \partial_t \boldsymbol{M}\, dV - T\frac{dS_i}{dt}\,. \tag{1.44}$$

At this point, introducing the Gibbs-Landau free energy so defined:

$$G_L = F(T, \boldsymbol{M}(.)) - \int_\Omega \mu_0 \boldsymbol{H}_a \cdot \boldsymbol{M}\, dV = G_L(T, \boldsymbol{H}_a; \boldsymbol{M}(.))\,, \tag{1.45}$$

we have

$$\frac{dG_L}{dt} = -\int_\Omega \mu_0 \boldsymbol{M} \cdot \partial_t \boldsymbol{H}_a\, dV - T\frac{dS_i}{dt}\,, \tag{1.46}$$

which for transformations at stationary applied field $\partial_t \boldsymbol{H}_a = \boldsymbol{0}$ becomes:

$$\frac{dG_L}{dt} = -T\,\frac{dS_i}{dt} \leq 0\,. \tag{1.47}$$

We obtain a minimization principle for the Gibbs-Landau potential. Indeed, as stated in equation (1.47) in an arbitrary transformation at constant temperature and stationary applied field can only decrease. In a transformation where the magnetization field changes, the conditions for a stable equilibrium are therefore:

$$\begin{aligned} &\delta G_L|_{(\boldsymbol{H}_a,T)} = \int_\Omega \left(\frac{\partial f}{\partial \boldsymbol{M}} - \mu_0 \boldsymbol{H}_a\right) \cdot \delta \boldsymbol{M}\, dV = 0\,, \\ &\delta^2 G_L|_{(\boldsymbol{H}_a,T)} > 0\,, \end{aligned} \tag{1.48}$$

namely the magnetization field of equilibrium is a minimum of G_L respect to any change of the magnetization distribution $\boldsymbol{M}(.)$ consistent with the constraint of uniform and constant temperature T and stationary applied field distribution $\boldsymbol{H}_a(.)$. In other words, the convexity of the Gibbs-Landau free energy guarantees the stability of the equilibrium magnetization state for every magnetization perturbation occuring at constant applied field and temperature value. In presence of multiplicity of local minima (multistability), such a concept of stability no holds anymore. In fact for a sufficiently large time scale, it is expected that the thermal fluctuations make the system visit all the magnetization configurations satisfying the conditions (1.48). This means that the stability has to be referred for a certain time scale. For this reason one speaks about metastability of a magnetic state. Interestingly the energetic formulation of the magnetostatic problem expressed in the equations (1.14),(1.16) and (1.17) can be connected to the thermodynamics of a magnetized body exposed in this section. In fact, once is recognized the equality $\varphi(\boldsymbol{M}) = f_m(T; \boldsymbol{M})$, we obtain $G = G_L$. This connection add a new information about the potential $\varphi(\boldsymbol{M})$ introduced talking about the constitutive relation. In fact, it is the Helmholtz free-energy of the magnetic body.
In the next section we characterize the two fundamental interactions originating the properties of ferromagnetic materials: exchange and anisotropy. Their mathematical description is used to characterize the Helmholz free-energy density $f(\boldsymbol{M})$, so far not revealed. In this way, we constitute the Gibbs-Landau free energy functional standing on the basis of the micromagnetic theory.

1.3 Exchange and Anysotropy

Two basic mechanisms are at the roots of the magnetic behaviour of ferromagnetic materials: exchange and anisotropy. Exchange derives from the combination of the electrostatic coupling between electron orbitals and the necessity to satisfy the Pauli exclusion principle. It results in spin-spin interaction that favours long-range spin ordering over macroscopic distances.

Anisotropy is instead mainly related to interactions of electron orbitals with the potential created by the hosting lattice. As well as the lattice symmetry is reflected in the symmetry of the potential, the spin orientation along certain symmetry axes of the hosting lattice becomes energetically favoured. In the following we start considering first the exchange interaction and then the anisotropy one. The study of the exchange interaction is splitted in two parts. In the first one we use the Weiss molecular field description to argue the spontaneous magnetization when the temperature is below the Curie value of the ferromagnet. In the second instead, a nonuniform magnetization distribution is considered and the associated free energy is derived. The anisotropy interaction is treated with symmetry arguments without going into the details of its physical origin.

Exchange

We start with a brief discussion of paramagnetism, which is the natural basis for the description of the exchange interaction in the ferromagnetism. Let us consider a paramagnet made by an assembly of identical noninteracting magnetic moments $\boldsymbol{\mu}_i$ of strength μ, subject to the action of the uniform external field $\boldsymbol{H}_a$. Each moment has a potential energy $-\mu_0 \boldsymbol{H}_a \cdot \boldsymbol{\mu}_i$ in the external field. Moreover, we consider the case where the moments are quantum moments with spin 1/2. Only two states are then possible, where the magnetic component along the field is either $+\mu$ or $-\mu$. The ensemble is in contact with a thermal bath with fixed temperature equal to T. The probability for a given magnetic state $\{\boldsymbol{\mu}_1, \boldsymbol{\mu}_2, \ldots, \boldsymbol{\mu}_N\}$ of the ensemble obeys in the thermodynamic equilibrium condition to the following Boltzmann statistics:

$$p(\boldsymbol{\mu}_{1,2,\ldots,N}) = \frac{1}{Z} \exp\left(- \frac{\sum_{i=1}^{N} -\mu_0 \boldsymbol{H}_a \cdot \boldsymbol{\mu}_i}{k_B T} \right) = \frac{1}{Z} \exp\left(\frac{\mu_0 H_a \, M_\mu \, \Delta V}{k_B T} \right), \tag{1.49}$$

where M_μ is the magnetization of the ensemble along the field direction for the magnetic state considered, ΔV the volume of the paramagnet and the term Z is called partition function [2]. Since the sum of the probabilities of

the all possible states is equal to 1, the partition function must be given by the following equation:

$$\begin{aligned} Z &= \sum_{states} \exp\left(-\frac{-\mu_0 H_a\, M_\mu\, \Delta V}{k_B T}\right) = \\ &= \prod_{i=1}^{N}\left(\sum_{states,\mu_i} \exp\left(-\frac{-\mu_0 \boldsymbol{H}_a \cdot \boldsymbol{\mu}_i}{k_B T}\right)\right) = Z_\mu^N\,, \end{aligned} \tag{1.50}$$

where Z_μ single-moment partition function given by the following equation:

$$Z_\mu = \exp\left(\frac{\mu_0 H_a \mu}{k_B T}\right) + \exp\left(-\frac{\mu_0 H_a \mu}{k_B T}\right) = 2\cosh a\,, \tag{1.51}$$

and the quantity a is the argument of the exponential functions. Notice that the inversion between the summation and product structure in equation (1.50) can be done due to the assumption of noninteracting magnetic moments. From the expression of the partition function (see eq. (1.50)), we can quickly calculate the average magnetization M of the ensemble, namely:

$$M = \frac{1}{Z}\sum_{states} M_\mu \exp\left(-\frac{-\mu_0 H_a\, M_\mu\, \Delta V}{k_B T}\right) = -\frac{N\, k_B T}{\mu_0 \Delta V}\partial_{H_a} \log Z_\mu\,, \tag{1.52}$$

where substituting eq.(1.51) one obtains the following expression:

$$M = \frac{N\,\mu}{\Delta V}\tanh\left(\frac{\mu_0 H_a \mu}{k_B T}\right) = M_0 \tanh a\,. \tag{1.53}$$

Fixed the temperature for small field values the magnetization depends linearly by the field while for $H_a \to \pm\infty \;\Rightarrow\; M \to \pm M_0$ respectively. In the case $a \ll 1$ we have $M \approx \chi H_a$, with $\chi(T) = \frac{C}{T}$. This last quantity is the magnetic susceptibility and its temperature dependence is known as the Curie law. In a ferromagnet, it is observed spontaneous magnetization also in case $H_a = 0$. This means that the simple theory of paramagnetism cannot take into account the ferromagnetism. However, since the spontaneous magnetization is the result of a strong interaction field which favors

collective alignment of the moments along the magnetization direction, it seems reasonable as a first approximation, to postulate for the interaction field the following expression:

$$H_W = N_W M \,, \tag{1.54}$$

where H_W is named Weiss molecular field and the term N_W measures the strength of the interaction. Under the presence of H_W each moment experiences an effective field that is sum of the applied and the molecular field. In this respect, eq.(1.53) becomes:

$$M = M_0 \tanh\left[\frac{\mu_0\,\mu}{k_B T}(H_a + N_W M)\right] . \tag{1.55}$$

Introducing the normalized magnetization $x = M/M_0$, he normalized external field $h_a = H_a/(N_W M_0)$ the quantity $T_C = (\mu_0\,\mu N_W M_0)/k_B$ and the normalized temperature $\mathcal{T} = T/T_C$, the equation (1.55) can be written as:

$$x = \tanh\left(\frac{x + h_a}{\mathcal{T}}\right) . \tag{1.56}$$

In figure 1.2 is plotted the solution of this equation for different values of h_a. When $H_a = 0$ for $T \ll T_C$ we have $M \approx M_0$ with $T = 0 \rightarrow M = M_0$. This means that when the temperature is well below the value T_C a spontaneous magnetization occurs. When $T \sim T_C$ instead, we have $M \ll M_0$ and for $T = T_C \rightarrow M = 0$. The temperature T_C is a threshold value after which the ferromagnet behaves like a paramagnet. For this reason, it is a characteristic temperature of the ferromagnet considered, called Curie temperature. Close to the Curie point, for $T > T_C$ with low value of the external field $h_a \ll 1$, equation (1.55) can be approximated by the following expression: $M = \chi(T)\, H_a$, where the temperature dependence of magnetic susceptibility for a ferromagnet is expressed by the Curie-Weiss law: $\chi(T) = \frac{C}{T - T_C}$. In the following, fixed the temperature T, we shall refer to the spontaneous magnetization with the symbol $M_s = M_s(T)$. Starting from the equation (1.56), we can calculate the amount of exchange energy when the magnetization is uniform and its strength is equal to $M_s(T)$. By

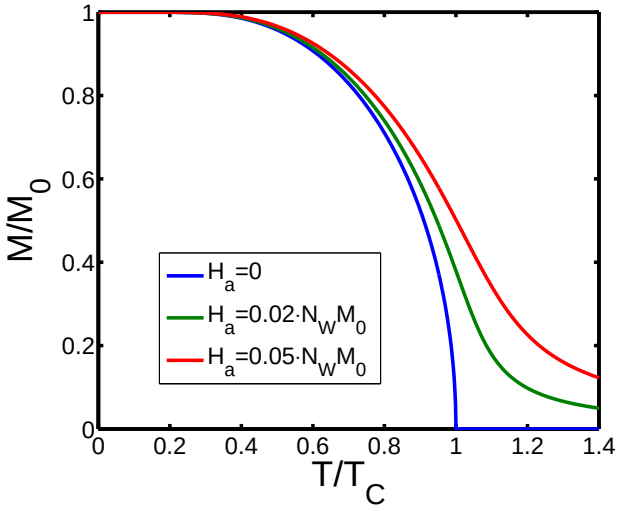

Figure 1.2: Spontaneous magnetization in function of the temperature for different values of the external field.

inverting the hyperbolic tangent in the equation (1.56), it can be written in the form

$$h_a = \frac{\mathcal{T}}{2} \log\left(\frac{1+x}{1-x}\right) - x\,. \tag{1.57}$$

According to the approach presented in the previous section, the above equation can be regarded as result of the condition

$$\frac{\partial g_{EX}}{\partial x} = 0\,, \tag{1.58}$$

where

$$g_{ex} = \mathcal{F}_{EX}(x) - h_a\, x\,, \tag{1.59}$$

is a Gibbs-Landau free energy for the exchange interaction considered, with

$$\mathcal{F}_{EX}(x) = \frac{\mathcal{T}}{2}\left[(1+x)\log(1+x) + (1-x)\log(1-x)\right] - \frac{x^2}{2} \tag{1.60}$$

the exchange free energy.

When in a magnetic body, the magnetization changes orientation from point to point $\boldsymbol{M}(\boldsymbol{r}) = M_s(T)\boldsymbol{m}(\boldsymbol{r})$, we have an extra exchange free energy cost. It is nonuniformity energy that is usually meant when one speaks of exchange energy. Therefore additional exchange contribution is present when the gradients ∇m_x, ∇m_y, ∇m_z of the unit magnetization vector $\boldsymbol{m}(\boldsymbol{r})$ are different from zero. We can make a Taylor expansion of the exchange energy, as a function of the magnetization gradients. If the variation is not too rapid, the lowest-order term in the energy density consistent with a cubic symmetry lattice of the ferromagnetic medium is given by:

$$f_{EX}(\boldsymbol{m}(\boldsymbol{r})) = const. + A\left[(\nabla m_x)^2 + (\nabla m_y)^2 + (\nabla m_z)^2\right], \tag{1.61}$$

where the constant term is the contribution due to the spontaneous magnetization, while the phenomenological constant A summarizes short-range exchange interactions.

Anisotropy

We have seen that the exchange energy depends by the reciprocal alignment of magnetic spin moments but not by their orientations in the space. This isotropic feature of the free energy is not conserved in presence of anisotropy effect, which energetically favours certain directions. The character of the anisotropy is reflected in the mathematical symmetry expressed by the anisotropy free energy density f_{AN}. In this respect, it is considered the development of f_{AN} in even powers of $\boldsymbol{m}$, since it is experimentally observed the invariance of f_{AN} with respect to inversion of $\boldsymbol{m}$. For example, in case of uniaxial anisotropy, say $\hat{\boldsymbol{e}}_{AN}$ the anisotropy axis, we have the following expression:

$$f_{AN}(\boldsymbol{m}) = K_0 + K_1[1 - (\boldsymbol{m}\cdot\hat{\boldsymbol{e}}_{AN})^2] + K_2[1 - (\boldsymbol{m}\cdot\hat{\boldsymbol{e}}_{AN})^2]^2 + \dots \tag{1.62}$$

where $(K_0, K_1, K_2, \dots, K_{i-th}, \dots)$ are the anisotropy constants of the i-th order, which have the dimensions of energy per unit of volume. In case of cubic anysotropy instead, we have three privileged directions, which we

take as (x, y, z) axes. The development of the anysotropy energy, consistent with the invariance under $\boldsymbol{m} \to -\boldsymbol{m}$, takes the following form:

$$f_{AN}(\boldsymbol{m}) = K_0 + K_1(m_x^2 m_y^2 + m_y^2 m_z^2 + m_z^2 m_x^2) + K_2 m_x^2 m_y^2 m_z^2 + \dots \quad (1.63)$$

where the terms $(m_x^4 + m_y^4 + m_z^4)$, $(m_x^6 + m_y^6 + m_z^6)$ and $(m_x^4 m_y^2 + m_y^4 m_z^2 + m_z^4 m_x^2)$ are not included since they are dependent by those ones written in equation (1.63).
At this point we are ready to express the Gibbs-Landau free energy functional showing for each contibution its dependence by the magnetization field. This is the first step to formulate the micromagnetic theory as discussed in the next section.

1.4 Micromagnetic energy and Brown's equations

Micromagnetic theory was developed as an effort to give a rigourous basis to ferromagnetic domains theory. The theory is applicable to a spatial scale "small enough to reveal details of the transition regions between domains, yet large enough to permit the use of continuous magnetization vector rather than of individual atomic spins". In micromagnetics, the state of the ferromagnet is described by the vector field $\boldsymbol{M}(\boldsymbol{r}; t)$, representing the local magnetization at every point inside the ferromagnet. When the temperature is well below the Curie temperature of the ferromagnet, the magnetization field respects the following fundamental constraint:

$$|\boldsymbol{M}(\boldsymbol{r})| = M_s(T)\,, \quad (1.64)$$

which means that the magnitude of the local magnetization vector at each point inside the ferromagnet is equal to the spontaneous magnetization M_s at the given temperature T. This constraint summarizes the effect of the atomic-scale exchange interaction, qualitatively discussed in the previous section with the Weiss molecular field model. The micromagnetic theory is based on the fact that for a ferromagnetic body occupying the region Ω,

with magnetization $\boldsymbol{M}(\boldsymbol{r})$, is associated the following free energy functional:

$$G_L(\boldsymbol{M};\boldsymbol{H}_a) = F_{EX} + F_{AN} + F_M + F_a = \\ = \int_\Omega \left[\frac{A}{M_s^2} \sum_i (\nabla M_i)^2 + f_{AN}(\boldsymbol{M}) - \frac{\mu_0}{2} \boldsymbol{H}_M[\boldsymbol{M}] \cdot \boldsymbol{M} - \mu_0 \boldsymbol{H}_a \cdot \boldsymbol{M} \right] dV \,. \tag{1.65}$$

The first term inside the integral represents the exchange energy. The constant A is the so-called exchange stiffness constant; its value in ferromagnets is usually of the order of $10^{11} Jm^{-1}$. The second term $f_{AN}(\boldsymbol{M})$ describes crystal anisotropy effects, while the two last terms represent magnetostatic energy and energy of interaction with the external magnetic field. The magnetostatic contribution is governed by the field $\boldsymbol{H}_M$, expressed in equation (1.8). The applied field $\boldsymbol{H}_a$ is produced by external sources and, in general, it is a given vector function of space and time. The micromagnetic free energy may contain additional terms describing other energy contributions, for example magnetoelastic effects. The magnetic body considered is assumed to be rigid, therefore such terms are not involved in our discussion. In the following, we omit the dependences on T, since the temperature will always be assumed to be uniform in space and constant in time. As argued in section 1.2, for a given applied field the micromagnetic equilibria can be found solving the following variational problem:

$$\begin{aligned} \delta G_L = & \int_\Omega -\mu_0 \left[\boldsymbol{H}_{EX} + \boldsymbol{H}_{AN} + \boldsymbol{H}_M + \boldsymbol{H}_a \right] \cdot \delta \boldsymbol{M} \, dV \\ & - \mu_0 \int_{\partial\Omega} \partial_n \boldsymbol{M} \cdot \delta \boldsymbol{M} \, dS = 0 \,, \end{aligned} \tag{1.66}$$

where $\boldsymbol{H}_{AN}$ and $\boldsymbol{H}_{EX}$ are the anisotropy field and the exchange field, respectively given by:

$$\boldsymbol{H}_{EX} = l_{EX}^2 \nabla^2 \boldsymbol{M} \,, \qquad\qquad \boldsymbol{H}_{AN} = -\frac{1}{\mu_0} \partial_{\boldsymbol{M}} f_{AN} \,, \tag{1.67}$$

where $l_{EX} = \sqrt{\frac{2A}{\mu_0 M_s^2}}$ is the so-called exchange length. Due to the fundamental micromagnetic constraint (1.64), the magnetization variation has to

have the following structure: $\delta \boldsymbol{M} = \boldsymbol{M} \times \delta\theta$, where $\delta\theta$ is an arbitrary small but otherwise arbitrary space-dependent vector. In this respect, equation (1.66) can be written as:

$$\begin{aligned} \delta G_L = & \int_\Omega \mu_0 \boldsymbol{M} \times \boldsymbol{H}_{eff} \cdot \delta\boldsymbol{\theta}\, dV \\ & + \int_{\partial\Omega} \mu_0 \boldsymbol{M} \times \partial_n \boldsymbol{M} \cdot \delta\boldsymbol{\theta}\, dS = 0\,. \end{aligned} \tag{1.68}$$

where the vector:

$$\boldsymbol{H}_{eff} = -\frac{1}{\mu_0}\frac{\delta G_L}{\delta \boldsymbol{M}} = \boldsymbol{H}_{EX} + \boldsymbol{H}_{AN} + \boldsymbol{H}_M + \boldsymbol{H}_a\,, \tag{1.69}$$

is called effective magnetic field because it resumes all the interactions we included in the free energy functional. The notation $\frac{\delta f(\boldsymbol{x})}{\delta \boldsymbol{x}}$ indicates the variational derivative. Due to the arbitrariness of the body shape and the magnetization variation, we obtain the so called Brown's equations [3], [4], [5] [6]:

$$\begin{aligned} & \boldsymbol{M} \times \boldsymbol{H}_{eff} = \boldsymbol{0} && in\ \Omega \\ & \partial_n \boldsymbol{M} = \boldsymbol{0} && on\ \partial\Omega\,, \end{aligned} \tag{1.70}$$

which define a nonlinear integro-differential problem where the boundary condition is given and not arbitrary.

1.5 Modelling of magnetization dynamics

When $\boldsymbol{M}(\boldsymbol{r};t)$ is not aligned with $\boldsymbol{H}_{eff}$ ($\boldsymbol{M}\times\boldsymbol{H}_{eff} \neq \boldsymbol{0}$), the magnetization dynamics takes place. The main is a precessional dynamics around $\boldsymbol{H}_{eff}$, described by the following equation:

$$\dot{\boldsymbol{M}} = -\gamma \boldsymbol{M} \times \boldsymbol{H}_{eff}\,, \tag{1.71}$$

where γ here is the absolute value of the gyromagnetic ratio of the electron spins. This equation proposed by Landau and Lifshitz in 1935 [7], describes conservative motion. This can be seen by the following equation:

$$\dot{G}_L = -\mu_0 \int_\Omega \left[\boldsymbol{H}_{eff} \cdot \dot{\boldsymbol{M}} - \boldsymbol{M} \cdot \dot{\boldsymbol{H}}_a\right] dV\,, \tag{1.72}$$

expressing the power balance during the magnetization dynamics assuming the boundary conditions (1.70). In case of motion described by the equation (1.71), it can be written as follows:

$$\dot{G}_L = \mu_0 \int_\Omega \boldsymbol{M} \cdot \dot{\boldsymbol{H}}_a \, dV \,, \tag{1.73}$$

where it is evident that $\dot{\boldsymbol{H}}_a = \boldsymbol{0} \Rightarrow \dot{G}_L = 0$.

1.6 Dissipations: Landau-Lifshitz vs Gilbert

In order to take into account dissipative effects, additional terms are added to LL equation. In this respect, the most used equation is the following [7]:

$$\dot{\boldsymbol{M}} = -\gamma_L \boldsymbol{M} \times \boldsymbol{H}_{eff} - \frac{\gamma_L \alpha}{M_s} \boldsymbol{M} \times (\boldsymbol{M} \times \boldsymbol{H}_{eff}) \,, \tag{1.74}$$

where γ_L is a gyromagnetic-type constant which can be different from γ, and the damping constant $0 < \alpha \ll 1$. The power balance in this case is given by:

$$\dot{G}_L = -\frac{\mu_0 \gamma_L \alpha}{M_s} \int_{\Omega_m} |\boldsymbol{M} \times \boldsymbol{H}_{eff}|^2 \, dV + \mu_0 \int_\Omega \boldsymbol{M} \cdot \dot{\boldsymbol{H}}_a \, dV \,, \tag{1.75}$$

which in case of time invariant applied field $\dot{\boldsymbol{H}}_a = \boldsymbol{0}$ becomes

$$\dot{G}_L = -\frac{\mu_0 \gamma_L \alpha}{M_s} \int_{\Omega_m} |\boldsymbol{M} \times \boldsymbol{H}_{eff}|^2 \, dV < 0 \,. \tag{1.76}$$

This relation expresses the fact that G_L decreases throughout the magnetization dynamics and only the magnetization fields $\boldsymbol{M}(.)$ which minimize it are possible equilibrium solutions, consistently to the thermostatic principle viewed in section section 1.2.

1.7 Gilbert theory of dissipations

The phenomenological introduction of the damping torque proposed by Landau and Lifshitz in their celebrated paper [7] is not the only way to do so. T. L. Gilbert proposed a different dissipative term [8], derived by using the Rayleigh dissipation function method [9], [10], [11]. Starting from a Lagrangian formulation of the conservative LL equation, with Lagrangian given by:

$$\mathcal{L}(\boldsymbol{M}, \dot{\boldsymbol{M}}) = \int_{\Omega} \boldsymbol{A}_M(\boldsymbol{M}) \cdot \dot{\boldsymbol{M}}\, dV - G_L(\boldsymbol{M})\,, \tag{1.77}$$

where the potential $\boldsymbol{A}_M$ satisfies the following equation:

$$\partial_{\boldsymbol{M}} \times \boldsymbol{A}_M(\boldsymbol{M}) = \boldsymbol{M}\,. \tag{1.78}$$

From the Lagrangian expressed in equation (1.77), the conservative Landau-Lifshitz equation (1.71) is obtained from the following Euler-Lagrange equation:

$$\frac{\delta \mathcal{L}}{\delta \boldsymbol{M}} - \frac{d}{dt}\frac{\delta \mathcal{L}}{\delta \dot{\boldsymbol{M}}} = \boldsymbol{0}\,. \tag{1.79}$$

At this point, the dissipation can be included by the following equation:

$$\frac{\delta \mathcal{L}}{\delta \boldsymbol{M}} - \frac{d}{dt}\frac{\delta \mathcal{L}}{\delta \dot{\boldsymbol{M}}} - \frac{\delta \mathcal{R}}{\delta \dot{\boldsymbol{M}}} = \boldsymbol{0}\,, \tag{1.80}$$

where $\mathcal{R}(\dot{\boldsymbol{M}})$ is the Rayleigh's dissipation functional, given by:

$$\mathcal{R}(\dot{\boldsymbol{M}}) = \frac{\eta}{2}\int_{\Omega} |\dot{\boldsymbol{M}}|^2\, dV\,. \tag{1.81}$$

where of $\eta > 0$. In this way the Landau Lifshitz equation with the addition of the Gilbert damping term, also called LLG equation is written as:

$$\dot{\boldsymbol{M}} - \frac{\alpha}{M_s}\boldsymbol{M} \times \dot{\boldsymbol{M}} = -\gamma_G \boldsymbol{M} \times \boldsymbol{H}_{eff}\,, \tag{1.82}$$

where $\alpha = \eta\gamma_G M_s$, and γ_G is the gyromagnetic constant for the Gilbert formulation. The dissipative nature of the LLG can be proved as for the

equation (1.74). In fact by using the equation (1.82), we have the following power balance:

$$\dot{G}_L = -\frac{\mu_0 \alpha}{M_s \gamma_G} \int_\Omega |\dot{\boldsymbol{M}}|^2 \, dV \; + \mu_0 \int_\Omega \boldsymbol{M} \cdot \dot{\boldsymbol{H}}_a \, dV \,, \tag{1.83}$$

where it is evident that the micromagnetic energy rate is negative ($\dot{G}_L < 0$) when $\dot{\boldsymbol{H}}_a = \boldsymbol{0}$.

The LLG equation can be putted in form of the equation (1.74). This can be done by expressing in the equation (1.82) the damping torque in function of the only magnetization and not of its time derivative. When we do that, we obtain the following equation:

$$\dot{\boldsymbol{M}} = -\frac{\gamma_G}{1+\alpha^2} \boldsymbol{M} \times \boldsymbol{H}_{eff} - \frac{\gamma_G}{1+\alpha^2} \frac{\alpha}{M_s} \boldsymbol{M} \times (\boldsymbol{M} \times \boldsymbol{H}_{eff}) \,, \tag{1.84}$$

which is equal to the non conservative Landau Lifshitz eq.(1.74) once are satisfied the following relations:

$$\gamma_G = \gamma_L (1 + \alpha^2) \,, \tag{1.85}$$

which is well approximated by an identity in case of $\alpha \ll 1$. Typical values of the damping are $\alpha \sim 0.001 \div 0.1$ for the most used magnetic materials (CoFeB [12], [13], Py [14], Ni [15]).

1.8 Spin transfer torque effect

When an electric current flows across a ferromagnet, electrons exert a torque of quantum-mechanical origin. This effect is called spin transfer torque and is most often investigated in multi-layer structures (see fig.1.3). The effect of spin transfer on magnetization dynamics can be studied (quite independently of the details of the microscopic mechanism responsible for it) by adding an appropriate spin-transfer torque term to the Landau-Lifshitz-Gilbert (LLG) equation for the free-layer magnetization. The mathematical form of this additional torque term in three-layer structures, consisting of two ferromagnetic layers separated by a nonmagnetic spacer (see fig1.3),

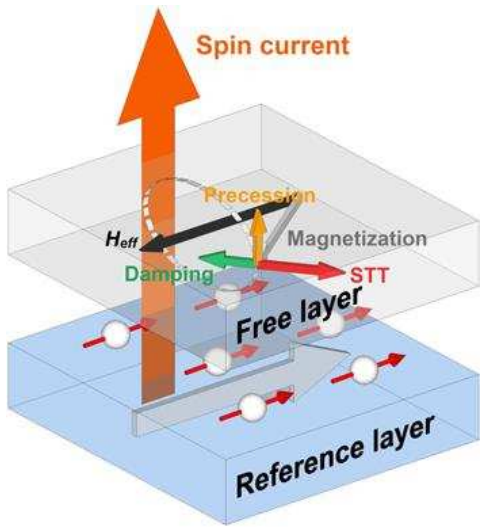

Figure 1.3: Trilayer structure. The reference layer has a fixed magnetization orientation. The injection of spin polarized current creates an additional torque (STT).

was derived by Slonczewski [16], [17], [18], [19]. This additional torque, in a general form independent on the kind of multilayer structure can be expressed by the following equation:

$$\boldsymbol{\tau}_{ST} = \varepsilon \frac{J_e}{J_p} \boldsymbol{M} \times (\boldsymbol{M} \times \boldsymbol{m}_p) \,, \tag{1.86}$$

where $\varepsilon(\eta; \boldsymbol{M} \cdot \boldsymbol{m}_p)$ is a function of the degree of spin polarization η and the reciprocal orientation between the magnetizations in the free layer and the reference layer (see fig.1.3). The term J_e is the spin-polarized current density, and J_p is a characteristic constant of the multilayer structure which has the dimension of a superficial density of electric current. The LLG equation (1.82) with the Slonczewski spin-transfer torque (LLGS) is given

by

$$\dot{\boldsymbol{M}} = -\gamma_G \, \boldsymbol{M} \times \left(\boldsymbol{H}_{eff} - \frac{\alpha}{\gamma_G \, M_s} \dot{\boldsymbol{M}} - \varepsilon \, \beta \boldsymbol{M} \times \boldsymbol{m}_p \right) , \tag{1.87}$$

where $\beta = J_e/J_p$. For typical multilayer devices where the magnetization dynamics is excited by spin-polarized current $J_p \sim 10^{10} \, A/cm^2$, while $J_e \sim 10^7 \, A/cm^2$. This means that the dimensionless spin-polarized-current is $\beta \sim \alpha$. It's interesting to notice that the spin-transfer torque term depending on the direction of $\boldsymbol{m}_p$ and the sign of J_e can act against the damping torque term. This concept can be formally understood if we explicit the power balance in the case $\dot{\boldsymbol{H}}_a = \boldsymbol{0}$ as in the previous sections:

$$\dot{G}_L = -\mu_0 \alpha \int_\Omega \left[\frac{|\dot{\boldsymbol{M}}|^2}{\gamma_G M_s} - \gamma_G \, \varepsilon \frac{\beta}{\alpha} (\boldsymbol{M} \times \boldsymbol{H}_{eff}) \cdot (\boldsymbol{M} \times \boldsymbol{m}_p) \right] dV \, , \tag{1.88}$$

where it is possible that for some orientation of the polarizer, the magnetic free energy can increase. This phenomenon is on the basis of current induced dynamics such as switching and the self-oscillations regime.

1.9 Normalized magnetization dynamics

It is useful to rewrite the equations describing the magnetization dynamics in normalized form, where magnetization and fields are measured in units of M_s, while energies are measured in units of $\mu_0 M_s^2 V$, where V is the volume of the ferromagnet. Then, the magnetization field is described by the unit vector:

$$\boldsymbol{m}(\boldsymbol{r}; t) = \frac{\boldsymbol{M}(\boldsymbol{r}; t)}{M_s} \, , \tag{1.89}$$

which lies on the unit sphere of the $\boldsymbol{m}-$space: $\boldsymbol{m}^2 = 1$. The normalized free energy g_L associated with the vector field $\boldsymbol{m}$ is the sum of normalized

exchange, anisotropy, magnetostatic, and Zeeman energies, respectively:

$$g_L(\boldsymbol{m};\boldsymbol{h}_a) = \frac{G_L(\boldsymbol{M};\boldsymbol{H}_a)}{\mu_0 M_s^2 V} = \frac{1}{V}\int_\Omega \left[\frac{l_{EX}^2}{2}\sum_i (\nabla m_i)^2 + \varphi_{AN}(\boldsymbol{m}) - \frac{\boldsymbol{h}_M}{2}\cdot\boldsymbol{m} - \boldsymbol{h}_a\cdot\boldsymbol{m}\right] dV\,. \tag{1.90}$$

where $\varphi_{AN} = \frac{f_{AN}}{\mu_0 M_s^2}$ is the normalized anisotropy energy, $\boldsymbol{h}_M = \boldsymbol{H}_M/M_s$ and $\boldsymbol{h}_a = \boldsymbol{H}_a/M_s$ are the normalized magnetostatic and applied fields respectively. At this point we can introduce the normalized effective field:

$$\boldsymbol{h}_{eff} = -\frac{\delta g_L}{\delta \boldsymbol{m}} = \frac{\boldsymbol{H}_{eff}}{M_s} = \boldsymbol{h}_{EX} + \boldsymbol{h}_{AN} + \boldsymbol{h}_M + \boldsymbol{h}_a\,, \tag{1.91}$$

and the following normalized Brown's equations:

$$\begin{aligned} &\boldsymbol{m}\times\boldsymbol{h}_{eff} = \boldsymbol{0} && in\ \Omega,\\ &\partial_n \boldsymbol{m} = \boldsymbol{0} && on\ \partial\Omega\,. \end{aligned} \tag{1.92}$$

The dynamics of the magnetization vector field $\boldsymbol{m}(\boldsymbol{r};t)$ is governed by the normalized version of the LL equation (1.74) or LLG equation (1.82). The dimensionless equations are obtained after a proper renormalization of time. It is convenient to choose the time unit in such a way that the coefficient in front of the precessional term is reduced to unity. Thus, by measuring time in units of $(\gamma_L M_s)$, from eq.(1.74) one obtains the normalized LL equation:

$$\dot{\boldsymbol{m}} = -\boldsymbol{m}\times\boldsymbol{h}_{eff} - \alpha\boldsymbol{m}\times(\boldsymbol{m}\times\boldsymbol{h}_{eff})\,, \tag{1.93}$$

while, by measuring time in units of $(\gamma_G M_s)$, from eq.(1.82) one obtains the normalized LLG equation:

$$\dot{\boldsymbol{m}} - \alpha\boldsymbol{m}\times\dot{\boldsymbol{m}} = -\boldsymbol{m}\times\boldsymbol{h}_{eff}\,. \tag{1.94}$$

When we add the spin-transfer torque the equation (1.93) becomes:

$$\dot{\boldsymbol{m}} = -\boldsymbol{m}\times\boldsymbol{h}_{eff} - \alpha\boldsymbol{m}\times(\boldsymbol{m}\times\boldsymbol{h}_{eff}) + \varepsilon\,\beta\boldsymbol{m}\times(\boldsymbol{m}\times\boldsymbol{m}_p)\,, \tag{1.95}$$

with the following power balance:

$$\dot{g}_L = -\alpha \int_\Omega \left[|\boldsymbol{m} \times \boldsymbol{h}_{eff}|^2 - \varepsilon \frac{\beta}{\alpha} (\boldsymbol{m} \times \boldsymbol{h}_{eff}) \cdot (\boldsymbol{m} \times \boldsymbol{m}_p) \right] dV \,. \tag{1.96}$$

On the other hand, the equation (1.94) adding the same term, becomes:

$$\dot{\boldsymbol{m}} - \alpha \boldsymbol{m} \times \dot{\boldsymbol{m}} = -\boldsymbol{m} \times \boldsymbol{h}_{eff} + \varepsilon \, \beta \boldsymbol{m} \times (\boldsymbol{m} \times \boldsymbol{m}_p) \,, \tag{1.97}$$

which admits the different and following power balance:

$$\dot{g}_L = -\alpha \int_\Omega \left[|\dot{\boldsymbol{m}}|^2 - \varepsilon \frac{\beta}{\alpha} (\boldsymbol{m} \times \boldsymbol{h}_{eff}) \cdot (\boldsymbol{m} \times \boldsymbol{m}_p) \right] dV \,. \tag{1.98}$$

It can be noticed that when we transform the equation (1.95) in its Gilbert form, we obtain an equation which is equal to the equation (1.97) except for an additional field like torque. Such torque is due to the transformation of the spin-transfer-torque term and it is weighted by the coefficient $\beta \, \alpha \sim \mathcal{O}(\alpha^2)$. For this reason, since $\alpha \ll 1$ the magnetization dynamics described by the two equations (1.95) and (1.97) are essentially equivalent. In the following of this thesis, the magnetization dynamics will be studied by using either the LL or the LLG form of the equations, as convenient. It is worth recalling that these two equations have been obtained by introducing different normalizations for the time scale. Therefore, these different normalizations will have to be taken into account whenever the equations are transformed from one form to another one.

1.10 Collective variables description of magnetization dynamics in nanostructure

Due to the nonlinear nature of the LLG equation (1.87), analytical solutions can be derived in very few special cases [20], [21], [22]. In general, the knowledge of the magnetization dynamics requires the integration of the LLG equation, defined in the region Ω occupied by the magnetic body. For this reason, different numerical schemes have been developed [23], [24], [25],

to integrate the LLG equation for different geometries, materials and excitation parameters. However, there exist several situations where, after a transient dynamics, the magnetization pattern can be approximately characterized by a finite set of coordinates. These coordinates play the role of degree of freedom of the magnetization dynamics and are called collective variables $\boldsymbol{X}(t) \equiv (X_1, \ldots, X_N)$. The study of the magnetization dynamics with the collective variables approach, is therefore based on the following ansatz:

$$\boldsymbol{m}(\boldsymbol{r}, t) = \boldsymbol{m}(\boldsymbol{r}, \boldsymbol{X}(t)) \,, \tag{1.99}$$

which implies the following law of variation:

$$\delta \boldsymbol{m} = \sum_{j=1}^{N} \partial_{X_j} \boldsymbol{m} \, \delta X_j \,. \tag{1.100}$$

Starting from these two equations, a dynamical model for the collective variables can be derived. The first step to do so is to write the LLG equation (1.97) in a variational form as in the following:

$$\int_\Omega \left(\boldsymbol{m} \times \dot{\boldsymbol{m}} + \frac{\delta g_L}{\delta \boldsymbol{m}} + \alpha \dot{\boldsymbol{m}} + \beta \, \varepsilon \, \boldsymbol{m} \times \boldsymbol{m}_p \right) \cdot \delta \boldsymbol{m} \, dV = 0 \,, \tag{1.101}$$

where in general $\delta \boldsymbol{m}(\boldsymbol{r}; t) = \boldsymbol{m}(\boldsymbol{r}; t) \times \delta \boldsymbol{\theta}(\boldsymbol{r}; t)$, and the function $\delta \boldsymbol{\theta}(\boldsymbol{r}; \boldsymbol{t})$is arbitrary. When we assume a collective variables description, substituting eq.(1.99) and the (1.100) in (1.101) we obtain:

$$\begin{aligned} \sum_{k=1}^{N} \Bigg[\int_\Omega \Bigg(\boldsymbol{m} \times \left(\dot{\boldsymbol{X}} \cdot \partial_{\boldsymbol{X}} \boldsymbol{m} \right) + \frac{\delta g_L}{\delta \boldsymbol{m}} + \alpha \, \dot{\boldsymbol{X}} \cdot \partial_{\boldsymbol{X}} \boldsymbol{m} + \\ + \beta \, \varepsilon \, \boldsymbol{m} \times \boldsymbol{m}_p \cdot \partial_{X_k} \boldsymbol{m} \Bigg) \, dV \Bigg] \delta X_k = 0 \,, \end{aligned} \tag{1.102}$$

or in a more compact form:

$$\sum_{k=1}^{N} \left[\sum_{h=1}^{N} G_{kh} \dot{X}_h + \partial_{X_k} W + \sum_{h=1}^{n} D_{kh} \dot{X}_h - F_{st,k} \right] \delta X_k = 0 \,, \tag{1.103}$$

which are fulfilled for every variation $\delta X_k,\ k = 1 \dots n.$ this implies the following dynamical model :

$$\sum_{h=1}^{n} G_{kh}\dot{X}_h + \partial_{X_k} W + \sum_{h=1}^{n} D_{kh}\dot{X}_h - F_{st,k} = 0\,, \tag{1.104}$$

or in vectorial form

$$\boldsymbol{G}\cdot\dot{\boldsymbol{X}} + \partial_{\boldsymbol{X}} W + \boldsymbol{D}\cdot\dot{\boldsymbol{X}} - \boldsymbol{F}_{st} = \boldsymbol{0}\,. \tag{1.105}$$

In the equation (1.104) the several coefficients of the collective variables are related to the magnetization structure through the following expressions :

$$G_{kh} = \int_\Omega \boldsymbol{m}\cdot\partial_{X_h}\boldsymbol{m}\times\partial_{X_k}\boldsymbol{m}\,dV\,, \tag{1.106}$$

$$\partial_{X_k} W = \int_\Omega \partial_{X_k} g_L\,dV\,, \tag{1.107}$$

$$D_{kh} = \alpha\int_\Omega \partial_{X_k}\boldsymbol{m}\cdot\partial_{X_h}\boldsymbol{m}\,dV\,, \tag{1.108}$$

$$F_{st,k} = \beta\int_\Omega \varepsilon(\boldsymbol{m},\boldsymbol{m}_p)\,\boldsymbol{m}_p\cdot\boldsymbol{m}\times\partial_{X_k}\boldsymbol{m}\,dV\,. \tag{1.109}$$

As an example of that, let us consider the case where the magnetization can be approximated to be in a uniform state. Then the natural choice for the collective variables is $X_k = m_k$. In this respect, the equations [1.106−1.109] in a (x, y, z) cartesian frame, becomes the following relations:

$$\boldsymbol{G} = |\Omega|\begin{bmatrix} 0 & -m_z & m_y \\ m_z & 0 & -m_x \\ -m_y & m_x & 0 \end{bmatrix}\,, \tag{1.110}$$

$$\partial_{\boldsymbol{X}} W = |\Omega|\,\partial_{\boldsymbol{m}} g_L = -|\Omega|\,\boldsymbol{h}_{eff}\,, \tag{1.111}$$

$$\boldsymbol{D} = |\Omega|\begin{bmatrix} 1 & 0 & 0 \\ 0 & 1 & 0 \\ 0 & 0 & 1 \end{bmatrix}\,, \tag{1.112}$$

$$\boldsymbol{F}_{st} = |\Omega|\,\beta\,\varepsilon(\boldsymbol{m},\boldsymbol{m}_p)\,\boldsymbol{m}_p \times \boldsymbol{m}\,. \tag{1.113}$$

At this point, if we substitute them in the equation (1.105) we get the following equation:

$$\boldsymbol{m} \times \dot{\boldsymbol{m}} + \alpha\,\dot{\boldsymbol{m}} - \boldsymbol{h}_{eff} + \beta\,\varepsilon\,\boldsymbol{m} \times \boldsymbol{m}_p = \boldsymbol{0}\,, \tag{1.114}$$

which is equivalent to the following:

$$\dot{\boldsymbol{m}} - \alpha\,\boldsymbol{m} \times \dot{\boldsymbol{m}} + \boldsymbol{m} \times \boldsymbol{h}_{eff} - \beta\,\varepsilon\,\boldsymbol{m} \times (\boldsymbol{m} \times \boldsymbol{m}_p) = \boldsymbol{0}\,. \tag{1.115}$$

The so obtained equation is formally equivalent to the equation (1.97), but the difference is in the effective field which is not an integro-differential operator of the magnetization (see eq.(1.69)) anymore. In the next chapter the magnetization dynamics in spatially uniform magnetized nanoparticles is explored for several aspects in a more detailed way. Such analysis is preparatory for the third chapter of this thesis. The main application of collective variables will be presented in chapter 4. there we consider the dynamics of magnetization where the magnetization pattern has the form of a vortex in a point-contact device.

Chapter 2

Nonlinear magnetization dynamics in spatially uniform magnetized nanoparticles

Abstract

This chapter introduces the reader to the analysis of uniformly magnetized ferromagnetic nanoparticles. We start with a brief discussion on the presence of uniform magnetic state in ellipsoidal shaped particles. Then, the study of the magnetic equilibrium states when there are not external excitations is investigated by means the Brown's equations. The effect of the magnetic field on the equilibria is shown for a spheroidal particle: the Stoner and Wohlfarth model is presented. The analysis of the magnetic equilibria is followed by the discussion on the dynamics. An overview on the structural properties of the magnetization dynamics is made in the conservative case and in the nonconservative case. For this last part, we start including first the damping torque and then the spin transfer torque to the conservative dynamical model. The introduction of the damping torque has two main effects in the dynamics. The first one considered is the Liapunov structure of the LLG equation which means that there is an energy function decreasing

along the trajectories. Such dissipative nature of the dynamics produces the division of the magnetization state space in the basins of attraction of the two stable magnetic equilibria. The second one instead, is the time scales separation between the precessional dynamics and the relaxation dynamics. This last effect justifies the use of a perturbative approach based on the Melnikov function. Such analysis is extended when the magnetization dynamics is excited by spin-polarized current. In particular, we show that the Melnikov function is a powerful tool to study the possible self-oscillation regimes and the switching dynamics. The whole analysis is conducted in the framework of the nonlinear dynamics theory for planar system. Several bifurcation mechanisms are introduced and their occurrence and role in the magnetization dynamics qualitatively discussed.

2.1 The uniformly magnetized nanoparticle

The uniformly magnetized nanoparticle represents the key model to understand the complex features of the nonlinear magnetization dynamics in nanosystems. Despite the reduced number of degree of freedom respect to the spatially distributed case, the uniform magnetization dynamics can exhibit several dynamical regimes, such as hysteresis, self-oscillations, switching dynamics, chaos, nonlinear resonance and so on. The study of these regimes is instrumental in the design of memory devices, magnetic nano-oscillators, magnetic-logic circuit , etc. From a physical point of view, it is expected to observe a uniform magnetization in small particle such that the exchange interaction dominates over the magnetostatics, which favours the formation of domains (poles avoidance principle). Such idea has found its mathematical proof in ref. [26], [27]. In addiction, the uniformly magnetized state is a rigorous solution of the LLG equation when the nanoparticle is ellipsoidal shaped and the initial condition is a spatially uniform magnetization distribution. However, in general in that case the stability of the magnetization is not guaranteed. It is expected that the spatially uniform motion is stable against spatially non uniform perturbations for a sufficiently small particle. In an experimental situation the shape of the ferromagnetic

nanoparticles cannot be perfectly controlled due to the fabrication process. For sufficiently small particles the nonuniformities are localized at the edge of the sample and their effect on the uniform motion can be neglected. In these cases, the uniform magnetization approximation is a powerful tool for describing the main dynamical features of the magnetization process.

2.2 Energy and effective field

Let us consider an ellipsoidal ferromagnetic particle, assumed to be uniformly magnetized. The exchange field is zero, while the magnetostatic field is given by the following relation [28]:

$$\boldsymbol{h}_M[\boldsymbol{m}] = -\boldsymbol{\mathcal{N}} \cdot \boldsymbol{m}\,, \tag{2.1}$$

where $\boldsymbol{\mathcal{N}}$ is the demagnetizing tensor. In a cartesian frame where the three directions are along the principal axis of the ellipsoid, we have that $\boldsymbol{\mathcal{N}}$ is a diagonal matrix and that its trace is unitary: $\mathcal{N}_x + \mathcal{N}_y + \mathcal{N}_z = 1$. The cartesian axes are chose such that $\mathcal{N}_x \leq \mathcal{N}_y \leq \mathcal{N}_z$. The quantities $(\mathcal{N}_x, \mathcal{N}_y, \mathcal{N}_z)$ depend only on the ratio of the ellipsoid axes lengths and not on the magnetic property of the medium. Analytical expressions of $(\mathcal{N}_x, \mathcal{N}_y, \mathcal{N}_z)$ are given in reference [28]. Without the exchange contribution and taking into account the equation (2.1), the free energy expressed in the equation (1.90) becomes:

$$g_L(\boldsymbol{m}, \boldsymbol{h}_a) = \frac{1}{2}\,\boldsymbol{m} \cdot \boldsymbol{\mathcal{N}} \cdot \boldsymbol{m} + k_1(1 - (\boldsymbol{m} \cdot \boldsymbol{e}_{AN})^2) - \boldsymbol{h}_a \cdot \boldsymbol{m}\,. \tag{2.2}$$

Introducing the diagonal tensor $\boldsymbol{D} = diag\{D_x, D_y, D_z\}$, where the diagonal elements are expressed by $D_{x_i} = \mathcal{N}_{x_i} - 2k_1(\boldsymbol{e}_{AN} \cdot \boldsymbol{e}_{x_i})$, up to a constant the free energy is given by

$$g_L(\boldsymbol{m}, \boldsymbol{h}_a) = \frac{1}{2}\,\boldsymbol{m} \cdot \boldsymbol{D} \cdot \boldsymbol{m} - \boldsymbol{h}_a \cdot \boldsymbol{m}\,. \tag{2.3}$$

The coefficients (D_x, D_y, D_z) reveal the interplay between the magnetostatic and the anisotropy interactions. In this respect, the magnetostatic effect is

also referred as shape-anisotropy. From the equation (2.3) we obtain the following expression for the effective field:

$$\boldsymbol{h}_{eff} = -\frac{\partial g_L}{\partial \boldsymbol{m}} = -\boldsymbol{D}\cdot\boldsymbol{m} + \boldsymbol{h}_a\,, \tag{2.4}$$

and therefore the Brown equation (1.92) is written as:

$$\boldsymbol{m}\times\boldsymbol{h}_{eff} = \boldsymbol{m}\times(\boldsymbol{h}_a - \boldsymbol{D}\cdot\boldsymbol{m}) = \boldsymbol{0}\,. \tag{2.5}$$

and in the cartesian frame (x, y, z), it takes the following form:

$$\begin{aligned}
&(D_z - Dy)\, m_z m_y - (h_{ay}\, mz - h_{az}\, my) = 0\,,\\
&(D_z - Dx)\, m_z m_x - (h_{az}\, mx - h_{ax}\, mz) = 0\,,\\
&(D_y - Dx)\, m_x m_y - (h_{ax}\, my - h_{ay}\, mx) = 0\,.
\end{aligned} \tag{2.6}$$

In case $\boldsymbol{h}_a = \boldsymbol{0}$, the solutions consistent with the fundamental constraint $\boldsymbol{m}^2 = 1$ are expressed by the following equations:

$$\begin{aligned}
&m_z = m_y = 0,\ m_x = \pm 1\,,\\
&m_x = m_z = 0,\ m_y = \pm 1\,,\\
&m_y = m_x = 0,\ m_z = \pm 1\,.
\end{aligned} \tag{2.7}$$

In fig.2.1 are represented the magnetic equilibria on the unit sphere in the $\boldsymbol{m}$-space expressed by the equations (2.7) and the curves corresponding to a fixed value of g_L in the range $[\frac{D_x}{2}, \frac{D_z}{2}]$ when $\boldsymbol{h}_a = \boldsymbol{0}$. According to the order relation among the coefficients D_{x_i}, these magnetic equilibria can be classified in minima, saddles and maxima of the free energy g_L. In particular, if $D_x \leq D_y \leq D_z$ holds again, we have that $m_x = \pm 1$ are minima, $m_y = \pm 1$ are saddles and $m_z = \pm 1$ are maxima of g_L. Therefore, a stable equilibrium condition is reached when the magnetization is aligned to the x axis. For this reason, x is called easy axis, while y and z are called intermediate and hard axes respectively.

When the external field $\boldsymbol{h}_a \neq \boldsymbol{0}$ the magnetic equlibria change depending on the field strength and direction. In the next section we present an example of that, which reveals the basics of the magnetic recording.

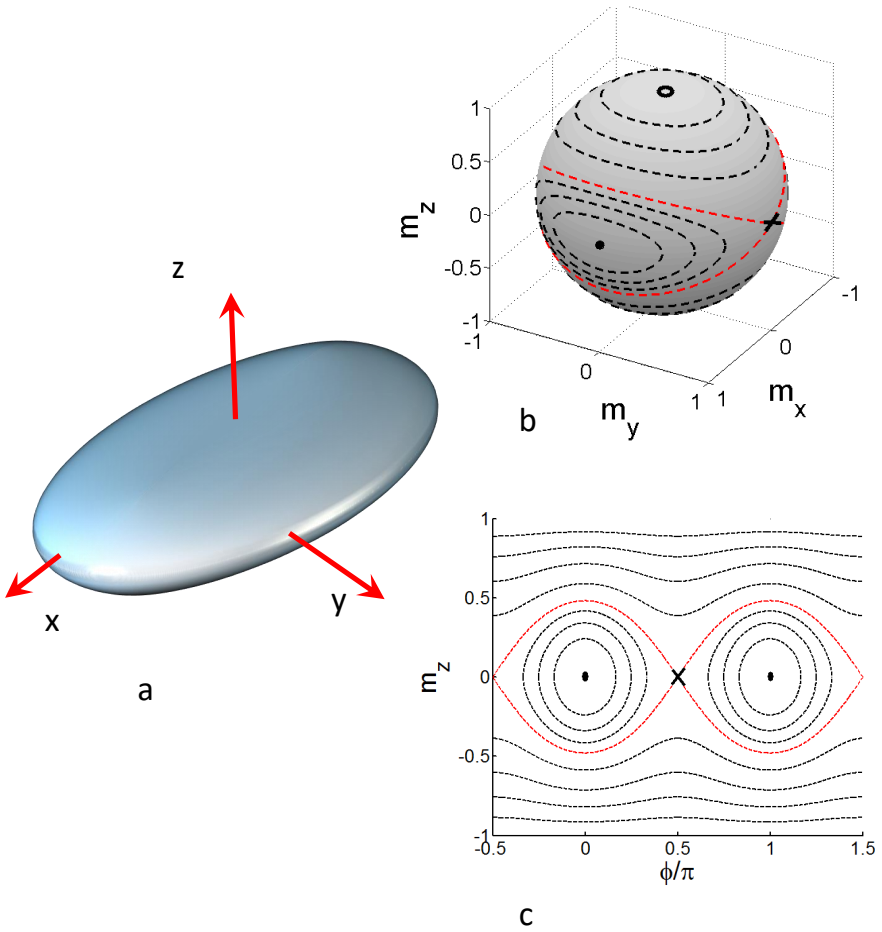

Figure 2.1: (a)Sketch of the ellipsoidal nanoparticle. Representation of the magnetic equilibria on the unit sphere in the $\boldsymbol{m}$-space (b) and in the $(\phi = tg^{-1}\left(\frac{m_y}{m_x}\right), m_z)$ plane (c) in the case $\boldsymbol{h}_a = \boldsymbol{0}$. The dotted lines are the contour curves of g_L.

2.3 Stoner and Wohlfarth model

Let us consider a spheroidal particle, where say z the direction of the rotational symmetry axis such that $D_x = D_y = D_\perp$. In this case, the free energy assumes the following form:

$$\begin{aligned} g_L(\boldsymbol{m}, \boldsymbol{h}_a) &= \frac{D_\perp}{2}\left(m_x^2 + m_y^2\right) + \frac{D_z}{2} m_z^2 - \boldsymbol{h}_a \cdot \boldsymbol{m} \\ &= \frac{D_\perp}{2} + \frac{(D_z - D_\perp)}{2} m_z^2 - \boldsymbol{h}_a \cdot \boldsymbol{m}\,. \end{aligned} \tag{2.8}$$

The relation between the effective field and g_L becomes:

$$\boldsymbol{h}_{eff} = -\frac{\partial g_L}{\partial \boldsymbol{m}} = k_{eff} \boldsymbol{m}_z + \boldsymbol{h}_a\,, \tag{2.9}$$

where the constant $k_{eff} = D_z - D_\perp$. In the following, the constant k_{eff} is assumed to be positive. This means that when $\boldsymbol{h}_a = \boldsymbol{0}$, z is the easy axis where $m_z \pm 1$ are the stable equilibria, while the circumference $m_x^2 + m_y^2 = 1$ represents a set of unstable equilibria. This picture changes when a magnetic field is applied in a certain direction. Let us indicate with θ_h the angle between the applied field direction and the z axis. Moreover, let us consider the case where the applied field has a component in the plane (x, y) aligned to the x axis. When we apply the external field $\boldsymbol{h}_a$, $\boldsymbol{m}$ rotates away from the easy axis, toward the field, by an angle θ depending of the relative strength of the anisotropy and the field. In this way, the angle θ between the magnetization direction and the easy axis (z) is the single degree of freedom for the magnetization direction. In this framework the free energy (2.8) is written as follows:

$$g_L(\theta; h_{a\perp}, h_{az}) = -\frac{k_{eff}}{2}\cos^2\theta - h_{az}\cos\theta - h_{a\perp}\sin\theta\,, \tag{2.10}$$

where $h_{az} = h_a \cos\theta_h$, $h_{a\perp} = h_a \sin\theta_h$. In order to find the magnetic equilibria, we have to solve the Brown equation $\boldsymbol{m} \times \boldsymbol{h}_{eff} = \boldsymbol{0}$, which in this case is written as:

$$\partial_\theta g_L = k_{eff}\sin\theta\cos\theta + h_{az}\sin\theta - h_{a\perp}\cos\theta = 0\,. \tag{2.11}$$

When $h_a = 0$, we find the equilibria defined before, namely $\sin\theta = 0$ corresponding to $m_z = \pm 1$ and $\cos\theta = 0$ corresponding to the circumference $m_x^2 + m_y^2 = 1$. Instead, when $h_a \neq 0$, the position and the stability depend on the direction and the strength of the applied field. According to the idea exposed in the previous section where are stable (unstable) the equilibria that minimize (maximize) the free energy, the critical condition corresponding to the change of stability of an equilibrium state is given by:

$$\partial_\theta^2 g_L = k_{eff}(\cos^2\theta - \sin^2\theta) + h_{az}\cos\theta + h_{a\perp}\sin\theta = 0\,. \tag{2.12}$$

Fixed θ and solving together the equations (2.11) and (2.12) in the variables $(h_{a\perp}, h_{az})$, we find the following parametric representation:

$$\begin{aligned} h_{a\perp} &= k_{eff}\sin^3\theta\,, \\ h_{az} &= -k_{eff}\cos^3\theta\,, \end{aligned} \tag{2.13}$$

where θ represents the direction of the magnetic state of equilibrium which is changing stability due to the external action of the applied field $(h_{a\perp}, h_{az})$. The curve generated by equation (2.13) when θ varies in the interval $(-\pi, \pi)$ is the astroid shown in fig.2.2. By eliminating θ from equation (2.13) we obtain the equation of the astroid in the control plane $(h_{a\perp}, h_{az})$, given by:

$$h_{a\perp}^{2/3} + h_{az}^{2/3} = k_{eff}^{2/3}\,. \tag{2.14}$$

The astroid has different geometrical properties which reveal hysteresis in the magnetization process. For a given θ, equation (3.3) defines a straight line in the plane $(h_{a\perp}, h_{az})$ starting and tangent to the astroid point $(h_{a\perp}(\theta), h_{az}(\theta))$ according to the equations (2.13). Any point $(h_{a\perp}, h_{az})$ on such a line represents a field for which the specific θ is a stable equilibrium state. Let us consider a point $(h_{a\perp,0}, h_{az,0})$ inside the region bounded by the astroid curve. It is possible to show that there are four tangents to the astroid to which the point belongs (see the green dot labeled 'A' in fig.2.2(a)). Moreover, by inspection, one can see that two of them refer to stable magnetization orientations ($\partial_\theta^2 g_L > 0$), while the other two refer to unstable magnetization orientations ($\partial_\theta^2 g_L < 0$). This means that for applied field values corresponding to a points inside the astroid in fig.2.2(a),

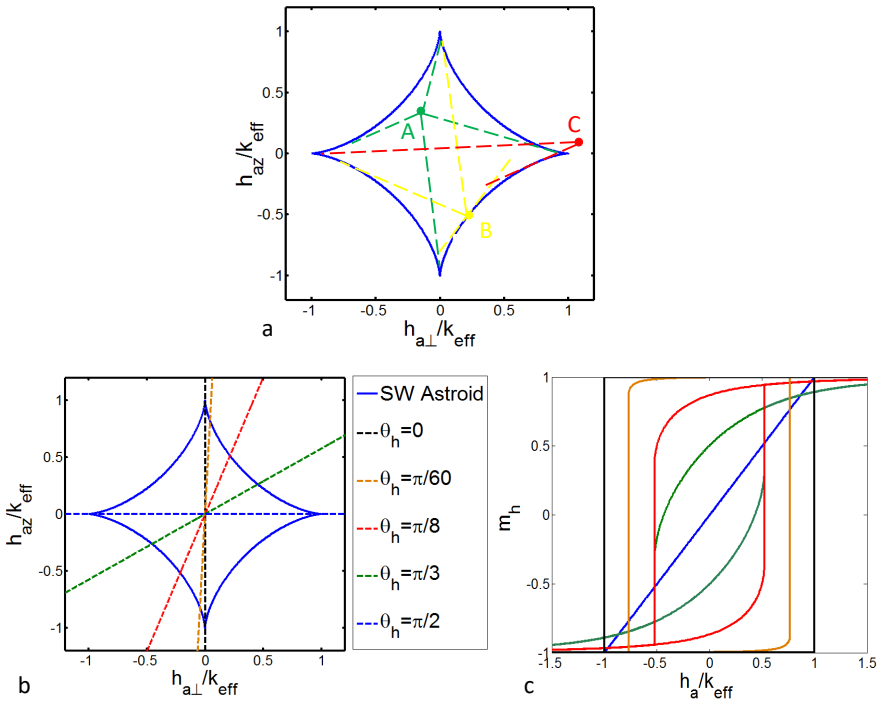

Figure 2.2: (a,b)Stoner and Wohlfarth astroid. (c) Hysteresis loops obtained ramping the field forward and backward along the dotted line with slope equal to tan θ_h in (b).

there are four equilibria: two of them are stable and the remaining two are unstable. When the point $(h_{a\perp,0}, h_{az,0})$ belongs to the astroid curve (see the yellow dot labeled 'B' in fig.2.2(a)), the tangents that intersect each other in it are three: one corresponding to a stable magnetization orientation, one to an unstable one and the third one, which is neither stable nor unstable ($\partial^2_\theta g_L = 0$). Finally the last case, when the point $(h_{a\perp,0}, h_{az,0})$ is outside the astroid curve (see the red dot labeled 'C' in fig.2.2(a)). In this case we have only two tangents, corresponding to a one stable and one unsta-

ble magnetization directions. At this point, if we imagine to ramp up and down the external field quasi-statically along the dotted lines in fig.2.2(b) and plot the magnetization component along the field direction m_h versus the strength of the external field h_a, we obtain the hysteretic curve represented in fig.2.2(c). The color of the hysteresis loop in (c) is connected to the color of the dotted line in (b), which changes according to the orientation of the applied field, indicates with θ_h. The hysteretic transitions of m_h in function of h_a are due to the presence of two stable magnetic states for points $(h_{a\perp}, h_{az})$ inside the astroid. Which one of them is observed, cannot be predicted from the magnetization statics but the equation of the uniform magnetization dynamics has to be added.

2.4 Macrospin dynamics

The uniform magnetization dynamics is also referred coherent spins motion or macrospin dynamics. In fact on 'micromagnetic' spatial scale the magnetic moments move coherently, like a single (macroscopic) spin. The LLG equation can be put in the following form:

$$\dot{\boldsymbol{m}} = \boldsymbol{v}(\boldsymbol{m}, \tau)\,, \tag{2.15}$$

where the vector field:

$$\boldsymbol{v}(\boldsymbol{m}, \tau) = -\boldsymbol{m} \times (\boldsymbol{h}_{eff} + \alpha\, \boldsymbol{m} \times \boldsymbol{h}_{eff} - \beta\, \varepsilon\, \boldsymbol{m} \times \boldsymbol{p})\,. \tag{2.16}$$

The vector field $\boldsymbol{v}$ depends explicitly on the time whenever the applied field $\boldsymbol{h}_a$ or the spin polarized current β are time-dependent.

The fact that the magnetization dynamics preserves the magnitude of $\boldsymbol{m}$ implies that the dynamical system (2.15) evolves on the surface of the unit sphere $|\boldsymbol{m}|^2 = 1$, consistently to the fact that the vector field $\boldsymbol{v}(\boldsymbol{m}; \tau)$ is tangential to this sphere at every point. Remarkably, a number of results concerning the magnetization dynamics derive from the unit sphere topology. We shall discuss the particular case when the dynamics is autonomous, i.e., the vector field $\boldsymbol{v}$ does not explicitly depend on time ($\boldsymbol{v} = \boldsymbol{v}(\boldsymbol{m})$). Autonomous dynamical systems on the unit sphere are characterized by the following properties:

- The number of equilibria is at least two and it is always even. This conclusion is derived from Poincaré index theorem [30], [31], which asserts that the number of nodes, foci and centers minus the number of saddles of any autonomous dynamics on the sphere is equal to two.

- Chaos is precluded, because the phase space is two-dimensional. This is the consequence of the generalized version of the Poincaré-Bendixson theorem [31], [32], which states that on two-dimensional manifolds the only possible steady states are either stationary states associated with equilibria or self-oscillations associated with limit cycles of the dynamics.

In order to go through the details of the magnetization dynamics, let us consider the power balance for the uniformly magnetized nanomagnet, given by the following equation:

$$\dot{g}_L = -\alpha|\boldsymbol{m} \times \boldsymbol{h}_{eff}|^2 + \beta\,\varepsilon\,(\boldsymbol{m} \times \boldsymbol{m}_p) \cdot (\boldsymbol{m} \times \boldsymbol{h}_{eff})\,. \tag{2.17}$$

In case of zero spin polarized current and damping values ($\beta = \alpha = 0$), the free energy is conserved. In fact, from the balance above written, we have:

$$\dot{g}_L = 0 \;\Rightarrow\; g_L(\tau) = g_0\,. \tag{2.18}$$

This means that the magnetization dynamics occurs on the unit sphere at constant free energy. In other words, $g_L(\boldsymbol{m})$ is an integral of motion of the magnetization dynamics and therefore this kind of motion is called conservative. For this reason, it follows that the dotted curves represented in fig.2.1 are the magnetization trajectories when $\boldsymbol{h}_a = \boldsymbol{0}$. According to this fact, the equilibria $m_z = \pm 1$ and $m_x = \pm 1$ are centers of the dynamical system (2.15) and the curves connecting the saddle equilibrium states $m_y = \pm 1$ are called heteroclinic trajectories. Fixed the initial condition $\boldsymbol{m}(t_0) = \boldsymbol{m}_0$ from the solution of the following equation:

$$\dot{\boldsymbol{m}} = \boldsymbol{m} \times \boldsymbol{D} \cdot \boldsymbol{m},, \tag{2.19}$$

it is possible to obtain the time parametrization for the trajectories associated to the free energy value $g_L(\boldsymbol{m}; \boldsymbol{h}_a = \boldsymbol{0}) = g_L(\boldsymbol{m}_0) = \frac{1}{2}\,\boldsymbol{m}_0 \cdot \boldsymbol{D} \cdot \boldsymbol{m}_0$.

In reference [20], [33] the authors solve eq.(2.19) in the general case when $\boldsymbol{h}_a \neq \mathbf{0}$ and it is aligned to one of the principal axes of the ellipsoid. When $\alpha \neq 0$ the magnetization dynamics is no longer conservative. In fact, the power balance is given by the following equation:

$$\dot{g}_L = -\alpha |\boldsymbol{m} \times \boldsymbol{h}_{eff}|^2 < 0\,, \tag{2.20}$$

which shows that the free energy is a decreasing function of time during the magnetization dynamics. Let us continue to consider the case $\boldsymbol{h}_a = \mathbf{0}$. In this scenario, the classification of the equilibria given in case of the conservative dynamics changes. In particular, the energy maxima $m_z = \pm 1$ become unstable equilibrium states, while the energy minima $m_x = \pm 1$ become stable equilibrium states. The saddle equilibria are unaffected by perturbing the dynamics with the dissipations. This fact, is a general result of nonlinear dynamical systems theory and has to do with the concept of structural stability [30], [31]. A center equilibrium is not structurally stable because even a small pertubation changes the qualitative behaviour of the trajectories in the phase portrait around it. This description does not apply to a saddle equilibrium and therefore it is structurally stable. In fig.2.3 it is shown an example of damped magnetization dynamics. The relaxation property of the free energy expressed in equation (2.20) is often referred to Liapunov structure for the LLG equation. As a consequence of that, the state space is naturally divided in 2 kind of regions: low energy and high energy regions. The low energy regions are those ones bounded by the heteroclinic curves and containing the stable equilibria $m_x = \pm 1$. The high energy regions instead are those ones bounded by the heteroclinic curves but containing the unstable equilibria $m_z = \pm 1$. From eq.(2.20) emerges that all the initial conditions in the low energy region containing $m_x = \pm 1$ will relax to it respectively, while for an initial condition in the high energy region which one of the two stable equilibria is reached at the end of the relaxation dynamics, is strongly affects by the initial condition itself. In figure 2.4 we divide the state space in two regions. The black (white) region is composed by all the initial conditions which for $t \to \infty$ relax to $m_x \to +1(-1)$. For this property, it is called basin of attraction of the equilibrium state $m_x = +1(-1)$. It appears also that in the high energy

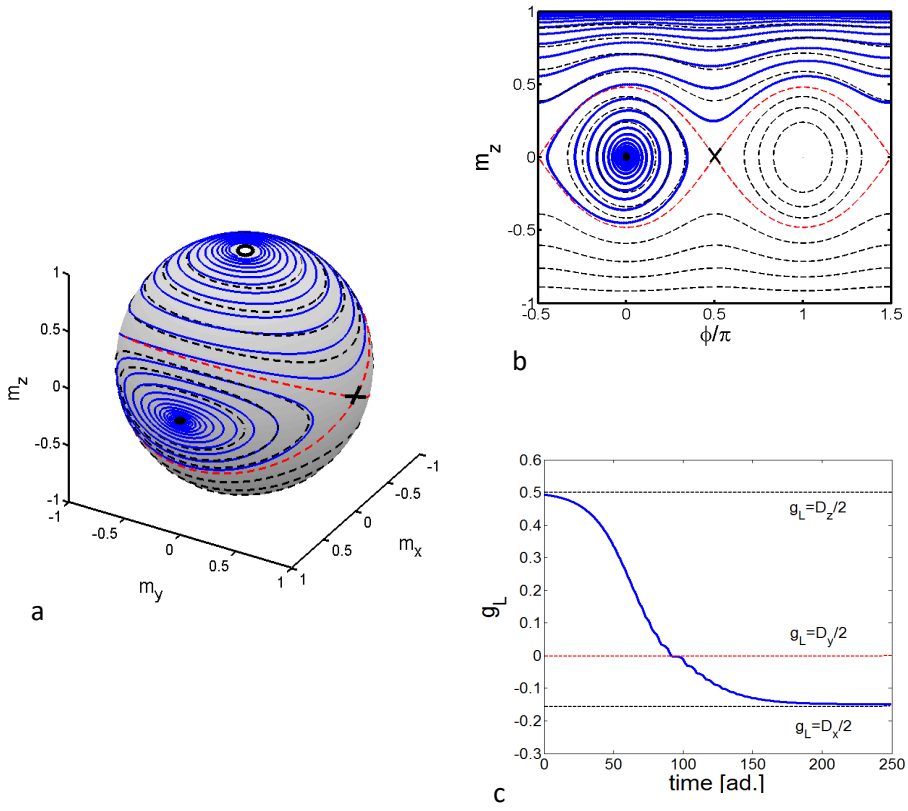

Figure 2.3: Representation of a non-conservative dynamics ($\alpha = 0.03$) on the unit sphere (a) and the in the plane (ϕ, m_z) (b). The blue trajectory is obtained integrating eq.(2.15) with $\beta = 0$, starting from the initial condition $\boldsymbol{m}_0 \equiv (0.1, 0, 0.95)$. (c) Relaxation dynamics of $g_L(\boldsymbol{m}(t))$. With the dotted lines are pointed out the energy value of the unstable and stable equilibria in black and the saddle equilibria in red.

regions the two attraction basins are finely interlaced. This effect is due to the smallness of the damping and is relevant for relaxation dynamics when

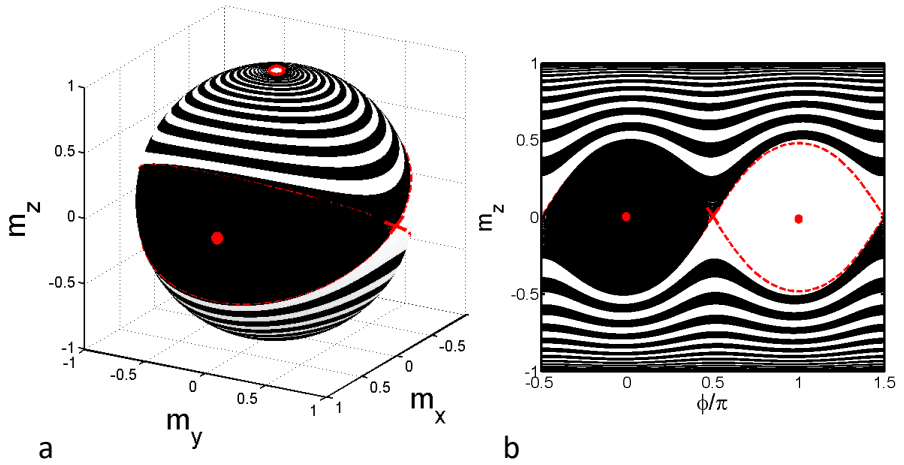

Figure 2.4: Basins of attraction of the two stable equilibria $m_x = \pm 1$ at zero applied field represented on the unit sphere (a) and in the plane (ϕ, m_z) (b).

the initial condition is in the high energy region and is affected by an uncertainty due to its preparation which is reflected on its exact knowledge. This problem has been investigated in the references [34], [35], [36]. Moreover, it has been taken into account for designing novel precessional-switching strategy based on pulse of magnetic field [37] or on pulse of spin-polarized current [38]. An other consequence of the damping smallness is the time scale separation between the precessional and the relaxation dynamics. Let us indicate with $T(g)$ the time period necessary for a complete precession along the conservative trajectory corresponding to $g_L = g$ in the conservative case. In a time interval $\Delta\tau \sim T(g)$, the magnetization dynamics is approximated $\mathcal{O}(\alpha)$ by the consevative one as sketched in fig.2.3(a,b) where the blue line indicating the damped magnetization dynamics for a single precession (single turn) is very close to a black-dotted line representing a conservative trajectory.

Starting from this consideration, we can write the energy balance during

the time-interval $[0, T(g)]$ as follows:

$$\Delta g_L = -\alpha \int_{T(g)} |\boldsymbol{m} \times \boldsymbol{h}_{eff}|^2 \, d\tau = -\alpha \, M(g) + \mathcal{O}(\alpha^2) \, . \tag{2.21}$$

The quantity $M(g)$ is called Melnikov function and is expressed by the following equation:

$$M(g) = \int_{T(g)} |\boldsymbol{m}_c \times \boldsymbol{h}_{eff}(\boldsymbol{m}_c)|^2 \, d\tau \, , \tag{2.22}$$

where $\boldsymbol{m}_c(\tau) = \boldsymbol{m}(g_L(\tau) = g)$is the conservative dynamics associated to the free energy value $g_L = g$. If we neglect $\mathcal{O}(\alpha^2)$ terms in eq.(2.21), the condition $\Delta g_L = 0$ corresponds to a vanishing Melnikov fucntion: $M(g) = 0$. For a pure relaxation dynamics ($\alpha \neq 0, \beta = 0$) this condition cannot occur since $M(g) > 0$ (see eq.(2.22)) . However in case of excitation by spin-polarized current, since $\beta \sim \alpha$ the time scale separation holds again and therefore we have the following energy balance:

$$\Delta g_L \approx -\alpha \, M(g) = -\alpha \left(M_\alpha - \frac{\beta}{\alpha} M_\beta \right) \, , \tag{2.23}$$

where the two Melnikov functions M_α and M_β are given by:

$$\begin{aligned} M_\alpha &= \int_{T(g)} |\boldsymbol{m}_c \times \boldsymbol{h}_{eff,c}|^2 \, d\tau \, , \\ M_\beta &= \int_{T(g)} \varepsilon(\boldsymbol{m}_c, \boldsymbol{p}) (\boldsymbol{m} \times \boldsymbol{p}) \cdot (\boldsymbol{m}_c \times \boldsymbol{h}_{eff,c}) \, d\tau \, . \end{aligned} \tag{2.24}$$

In this case, for $M_\beta \neq 0$ fixed $g_L = g$, there exists a spin-polarized current value such that

$$\Delta g_L(g) = 0 \; \Rightarrow \; \beta(g) = \alpha \, \frac{M_\alpha(g)}{M_\beta(g)} \, . \tag{2.25}$$

This means that there is a magnetization trajectory $\boldsymbol{m}(t) = \boldsymbol{m}_c(t; g) + \mathcal{O}(\alpha)$ where the magnetization precession is continuously sustained due to the spin-transfer-torque mechanism.

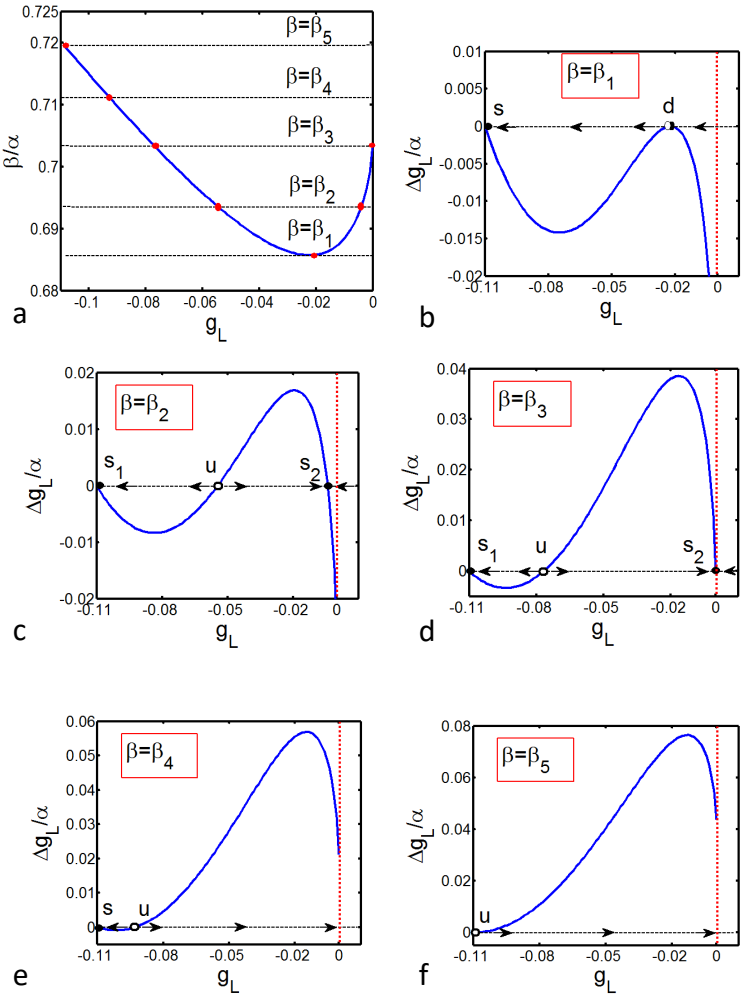

Figure 2.5: (a) Spin-polarized current which vanishes the Melnikov function according to eq.(2.25). (b-f) Representation of the free energy variation due to a single precession on the conservative trajectory corresponding to the free energy value g_L (abscissa), for 5 current values $\beta_{1\to5}$. The symbols in each figure indicate a free energy value where $\Delta g_L = 0$. The black arrows show the energy dynamics for non stationary free energy values $\Delta g_L \neq 0$. According to this, the labelling 's,d,u' indicate a stable, saddle and unstable stationary free energy value respectively. The vertical red-dotted line corresponds to $g_L = D_y/2$. Nanomagnet parameters: $D_x = -0.22$, $D_y = 0$, $D_z = 1$

For example, let's consider the case where the polarizer is oriented along the easy axis $\boldsymbol{p} = \boldsymbol{e}_x$ and that $\varepsilon(\boldsymbol{m}_c) = 1$. Varying g_L in $[D_x/2, D_y/2]$, according to eq.(2.25), we obtain the fig.2.5(a). Let us imagine to increase the current starting from $\beta < \beta_1$:

- $0 \leq \beta < \beta_1$: there is only a stationary stable free energy state $g_L(s) = Dx/2$ corresponding $m_x = \pm 1$.

- $\beta = \beta_1$: It appears a self-oscillations trajectory (limit cycle), corresponding to the free energy value $g_L(d) < D_y/2$. This regime is stable (unstable) for perturbations $\delta g_L = g_L - g_L(d) > 0$ ($\delta g_L < 0$). The mechanism of formation of a such dynamics corresponds to a saddle-node bifurcation of limit cycles in the $\boldsymbol{m}$-space. In fact a further small increasing of β splits it in two limit cycles: one stable and the other one unstable. In the plane $(g_L, \Delta g_L)$ a parallel 1-dimensional bifurcation analysis can be done. In particular, the saddle node bifurcation of limit cycle corresponds to a transcritical bifurcation [31].

- $\beta = \beta_2$: there are two self-oscillations regimes, a stable one corresponding to the free energy value $g_L = g_L(s_2)$ and an unstable one corresponding to $g_L = g_L(u)$ (see fig.2.6).

- $\beta = \beta_3$: $g_L(s_2) = D_y/2$. The two saddle equilibria $m_y = \pm 1$ are connected by a closed trajectory approximately $\mathcal{O}(\alpha)$ described by $\boldsymbol{m}_c(\tau; g_L(s_2))$ and therefore the self-oscillations cannot occur anymore. This event attests the occurring of the so called heteroclinic-connection bifurcation in the $\boldsymbol{m}$-space [30], [31].

- $\beta = \beta_4$: all the initial conditions with free energy value $g_L < g_L(u)$ relax to $m_x = 1$, while all those with $g_L > g_L(u)$ go to $m_x = -1$ and then switch stable magnetic equilibrium state (see fig.2.7).

- $\beta = \beta_5$: the unstable limit cycle 'u' contracts on the stable equilibrium $m_x = 1$ and disappears, making it unstable. This fact corresponds to an Hopf-subcritical bifurcation in the $\boldsymbol{m}$-space [30], [31] and in the plane $(g_L, \Delta g_L)$ to a transcritical bifurcation. Therefore, it follows

that the current value β_5 is the switching current for the initial condition $m_x = 1$ (see fig.2.8).

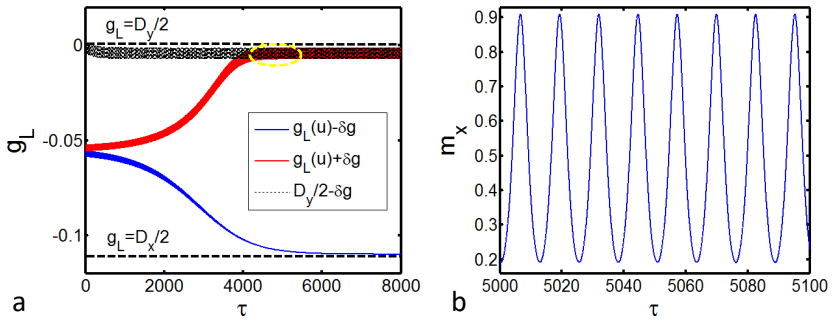

Figure 2.6: (a) Energy dynamics when $\beta = \beta_2$ starting from three different initial conditions, represented with the colored legend. (b) Self-oscillation dynamics of the magnetization (x-component), corresponding to the energy dynamics pointed out by the yellow circle.

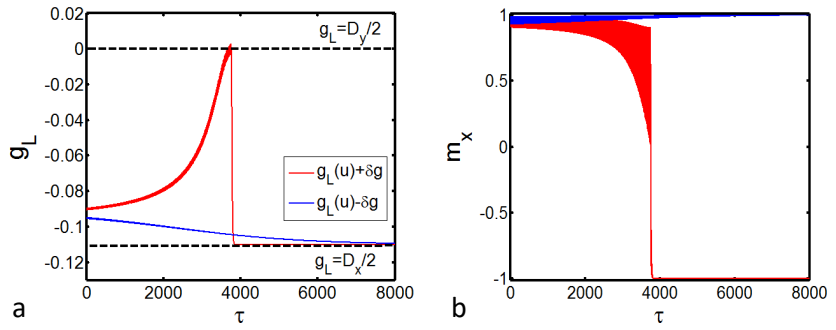

Figure 2.7: (a) Energy dynamics when $\beta = \beta_4$, starting from the two different initial conditions represented in the colored legend. (b) Magnetization dynamics (x-component), according to the energy color legend.

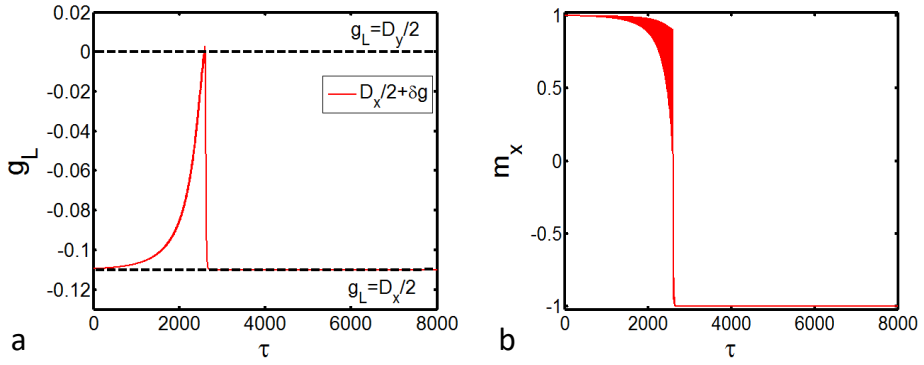

Figure 2.8: (a) Energy dynamics when $\beta = \beta_5$, starting from $m_x = 1$. (b) Switching dynamics of the magnetization (x-component), corresponding to the energy dynamics represented in (a).

Just for sake of completeness, we remark that changing the nanomagnet parameters D_x, D_y and D_z, change also the order and the occurence of certain bifurcation mechanisms respect to the scenario depicted in fig.2.5.

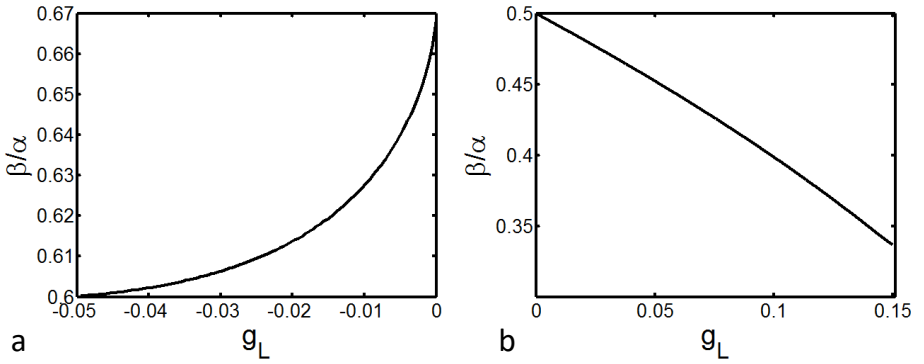

Figure 2.9: Spin-polarized current value which vanishes the Melnikov function according to eq.(2.25) for the folling two set of parameters: (a) $D_x = -0.1$, $D_y = 0$, $D_z = 1$; (b) $D_x = 0$, $D_y = 0.3$, $D_z = 0.7$.

For example in the figure 2.9 are shown two different cases where the saddle-node bifurcation of limit cycle does not occur. In fact, increasing the current starting from a zero value, just two of them occur: Hopf and heteroclinic-connection bifurcation. It is possible to show by using the same energetic analysis used above that the occurrence order is opposite and that there is not coexistence between a stable magnetic equilibria and a stable self-oscillation regime. In conclusion, we want to stress that the bifurcational analysis joint to the Melnikov theory are powerful tools to reveal the main features of the nonlinear magnetization dynamics excited by stationary spin-polarized current. In this part of the thesis the quantitative aspects have left room for the qualitative discussion sustained by numerical simulations. In the next chapter it is shown that a such approach allows a quantitative description of the several dynamical regimes.

Chapter 3

Influence of Second Order Anisotropy in STT-MTJ Nanodevices

3.1 Introduction

The magnetic tunnel junctions from a technological point of view, characterized by a large tunnel magnetoresistance (TMR), are very promising devices to drive new routes for the design of spin-transfer-torque magnetic random access memories (STT-MRAMs) [39], [40], [41], microwave oscillators [42], [43], and detectors [44], [45]. In particular, the discovery of the interfacial perpendicular anisotropy (IPA) in Fe-rich CoFeB-MgO magnetic tunnel junctions (MTJs) has been fundamental for the design of perpendicular MTJs [46], [47], [48]. In details, by controlling the thicknesses of both free and polarizer ferromagnets, the IPA can be engineered (i) to have an out-of-plane easy axis in both ferromagnets, (ii) to reduce the out-of-plane demagnetizing field while maintaining the orientation of both magnetizations in the plane, (iii) to have an in-plane the polarizer and a tilted or out-of-plane free layer magnetization. For storage applications where both ferromagnets are perpendicular, the IPA improved the dynamical propri-

eties of STT-MRAMs in terms of reduction of the switching current density, energy dissipation and writing speed [47], [49]. At this stage of the research, those devices seem that can be a valid alternative to the CMOS technology for moving storage beyond the Moore's law [50]. For microwave emissions, superior performances, such as low critical current density below than $10^6 A/cm^2$ and large output power approaching μW have been observed [51], [52], [53], [54], [55], [56]. Finally, detection sensitivities exceeding the one of Schottky diodes have also been observed [44], [45]. The transition from out-of-plane to in-plane easy axis occurs at a critical value of the thickness [46]. Most of the experimental and theoretical works have studied the effect of the IPA far from that value. However, near the critical thickness, the effective anisotropy field, including IPA and demagnetizing field, tends to be zero and the effect of the second order uniaxial perpendicular anisotropy becomes dominant, even though its anisotropy constant is one order of magnitude lower ($< 10^5 J/m^3$). The aim of the present chapter is to show, within a micromagnetic framework, the effect of the second order anisotropy in the dynamical proprieties of STT-MRAMs and microwave oscillators designed to have the free layer thickness near the critical size defined above, characterized by reduced effective out-of-plane anisotropy . For the STT-MRAM, the polarizer is considered out-of-plane, while for the microwave oscillators it is in-plane. Such a choice permits in fact to detect the magnetization state and dynamics due to the TMR effect for the respective cases of interest.

3.2 Device and modelling

The MTJ under investigation has a circular cross section with a diameter $D = 100\,nm.$ and a thickness of $t = 1.4\,nm$ [47]. The physical parameters are: $M_s = 950\,kA/m$, exchange constant $A = 20\,pJ/m$, $\alpha = 0.03$ [55], spin-torque efficiency $\eta = 0.66$ [57]. In the simulations, we considered first order perpendicular anisotropy constant $k_1 \geq 0.56 MJ/m^3$. The value $k_1 = 0.56 MJ/m^3$ has been computed by means of static micromagnetic simulations in order that at the thickness value considered the free layer

easy axis starts to be out-of-plane. The micromagnetic computations [58] are based on the numerical solution of the Landau-Lifshitz-Gilbert equation with the spin transfer torque efficiency for MTJ device [18], [19]:

$$\begin{aligned} b(\boldsymbol{m}\cdot\boldsymbol{m}_p) &= \frac{2\eta}{1+\eta^2\boldsymbol{m}\cdot\boldsymbol{m}_p}\,, \\ \beta &= \frac{g\,\mu_B}{e\gamma_0\,M_s^2\,L}\,J_{MTJ} = \frac{J_{MTJ}}{J_{0,MTJ}}\,, \end{aligned} \tag{3.1}$$

where the coefficient η indicates the spin polarization factor. In the following we introduce a cylindrical coordinates system with the z-axis oriented along the out-of-plane direction and the polar angle ϕ lying in the film-plane. The analytical theory developed is based on the assumption of uniform magnetization dynamics in the free layer of the MTJ device considered.

3.3 Analytical stability diagram

We start focusing our attention on the study of magnetization equilibria and how the uniaxial second order anysotropy effect affects their directions and stabilities when the system is not excited by external source. Therefore, the free energy and the effective field are given by the following relations [6]:

$$\begin{aligned} g_L(\boldsymbol{m}) &= \frac{1}{\mu_0 M_s^2}\left[k_{1eff}(1-m_z^2)+k_2(1-m_z^2)^2\right]\,, \\ \boldsymbol{h}_{eff} &= -\partial_{m_z} g_L\,\boldsymbol{e}_z = \frac{1}{\mu_0 M_s^2}\left[2k_{1eff}m_z + 4k_2 m_z(1-m_z^2)\right]\,\boldsymbol{e}_z, \end{aligned} \tag{3.2}$$

where $g_L(\boldsymbol{m})$ is the normalized magnetic energy with $k_{1eff} = k1 - 0.5\mu_0 M_s^2(D_z - D_p)$ the effective first order anisotropy constant, with k_1 the IPA first order anisotropy constant, $(D_z - D_p)$ the difference between the demagnetizing factors for the out of plane (z) and the in-plane (x, y) directions respectively, and k_2 is the second order anisotropy constant. First of all, we evaluate the equilibrium points when no external excitation are present. In that case the Brown equation (1.70) expressed in cylindrical

coordinates reads as:

$$\begin{aligned} &\partial_{m_z} g_L = 0\,, \\ &m_z = \pm 1\,. \end{aligned} \tag{3.3}$$

According to the thermostatic minimization principle (see the chapter 1), the stability of the equilibrium state is guaranteed if it is a minimum of the free energy. In this respect, for the equilibria defined by the first one of the eq. (3.3), are stable if:

$$\partial^2_{m_z} g_L \geq 0\,, \tag{3.4}$$

while for those ones defined by the 2nd one, it requires the following condition:

$$\begin{aligned} &m_z = +1 \Rightarrow \partial_{m_z} g_L \geq 0\,, \\ &m_z = -1 \Rightarrow \partial_{m_z} g_L \leq 0\,. \end{aligned} \tag{3.5}$$

We notice that that, both the existence and the stability depend on the m_z coordinate of the magnetic state. From Eqs(3.3), we obtain the fig.3.1, where the phase diagram of the magnetization equilibrium states as a function of the coefficients k_{1eff} and k_2 is displayed. Four stability regions are observed: i) Easy Axis region (EA, red color); ii) Easy Cone region (EC, green color); iii) Easy Plane region (EP, blue color); iv) Easy Axis-Plane region (EAP, yellow color). Each region is separated by the other ones via solid black lines where the couple (k_{1eff}, k_2) indicate the threshold values for a change of number and type of equilibria (bifurcation lines). i) EA. It is characterized by two equilibrium points for $m_z = \pm 1$, which means two out-of-plane equilibrium axes, and one circumference of unstable equilibrium points for $m_z = 0$, namely the in-plane state is not stable. This region is obtained for of $k_{1eff} \geq 0$ and for values of $k_2 \geq -k_{1eff}/2$. ii) EC. It includes two circumferences of stable equilibrium points for $m_z = \pm\sqrt{1 + \frac{k_{1eff}}{2k_2}}$ two unstable equilibrium points for $m_z = \pm 1$ and one circumference of unstable equilibrium points for $m_z = 0$, which means that neither in-plane nor out-of-plane states are stable. This region is achieved for $k_{1eff} \leq 0$ and for values of $k_2 \geq -k_{1eff}/2$.

iii) EP. Differently from EA, here the stable equilibrium points belong to the circumference for $m_z = 0$, whereas the points $m_z = \pm 1$ are unsta-

ble equilibria. This region is reached when $k_{1eff} \leq 0$ and for values of $k2 \leq -k_{1eff}/2$.. iv) EAP. The stable equilibrium states include both the out-of-plane $m_z = \pm 1$ and the in-plane $m_z = 0$ configuration, while the unstable equilibrium points are attained for $m_z = \pm\sqrt{1 + \frac{k_{1eff}}{2k_2}}$. This region is obtained for positive values of k_{1eff} and when k_2 is lower than $-k_{1eff}/2$. In the rest of the paper, we study the EA region where k_{1eff} and k_2 have both positive values .

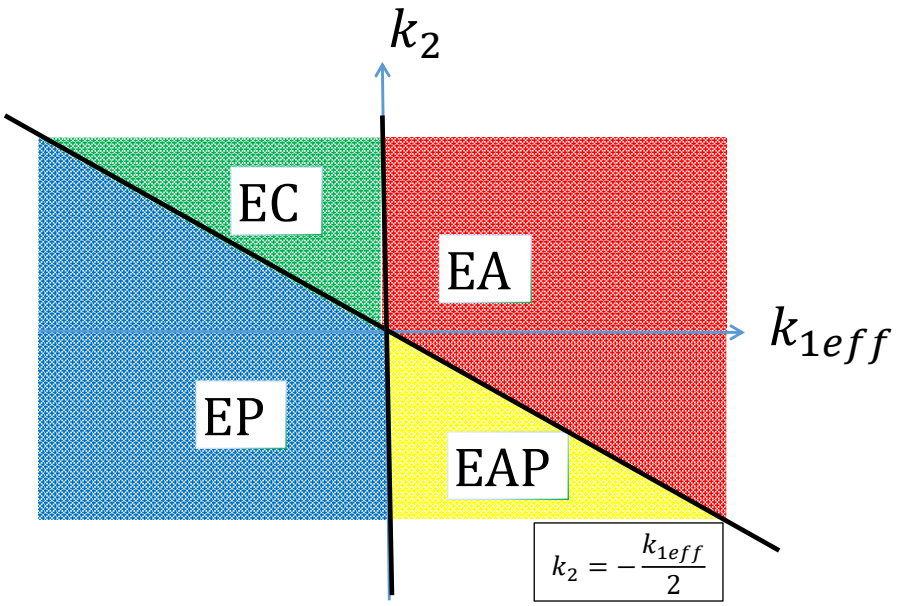

Figure 3.1: Stability diagram of the magnetization states as a function of k_{1eff} and k_2. Four regions can be identified: EA region (red color), EC region (green color), (EP) region, blue color), and EA-plane region (EAP) (yellow color). Black solid lines: bifurcation lines.

3.4 Switching Dynamics

Calculation of switching current when k_{1eff}, k_2 have both positive values, are crucial in the design of MTJ devices working as solid state magnetic memory. Then in this context, we have to study how the second order anysotropy effect influences the switching current. Let us consider the polarizer oriented along the symmetry axis of the particle, namely the z direction. In this framework, it is convenient to write the LLGS equation (1.115) in cylindrical coordinates:

$$\begin{aligned} (1+\alpha^2)\,\dot{m}_z &= -\alpha(1-m_z^2)\partial_{m_z} g_L - \beta\,\varepsilon(m_z)(1-m_z^2)\,, \\ (1+\alpha^2)\,\sqrt{1-m_z^2}\,\dot{\phi} &= -\sqrt{1-m_z^2}\,\partial_{m_z} g_L\,. \end{aligned} \tag{3.6}$$

In absence of dissipation ($\alpha = 0$) and external excitation ($h_a = 0, \beta = 0$) the magnetization equilibria are those ones descripted about the region EA of the stability diagram in fig.3.1. We have to note that the introduction of the current does not affect the equilibria $m_z = \pm 1$, and that the polarizer direction does not affect the cylindrical symmetry of the system. The current indeed changes the stability of the equilibria. At zero current the stability region of the equilibrium $m_z = +1(-1)$ is given by the magnetic states which have m_z positive (negative). These two stability regions also called basin of attraction of the two equilibria are separated by the circumference $m_x^2 + m_y^2 = 1$, constituted by a set of unstable equilibria. When a current is injected, this picture changes and in particular the basins of attraction are separated by an unstable limit cycle [20], namely an unstable self-oscillations trajectory, defined by the following equations:

$$\begin{aligned} &\dot{m}_z = 0\,, \;\; m_z \neq \pm 1\,, \\ &\dot{\phi} = -\frac{1}{(1+\alpha^2)}\partial_{m_z} g_L\,, \end{aligned} \tag{3.7}$$

where the last equality indicates the angular frequency of the magnetization precessions. The dynamical systems (3.7) defining the self oscillation trajectory of the magnetization dynamics is exactly the one in the conservative case. For this reason the self-oscillation trajectory at a fixed m_z^u is

the conservative trajectory corresponding to $g_L = g_L(m_z^u)$.
At this point, let us imagine the magnetic state to be in the equilibrium $m_z = +1$ and to increase the spin polarized current starting from the zero value ($\beta > 0$). Two are the possibles scenarios for the switching dynamics. The first one, where increasing the current the unstable limit cycle reaches the equilibrium $m_z = +1$. A so called Hopf bifurcation occurs and the limit cycle disappears on the equilibrium changing its stability. At this point the equilibrium $m_z = +1$ is unstable and a small kick to the magnetization causes the dynamics to occur and lead the magnetization to the only stable state of equilibrium $m_z = -1$. From this follows that the switching current is the one at which this bifurcation mechanism occurs. In the second scenario instead, increasing the current the unstable limit cycle moves toward $m_z = +1$ too, but for a certain current value an other Hopf bifurcation occurs in the equilibrium state $m_z = +1$, generating a stable limit cycle before the unstable limit cycle reach the equilibrium itself. The appearance of the stable limit cycle produces the change of stability of the equilibrium $m_z = +1$, which becomes unstable. In this respect, if the magnetization is in $m_z = +1$ and we kick it, the dynamics will lead the magnetization to oscillate along the stable self-oscillation trajectory. Therefore the MTJ device for such current value behaves like an oscillator. A further increment of the current makes the two limit cycles meet and annihilate each other. That process is the so called bifurcation mechanism saddle-node of limit cycles. After that we have that $m_z = +1$ is unstable and there are not stable attractors like limit cycles between the two equilibria. Therefore the switching dynamics can occur. Then, the threshold switching current in this scenario is the value at which the saddle-node bifurcation of the limit cycle occurs. Which one of the two scenario occurs, depends on k_{1eff} and k_2. A general criteria to find the switching current in both cases can be stated. In fact, the condition to be satisfied is:

$$\dot{m_z} > 0 \ , \ \forall \ m_z \neq \pm 1 \ \Rightarrow \beta \geq \max_{m_z} \left[\frac{\alpha \, \partial_{m_z} g_L}{\varepsilon(m_z)} \right] , \tag{3.8}$$

where the threshold switching current is obtained considering the equality sign. Let us call m_z^* the z-component of the magnetization which maximizes

the right hand side of (3.8). Then, by substituting it in eq. (3.9), we obtain the following expression for the switching current density:

$$J_{MTJ} = \frac{e\,\gamma_0\,M_s^2\,L}{g\,|\mu_B|}\left[\frac{\alpha\,m_z^*\left[k_{1eff}+2k_2\left(1-m_z^{*2}\right)\right]}{\varepsilon(m_z^*)}\right], \tag{3.9}$$

which is represented in comparison with micromagnetic simulations in fig.3.2 for several values of the second order anisotropy constant k_2. The demagnetizing factors that affect the value of k_{1eff} are evaluated in the non-ellipsoidal geometry hypothesis. In fact, once found m_z^* for every value of k_2, an inaccurate estimate of the demagnetizing factors produces an offset in the estimation of the switching current, that is exactly compensated if the analytical expressions obtained in ref. [59] in the case of a thin circular disk. In detail, we performed micromagnetic simulations of the switching current density as a function of k_2 in the range $(0, 4.0\times10^4 J/m^3)$ for three values of $k_1 0.56 MJ/m^3$, $0.58 MJ/m^3$, and $0.60 MJ/m^3$. In this way, a partial compensation of the first order anisotropy field due to the demagnetizing field is reached. The results are illustrated in fig.3.2, together with a comparison with the analytical computations obtained by solving equation (3.9). The switching current density is higher either when k_2 is increased for a given value of k_1 or when k_1 is increased while keeping k_2 constant, because of the out-of-plane easy axis of the magnetization. The analytical calculations based on the macrospin theory shows quantitative agreement with the numerical micromagnetic results. This confirms the foundation of our starting hypothesis.

3.5 Self-Oscillation Dynamics

In this section, we study the possibility to maintain self-oscillations [60], [61], [62], [63], [64], [65] of the magnetic state when a dc spin polarized current is applied. Here the polarizer has an in-plane direction needed to have a magnetoresistive signal from the magnetization precession. This different polarizer direction breaks the cylindrical symmetry. The possibility to obtain self-oscillations can be investigated by deriving the equation for the

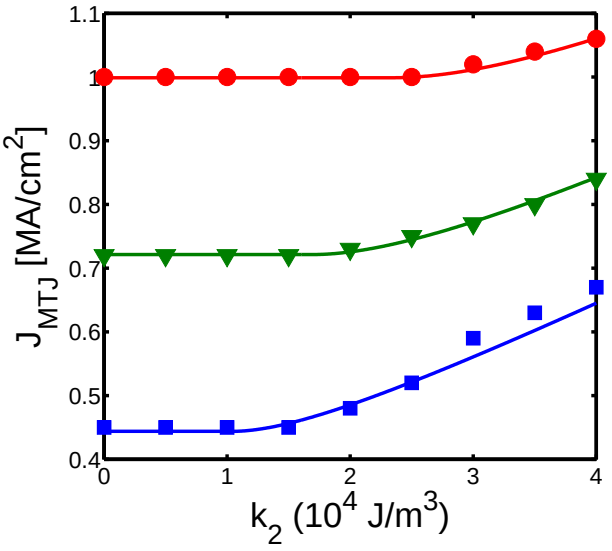

Figure 3.2: Switching current density as a function of the second-order perpendicular anisotropy constant k_2 for three values of the first-order perpendicular anisotropy constant k_1. Solid lines: analytical results. Symbols: micromagnetic results. Symbol shape and colors are linked to the values of k_1: blue $k_1 = 0.56MJ/m^3$, green $k_1 = 0.58MJ/m^3$ and red $k_1 = 0.60MJ/m^3$.

time evolution of the free energy. From eqs.(1.88) considering the polarizer aligned along the x-axis, we have :

$$\begin{aligned}(1+\alpha^2)\dot{g}_L = &-\alpha\left(\partial_{m_z} g_L\right)^2\left(1-m_z^2\right)+\\ &+\beta\,\varepsilon(m_z,m_x)\,\partial_{m_z} g_L\left(m_z\sqrt{1-m_z^2}\,\cos\phi\right)\,.\end{aligned} \tag{3.10}$$

When a self-oscillation occurs, we have that the total energy lost along the closed trajectory described by the magnetization precession (limit cycle or self-oscillation trajectory) is zero. This condition can be expressed as in

the following:

$$\Delta g_L = g_L(t_0 + T) - g_L(t_0) = \int_{t_0}^{t_0+T} \dot{g}_L \, d\tau = 0 \,, \tag{3.11}$$

where T is the time period for a complete and single magnetization precession. Substituting the (3.10) in the latter equation we obtain the energy balance between the dissipated energy due to the damping effects and the energy supplied by the external excitation, namely the spin transfer torque. The current value that satisfies this energy balance corresponds to the critical current that stabilizes the self-oscillation dynamics. Since $\beta \sim \alpha \ll 1$ the critical current producing self-oscillations of the magnetization can be estimated with the perturbative technique discussed in the chapter 2, called the Melnikov function theory. The Melnikov function can be calculated starting from the equation (3.11), where the expression of $\dot{g}_L$ is given by the equation (3.10) and the time dependence $\phi(\tau), m_z(\tau)$ are taken according to the unperturbed (conservative) dynamics (3.7), namely:

$$M(g) = \int_0^{2\pi} \left[\partial_{m_z} g_L \left(1 - m_z^2\right) - \frac{\beta}{\alpha} \, \varepsilon(m_z, m_x) \, m_z \sqrt{1 - m_z^2} \cos\phi \right] d\phi \,, \tag{3.12}$$

where $M(g)$ indicates the Melnikov function associated to the conservative trajectory of constant free energy $g = g_L(m_z)$. From the Melnikov function theory, we obtain an approximation $\mathcal{O}(\alpha^2)$ of the energy losses along the conservative trajectory, namely $\Delta g_L = -\alpha \, M(g) + \mathcal{O}(\alpha^2)$. Therefore, at the same approximation order, the condition (3.11) reduces to:

$$M(g) = M(m_z) = 0 \,. \tag{3.13}$$

The closed form expression for $M(m_z)$ is given by the following expression:

$$M(m_z) = -2\pi \partial_{m_z} g_L \, \left(1 - m_z^2\right) + \beta \frac{4\pi \, m_z}{\alpha\eta} \left[\frac{\sqrt{1 - \eta^4 \left(1 - m_z^2\right)} - 1}{\sqrt{1 - \eta^4 \left(1 - m_z^2\right)}} \right] , \tag{3.14}$$

which substituted into the equation (3.13) permits to obtain the expression of the critical current density which sustains the self-oscillations, expressed by the relation

$$J_{MTJ} = \frac{e\,\gamma_0\,L}{g\,|\mu_B|\mu_0}\left[\frac{\alpha\,\eta\,\left(1-m_z^2\right)\left(k_{1eff}+2k_2\left(1-m_z^2\right)\right)\sqrt{1-\eta^4\left(1-m_z^2\right)}}{\left(1-\sqrt{1-\eta^4\left(1-m_z^2\right)}\right)}\right]. \tag{3.15}$$

Since for the conservative dynamics it exists a one-to-one correspondence between m_z and the angular frequency of the magnetization precession $\omega(m_z)$, this relation can be read as $J_{MTJ} = J_{MTJ}(\omega(m_z); k_{1eff}, k_2)$. The Melnikov theory permits also to evaluate the stability of the self-oscillation regime under a perturbation of the free energy. This can be done by looking at the slope of the Melnikov function for the free energy value corresponding to the self-oscillations [20], [30], [31]. Positive slope means stable self-oscillations whereas negative slope indicates unstable self-oscillations. By applying this technique to our case, we found that the magnetization self-oscillations are always stable for each value of the current that produces them. In Fig.3.3, the self-oscillations predicted by the Melnikov theory versus the micromagnetic simulations are compared. The Melnikov theory reproduces quantitatively the relation between current and frequency in the range of current values in which the self-oscillation regimes are observed by the micromagnetic simulations. Outside this range, the theoretical predictions are not sustained by the numerical confirmation. This feature is due to the fact that the Melnikov theory does not take into account the bifurcation mechanisms induced by the asymmetry of the system enhanced by spin transfer torque interaction at larger currents.

The disappearance of stable magnetization self-oscillations can be explained by reconstructing the whole sequence of bifurcations occurring when the current is increased. When a spin-polarized current with polarizer along the x-axis is applied, the cylindrical symmetry of the system is broken. This produces a saddle-node bifurcation which creates a saddle equilibrium in $m_x = -1$, and an unstable equilibrium in $m_x = +1$. By increasing the current, the saddle $m_x = -1$ pass through an other saddle node bifurcation

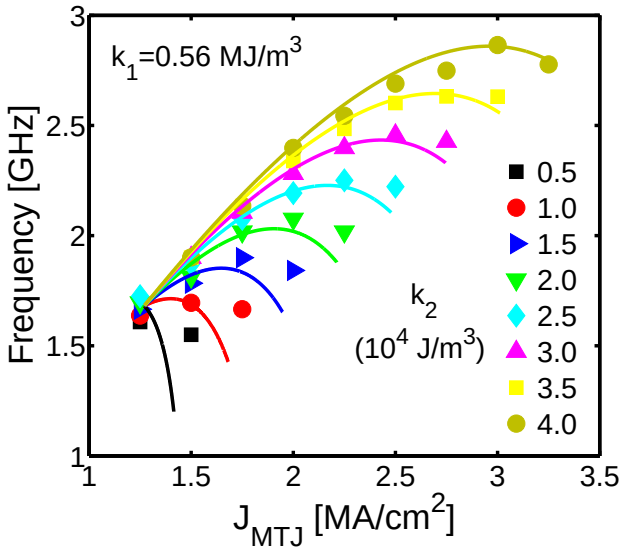

Figure 3.3: Self-oscillation frequency as a function of the current density, for eight values of the second-order perpendicular anisotropy constant k_2, when k_1 is fixed to $0.56 MJ/m^3$. Solid lines: analytical results. Symbols: micromagnetic results. Symbol shape and color are linked to the values of k_2, as indicated in the figure. In order to obtain a better fit of (3.15) with micromagnetic simulations, we considered $M_s = 950.3 kA/m$, namely, a variation of 0.32%.

which changes its stability making it stable and creating other two saddle equilibria. This argument can be easily proved by applying the perturbation theory to eq.(1.87). In order to do that, first of all we write down the dynamical equations in cylindrical coordinates when the polarizer is oriented along the x-axis :

$$\begin{aligned} (1+\alpha^2)\,\dot{m}_z &= -\alpha(1-m_z^2)\partial_{m_z} g_L - \beta\,\varepsilon(m_z,\boldsymbol{x})\,m_z\sqrt{1-m_z^2}\cos\phi\,, \\ (1+\alpha^2)\,\sqrt{1-m_z^2}\,\dot{\phi} &= -\sqrt{1-m_z^2}\,\partial_{m_z} g_L + \beta\,\varepsilon(m_z,\boldsymbol{x}) m_z \sin\phi. \end{aligned} \tag{3.16}$$

Then we linearize the above system of equations around $m_z = -1$:

$$\begin{aligned}(1+\alpha^2)\,\delta\dot{m}_z &= \left[\alpha\,(2k_{1eff}+4k_2) - \beta\frac{2\eta}{1-\eta^2}\right]\delta m_z\,,\\ (1+\alpha^2)\;\delta\dot{\phi} &= (2k_{1eff}+4k_2)\,\delta m_z + \beta\frac{2\eta}{1-\eta^2}\delta\phi\,,\end{aligned} \tag{3.17}$$

where we can directly find the two eigenvalues :

$$\begin{aligned}\lambda_{m_z} &= \alpha\,(2k_{1eff}+4k_2) - \beta\frac{2\eta}{1-\eta^2}\,,\\ \lambda_{\phi} &= -\beta\frac{2\eta}{1-\eta^2}\,.\end{aligned} \tag{3.18}$$

For a very small positive current value, we have a saddle equilibrium point in $m_x = -1$, and increasing it, λ_{m_z} becomes zero (a saddle node bifurcation occurs) when it reaches the value:

$$J_{MTJ} = \frac{e\,\gamma_0\,L\,\alpha}{g\,|\mu_B|\mu_0}\frac{1-\eta^2}{\eta}\,(k_{1eff}+2k_2)\;. \tag{3.19}$$

This value of current is smaller than the threshold of the self-oscillation for the considered range of the second order anisotropy constant k_2. By increasing the current density, we have that the two saddles equilibria, move from $m_x = -1$. On the other hand, there is the change of stability of the equilibria $m_z = \pm 1$ and the respective appearance of a stable limit cycle around them which corresponds to the so called Hopf bifurcation [30], [31]. Such bifurcation mechanism gives birth to the self-oscillation dynamics of the magnetization. Therefore, we can estimate the critical current density value at which the Hopf bifurcation occurs by simply making the following limit:

$$J_{MTJ,Hopf} = \lim_{m_z\to\pm 1} J_{MTJ}\,, \tag{3.20}$$

where J_{MTJ} is taken from the equation (3.15). In this way, we obtain the following formula:

$$J_{MTJ,Hopf} = \frac{e\,\gamma_0\,L}{g\,|\mu_B|\mu_0}\frac{2\,\alpha\,k_{1eff}}{\eta^3}\,. \tag{3.21}$$

This approach is approximated because we do not take into account the displacement of the equilibria that only for zero current are in $m_z = \pm 1$. We have checked the validity of this assumption, verifying that the displacement of the equilibria $m_z = \pm 1$ is less than $\delta m_z < 0.1$ in the whole range of current values considered. We notice that $J_{MTJ,Hopf}$ is independent of the second order anisotropy constant. This feature can be seen in Fig.3.3 where all the curves start from the same current density value, namely $J_{MTJ} = J_{MTJ,Hopf}$. As we said before for the current density values that sustain self-oscillations, we have that the two saddle equilibria move from $m_x = -1$ in the two hemisphere of the state space (unit sphere (m_x, m_y, m_z)-space). This can be seen solving the equilibrium equations obtained by imposing the condition $\dot{\phi} = \dot{m}_z = 0$ in the equations (3.16). At the same time, the self-oscillation orbit (limit cycle) is asymmetric with respect to rotations around the z-axis. This is due to the angular dependence of the spin transfer torque expression. As the current density increases, the limit cycle moves down and enlarges, while the saddle equilibria moves toward the limit cycles in the respective hemisphere of the unit sphere in the $\boldsymbol{m}$-space. Then, there will be a current density value at which the saddle equilibria intersect the limit cycle orbit, giving rise to a homoclinic-saddle-connection bifurcation [30], [31]. When this occurs, the limit cycle is broken, and no self-oscillations can be observed anymore. Moreover for such a current value the magnetization is switched to $m_x = -1$. This bifurcation mechanism is responsible of the maximum current value at which we can observe magnetization self-oscillation dynamics fixed the constants $k_1 eff$ and k_2. We estimate this critical current value by macrospin numerical simulations fixing the value of $k_1 = 0.56 MJ/m^3$, ranging k_2 from 0.5 to $4.0 \cdot 10^4$ J/m^3. As k_2 increases, the oscillations are excited for a larger range of current densities, because it makes the out-of-plane magnetization more stable. The agreement between analytical and numerical results improves as k_2 is increased.

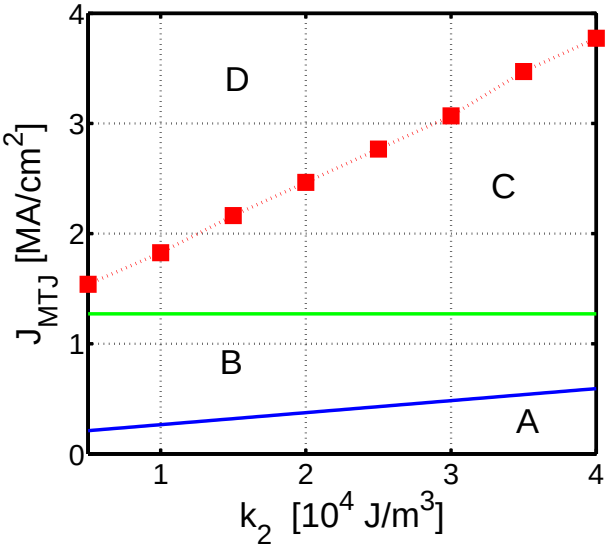

Figure 3.4: Bifurcation lines in the plane (k_2, J_{MTJ}) with $k_1 = 0.56MJ/m^3$ and $M_s = 950kA/m$.

3.6 Phase Diagram of equilibria and self-oscillation dynamics

The complete stability diagram showing the various bifurcation lines discussed in the previous paragraph is shown in fig.3.4 . We can distinguish four different regions in which the dynamical behaviour of the magnetic state is different, called A, B, C and D. The region A is characterized by two stable equilibria close to the magnetic states $m_z = \pm 1$, a saddle and an unstable equilibrium point in $m_x = -1$ and $m_x = +1$ respectively. The blue line that separates the A and B regions identifies the points (k_2, J_{MTJ}) defined by eq.(3.19), where the saddle node bifurcation in $m_x = -1$ occurs. In the B region, the equilibrium point in $m_x = -1$ is stable, but we have other two saddle equilibria arising from the saddle node bifurcation.

The green line separating the regions B and C is related to the Hopf bifurcation for the equilibria close to the magnetic states $m_z = \pm 1$ which become unstable with the presence of stable self-oscillation precession.The current density values for the points of this bifurcation line do not depend on k_2. In the C region we have stable magnetization self-oscillations. The red dotted line with squares separating the C and D regions represents the homoclinic connection bifurcation line. The current range at which self-oscillations exist for a fixed value of k_2 can be measured as the range of current density values between the red and the green line. Finally, in the D region, we have a stable state in $m_x = -1$, an unstable state in $m_x = +1$, and other 4 unstable states (two saddles and two nodes) that disappear for higher current values with a saddle node mechanism. In conclusion, we found that the second order uniaxial anisotropy plays a fundamental role near the compensation point in perpendicular magnetized ferromagnet. We have developed an analytical framework to predict both switching and self-oscillation proprieties that has been benchmarked with full micromagnetic simulations and a quantitative agreement is found.

Chapter 4

Synchronization of magnetic vortex oscillations in a pointcontact nanodevice by microwave field

4.1 Introduction

Spin-transfer nano-oscillators (STNOs) based on nanocontact geometry are future candidates to develop nanoscale devices in the area of information and communication technologies. Their current-field frequency tunability, narrow linewidth and stability at room temperature [66, 67] suggest their potential use in the microwave technology for realizing generators, detectors, modulators, etc. Furthermore, the micron size dimensions allow easy integration with the semiconductor technology. The main issues that limit their applicability are the low output power of the single device compared with LC voltage controlled oscillators [68] (VCO). A potential solution to this issue is the synchronization of an arbitrary number of non interacting STNOs with a small amplitude external source, often referred to as injection-locking [69]. The synchronization of magnetization oscillations

in nanopillars of submicron dimensions with nearly-uniform magnetization has been extensively studied in the last decade [69–75], showing that the transitions among the possible regimes are governed by strongly nonlinear effects [76–80]. In particular, the hysteretic behavior of the synchronization mechanism, first predicted theoretically [81–83] and later on observed experimentally [84, 85] , allowed a step forward towards understanding the synchronization of STNOs by means of a 'weak' microwave source.

Here, we study the synchronization mechanism between the dc current-induced vortex oscillations and a microwave external magnetic field in a thin film point-contact STNO [86]. These oscillation regimes in micron-sized thin-film STNO have been experimentally observed [87,88] and theoretically studied mostly by means the rigid vortex theory [89]. The latter model describes a linear dependence of the vortex oscillation frequency on the current as well as a current independent distance of the vortex core from the center of the nanocontact. Neverthless, further experiments on vortex core polarity switching [90, 91] and vortex oscillations driven by magnetic field and spin polarized current [92] were not in agreement with the predictions from the rigid vortex model. Indeed, numerical micromagnetic studies consistent with experimental results confirmed the presence of a vortex characterized by a deformed structure [93, 94]. This effect, which is more pronounced close to the vortex core, has been also observed experimentally [95].

Here we present a theoretical approach capable of taking into account the vortex structure deformation and apply the model to study the synchronization of current-driven magnetic vortex oscillations with an external microwave magnetic field for a disk-shaped point-contact STNO, as sketched in fig.4.1.

The main result of the work is the analytical derivation of the phase locking diagram (reported in fig.4.10(a,b)). This diagram describes all possible mechanisms of synchronization between vortex oscillations and external microwave magnetic field. Several insights emerge from our study. First of all, coexistence of synchronized and unsynchronized vortex oscillations is predicted for appropriate choices of amplitude and frequency of the microwave field. As a consequence of that, we show that the synchronization has a strong hysteretic nature. In addition, for microwave fields with mod-

erately high amplitude (order of mT), the locking frequency bands exhibit a pronounced asymmetry, which reveals complex nonlinear behaviour in the synchronization regime. The theoretical predictions are in good agreement with micromagnetic simulations of injection-locking experiments.

In the proposed theoretical model, vortex dynamics is modelled in terms of the vortex core position using a combined analytical-numerical approach. The analytical part consists of a collective variables description [96] of the vortex core dynamics. The numerical one allows us to introduce an additional current dependence describing the vortex deformation that a current independent ansatz [89, 97] cannot take into account.

4.2 Nonlinear vortex dynamics in pointcontact

Let us consider a point-contact device where the free layer is disk shaped with radius $R = 1\,\mu m$ and thickness $L = 4\,nm$. The magnetization field of this layer is free to evolve and the dynamics can be excited applying a magnetic field or making pass through it a spin polarized electric current thanks to a circular nanocontact of radius $R_{pc} = 50\,nm$ centered on the disk layer. The current is assumed to pass vertically to the disk plane in a confined region indicated in fig. by the red dotted lines. The magnetic state of the magnetic disk is assumed to be in a vortex state. This fact can be justified saying that increasing the size of the magnetic layer the vortex configuration is preferred because it minimizes the total micromagnetic energy sum of the exchange, the magnetostatic and the Zeeman energy. Furthermore when we excite the dynamics with an electric current passing through the nanocontact, the strong contribution of the total micromagnetic energy due to the Oersted-Ampere field generated by the electric current prefers curling patterns of the magnetization field instead of the uniform one. In case we choose as collective variables the in-plane coordinates of the vortex core center namely $\boldsymbol{X} \equiv (X_c, Y_c)$, then due to the circular symmetry of the free layer eq.(1.105) can be written as:

$$G(X)\hat{\boldsymbol{z}} \times \dot{\boldsymbol{X}} + \partial_{\boldsymbol{X}} W(X) + D(X)\dot{\boldsymbol{X}} - \boldsymbol{F}_{st} = \boldsymbol{0}\,. \tag{4.1}$$

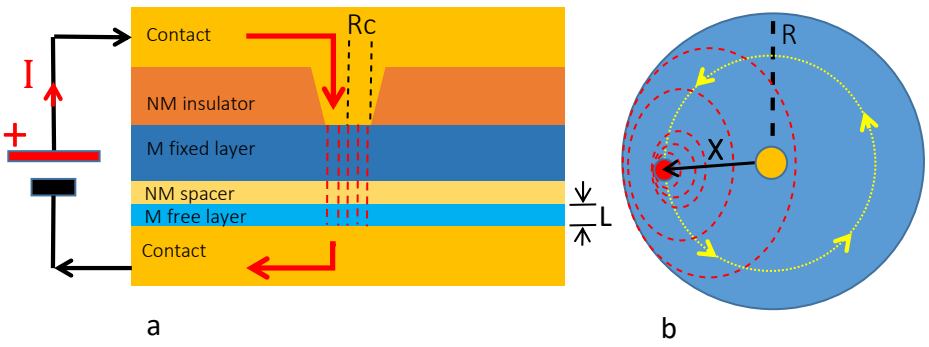

Figure 4.1: (a) Sketch of the point-contact STNO. (b) Sketch of the free layer. The filled orange dot located in the disk center is the cross-section of the nanocontact through which the electric current flows. The trajectory of the vortex core (red dot) around the nanocontact is represented by the yellow line. The dashed red lines represent the curling magnetization around the vortex core.

where $G_{X_cY_c} = -G_{Y_cX_c} = G(X)$ and $D_{X_cY_c} = D_{Y_cX_c} = 0$, $D_{X_cX_c} = D_{Y_cY_c} = D(X)$, with $X = |\boldsymbol{X}|$.

4.3 The Rigid Vortex Theory

When the external exctitations are turned off, the vortex core is centered in the free layer ($\boldsymbol{X} = \boldsymbol{0}$). When we excite the system instead, the vortex start to move. Let us imagine that the excitation realized by spin polarized current is such that the vortex motion occurs along a circular orbit of radius equal to the distance X of the vortex core from the center. The rigid vortex description of such a magnetization dynamics means that when the vortex moves around the magnetization pattern is not affected by the motion, which corresponds to the condition $\boldsymbol{m}(\boldsymbol{r}, \boldsymbol{X}(t)) = \boldsymbol{m}(\boldsymbol{r} - \boldsymbol{X}(t))$. In the

following, as it is typical in point-contact geometry, we shall consider the vortex dynamics occurring outside the nanocontact region which means $X > R_{pc}$. Taking the magnetization ansatz from the work of Usov and Peschany [98], it is possible to obtain the following expressions:

$$G(X) = G = \frac{2\pi\, M_s\, L}{\gamma}\,, \tag{4.2}$$

$$D(X) = D = \frac{2\pi\, M_s\, L}{\gamma} \log \frac{R}{r_c}\,, \tag{4.3}$$

$$W(X) \approx k_{Oe}\, I X\,, \tag{4.4}$$

$$\boldsymbol{F}_{st} = \boldsymbol{F}^z_{st} = \frac{k_{st,z}\, I}{X} \hat{\boldsymbol{z}} \times \hat{\boldsymbol{X}}\,. \tag{4.5}$$

where the expression for G is derived from the conservation of the topological charge, the term D is taken constant and calculated just considering the out of vortex core magnetization pattern when the vortex is centered in the device $\boldsymbol{X} = \boldsymbol{0}$ with r_c indicating the radius of the vortex core. The energy of the vortex configuration $W(X)$ is calculated taking only the Zeeman contribution due to the Oersted field in the limit case $R \to +\infty$, neglecting the out of plane component of the magnetization in the region of the vortex core. The force term due to the spin-transfer-torque interaction depends only by the out of plane component of the polarizer because the magnetization field under the nanocontact is in plane. If for the vortex core coordinates we adopt the in-plane polar coordinates $\boldsymbol{X} \equiv (X, \Phi) \Rightarrow \dot{\boldsymbol{X}} = (\dot{X}, X\dot{\Phi})$, the eq.(4.1) can be written:

$$\begin{aligned} \dot{X} &= \frac{G}{G^2 + D^2} \left[F^z_{st} - D\Omega X \right]\,, \\ \dot{\Phi} &= \frac{G}{G^2 + D^2} \left[\frac{D\, F^z_{st}}{G\, X} + G\, \Omega \right]\,, \end{aligned} \tag{4.6}$$

where

$$\Omega(X) = \frac{\partial_X W}{GX}\,, \tag{4.7}$$

is the angular frequency of the vortex core oscillating at constant X. In fact, considering the case of stationary oscillation $\dot{X} = 0$, one has

$$\begin{aligned} \dot{\Phi} &= \Omega(X)\,, \\ \Omega(X) &= \omega_0\,, \end{aligned} \tag{4.8}$$

where $\omega_0 = F^z_{st}/(D\,X)$. In this description the term D does not depend on the current, while both Ω and ω_0 depend linearly on it. Consequently, the stationary orbit radius X of the vortex core precession around the nanocontact is current-independent. From micromagnetic simulation of vortex oscillation driven by spin polarized current shown in fig.4.8 we observe a total disagreement with the rigid vortex theory predictions. In particular, in both cases with out-of-plane (see fig. 4.8(a,b)) and almost in-plane (see fig. 4.8(c,d)) polarizer, the dependence $X(I)$ is not negligible and the oscillation frequency is not linear with respect to the current value. Giving a look to the rigid vortex modelling those dependencies could be addicted to the fact that the magnetostatic energy is neglected. In fact since the magnetostatic energy is current independent, considering it we have that the term $\Omega(X)$ is not linear with the current anymore and then the stationary vortex oscillation radius X is current dependent. However reasoning on scaling argument we can prove that the $X(I)$ dependence in fig.4.2 is not a result of such an approximation. In order to show that, let us consider a disk of radius R being in a magnetic vortex state, assumed to be rigid with the vortex core center occupying a fixed position $\boldsymbol{X}$. The magnetostatic energy is expressed by the following equation:

$$F_M = -\mu_0 \int_\Omega \boldsymbol{H}_M[\boldsymbol{M}] \cdot \boldsymbol{M}\, dV = \frac{\mu_0}{2} \int_{\Omega_\infty} \boldsymbol{H}^2_M[\boldsymbol{M}]\, dV\,, \tag{4.9}$$

where $\boldsymbol{H}_M$ is the magnetostatic field expressed by the equation (1.8). It is convenient to report the magnetostatic field expression here since it is the core of the discussion. In this respect, we have

$$\boldsymbol{H}_M[\boldsymbol{M}] = -\frac{\nabla_P}{4\pi} \left[\int_{\Omega_m} \frac{\nabla_Q \cdot \boldsymbol{M}(\boldsymbol{Q})}{r_{PQ}}\, dV_Q - \int_{\partial\Omega_m} \frac{\boldsymbol{M} \cdot \boldsymbol{n}_Q}{r_{PQ}}\, dS_Q \right], \tag{4.10}$$

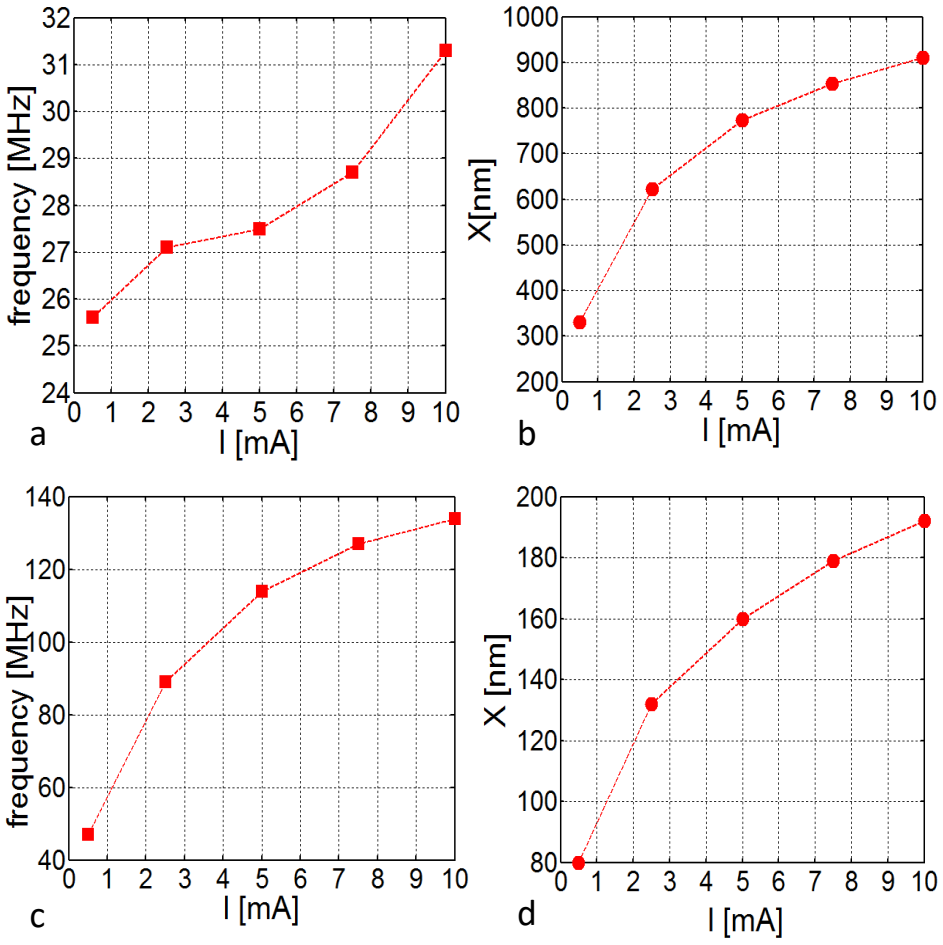

Figure 4.2: Oscillation frequency $f = \Omega/(2\pi)$ and stable orbit radius X as function of the spin-polarized current obtained fro micromagnetic simulations: (a) $f(I)$, (b) $X(I)$ for $\theta_p = 0$ (out-of-plane polarizer); (c) $f(I)$, (d) $X(I)$ for $\theta_p = 84°$ (in-plane polarizer).

where the first integral in the right hand side is the contribution due to the magnetic volume charges, while the second integral is the contribution due to the surface charges. When $R \to \infty$, fixed $\boldsymbol{X}$ we have $\boldsymbol{M} \cdot \boldsymbol{n}_Q \to 0$ and therefore the surface integral tends to zero. Moreover, if we assume a rigid vortex magnetization distribution we have that the volume charges are concentrate only in the vortex core and the magnetostatic field energy tends to be constant with respect to the position of the vortex core $\boldsymbol{X}$. In conclusion the current dependence of the orbit radius $X(I)$ should tends to zero when we increase the radius of the free layer and disappear in the limit case $R \to \infty$. In fig.4.17 is evident that this is not the case. In fact

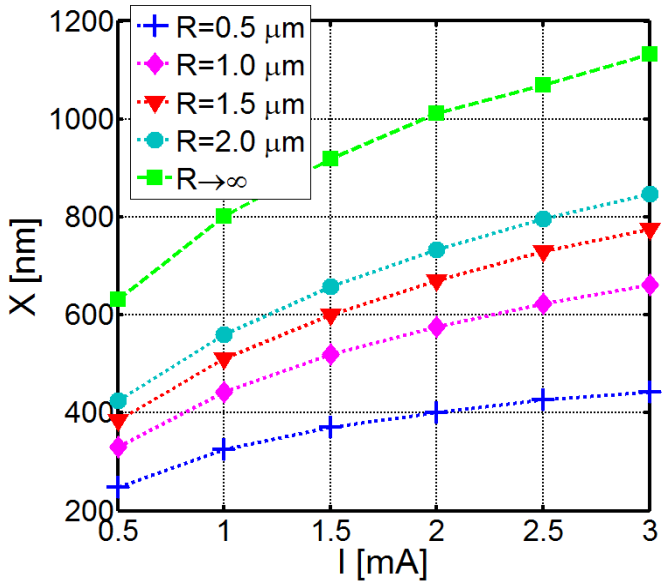

Figure 4.3: Stationary oscillation orbit radius X as a function of the out of plane $\theta_p = 0$ spin polarized current I, obtained from micromagnetic simulations.

increasing the size of the free layer the so plotted $X(I)$ dependence is more pronounced. Therefore, the anomalous current dependences showed up in

fig.4.2 are not a result of the inaccurate estimation of the vortex state energy, but rather of the fundamental hypothesis of rigid structure of the magnetic vortex. In the following section we propose a different approach where the magnetization distribution is not described by an ansatz anymore.

4.4 Free ansatz model identification

The aim of the previous section was to show the failure of the rigid vortex description for studying the magnetization dynamics in the point-contact device considered. The limitation of the rigid vortex theory to describe the vortex dynamics in submicron-size disks have been already discussed in reference [99]. However, to overcome such limitation the approach followed was to adopt for the magnetization pattern the two vortices ansatz [97] connected to the theory of the Beljavin-Poliakov soliton. In this section we show that either this last description is not able to reproduce the dynamical features of the vortex dynamics observed by means micromagnetic simulations. The reason is the deformation of the vortex structure due to the Oersted filed generated by the current flowing through the nanocontact. It is clear that if the discrepancy depends on the current, a current-independent ansatz cannot be the solution to our problem. In the following this argument will be validated with a combined analytical-numerical approach, where the numerical part of our study is developed in the environment MUMAX [24].

4.5 Conservative dynamics

The starting point of our analysis is the micromagnetic energy of the vortex configuration. In fact the main features of the vortex dynamics, in particular the deformation of the vortex structure and its impact on the dynamics can be understood with a combined analysis of the energy and the magnetization pattern. A numerical estimation of the several energetic contributions can be done considering the conservative dynamics $\alpha = 0$, $\beta = 0$. In that case

eq.(4.6) becomes:

$$\begin{aligned} \dot{X} &= 0\,, \\ \dot{\Phi} &= \Omega(X) = \frac{\partial_X W}{G\,X}\,, \end{aligned} \tag{4.11}$$

which describes a precession of the vortex core on a circular orbit of radius X at constant energy $W(X)$. In principle the conservative dynamics can be simulated setting the damping constant and the spin polarized current zero in the simulation software. However while that is immediate for the spin polarized current, the explicit structure of the solver used does not allow to set damping zero without increasing considerably the simulation error. We choose for these kind of simulations a damping constant $\alpha = 1.3{\times}10^{-3}$. This value is small enough to assume that for a sufficient long time the dynamics occurs at constant energy. On the other end it is big enough to contain the simulation error. Micromagnetic analysis shows that the rigid vortex theory cannot be applied for a quantitative description of nanocontact STNOs. In fig. 4.4, the behavior of the different energy terms as function of X and I is reported. One can clearly see that the exchange and the magnetostatic energy (fig.4.4(a,b)) which within the context of a rigid vortex model are considered to be independent of the vortex core position and current, exhibit monotonically increasing behavior as function of X, but also with respect to I in a nonnegligible way. In addition, the Zeeman energy associated with the Oersted field (fig.4.4(c)) shows a weak dependence on X compared to what a rigid vortex description would predict (see yellow curve).

The strong dependence on the current can be also explained by looking at the micromagnetically computed magnetization configuration, where a strong deformation of the vortex magnetization pattern is clearly visible (see fig.4.5(b)). The in-plane deformation is responsible for the weak dependence on X of the Zeeman energy and for the dependencies on both X and I of the exchange energy (see fig.4.4(a,c)). In fact, while for large enough distance from the vortex core the magnetization aligns with the Oersted field, in a small region around the line connecting the core center and the nanocontact center (line A-A' in fig. 4.5(a)) there is a sharp change of the magnetization direction. This change of direction is associated with a consistent amount

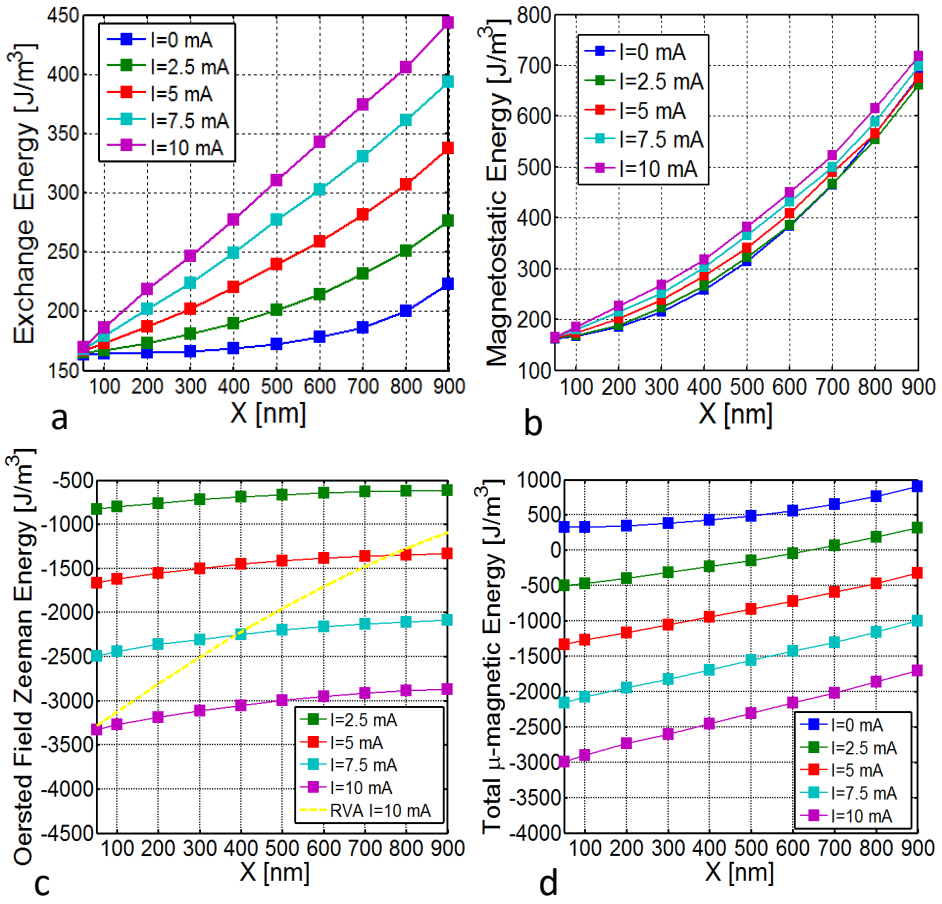

Figure 4.4: Energies as function of X and I computed from micromagnetic simulations. (a) exchange energy; (b) magnetostatic energy; (c) Zeeman energy; (d) total energy. Solid lines of different colors refer to different values of I, dashed yellow line in (c) refers to the Zeeman energy predicted by a rigid vortex description.

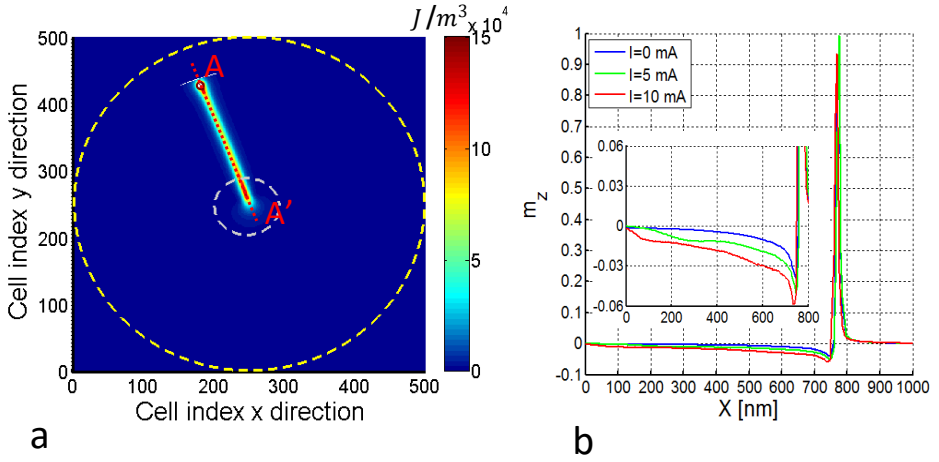

Figure 4.5: (a) Exchange energy density of the vortex configuration for $I = 10mA$ and $X = 800nm$; (b) m_z along the line A-A' represented in (a) for different current values I. Inset: magnified view.

of exchange energy stored along this branch structure, as in fig.4.5(a) where the exchange energy density is represented.

We also observe that the deformation of the vortex structure affects not only the in-plane magnetization components m_x, m_y, but also m_z. In fact, one can see in fig.4.5-(b) that, as far as the current is increased, in the region along the line A-A' except the vortex core region, the out-of-plane magnetization m_z exhibits a nonzero tilting downwards which increases with X and I. This deformation of the vortex structure can explain the current dependence of the magnetostatic energy reported in fig.4.4(b).

The gyrovector module is $G \approx 2\pi p \mu_0 M_s L/\gamma$, where p is the vortex core polarity, while the total energy is approximated with the following fourth degree polynomial $W(X, I) = W_0 + c_1 X + c_2 X^2 + c_4 X^4$, where the coefficients are obtained with a least squares fitting to the results of full micromagnetic simulations of the conservative dynamics. In fig.4.6(a), we show that the reduced order model where the current dependence of the

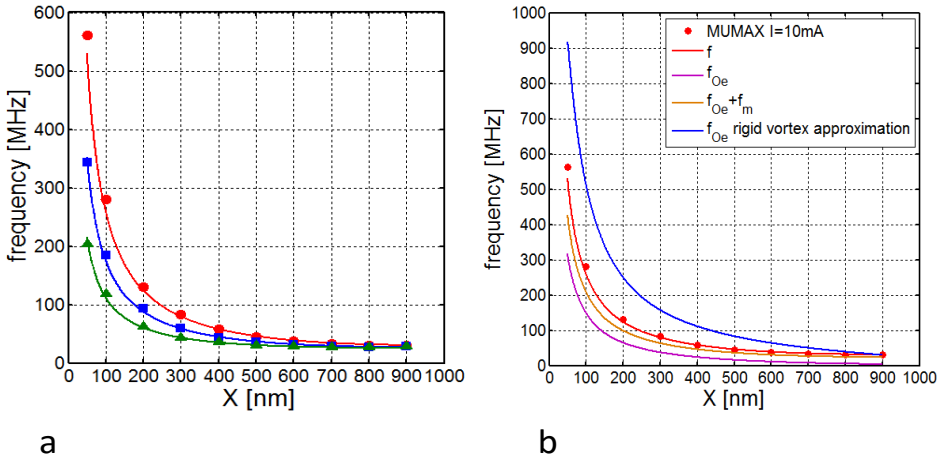

Figure 4.6: Comparison between the vortex oscillation frequency estimated with full micromagnetic simulations and evaluated with reduced order model for different current values. (a)The red circles, blue squares and green triangles are obtained from MUMAX [24] for $I = 10mA, I = 5mA$ and $I = 2.5mA$ respectively. The continuous line of the same color is related to the same current value but is obtained from eq. (4.11) using the polynomial expression for $W(X, I)$. (b)Different contributions to the total frequency f. The blue curve represents the frequency estimated according to eq. (4.11) under the assumption of rigid vortex profile for the magnetization distribution and considering only the Zeeman energy due to the Oersted field.

energy $W(X, I)$ is identified from micromagnetic computation of the energies is in good agreement with the oscillation frequency resulting from full micromagnetic simulations of conservative vortex gyration. Furthermore, in fig.4.6(b) one can see that each contribution (exchange f_{ex}, Oersted f_{Oe} and magnetostatic f_m) is important for the correct estimation of the conservative gyration frequency. In addition, it is important to notice that the rigid vortex theory is not able to reproduce the vortex dynamics in this case.

In fact by looking at the blue line in fig.4.6(b) computed assuming a rigid vortex state with $W(X,I) \approx W_{Oe}(X,I) \Leftrightarrow f(X,I) \approx f_{Oe}(X,I)$ [87] , [89] ,it is apparent that the frequency so predicted overestimates the frequency estimated by full micromagnetic simulations by a large amount. Notice that the matching of the frequency values validates the approximated expression for the gyrofactor which is rigorous only in case of rigid vortex. In the following we add nonconservative effects to the vortex dynamics, such as damping and spin-polarized-current.

4.6 Current driven dynamics

In order to reproduce the correct current dependence of the stationary orbit radius and oscillation frequency, we found out that it is necessary to fit both the energy W and the damping term coefficient D with micromagnetic simulations. The identification procedure of D can be inferred from the reduced order model described by eq.(4.1) in the absence of spin torque force $\boldsymbol{F}_{st} = \mathbf{0}$. In this framework, we end up with the following equation:

$$D^2\dot{X} + D\partial_X W + G^2\dot{X} = 0 \ , \tag{4.12}$$

which is a second degree polynomial equation in D that can be solved once $\dot{X}$ is known. This last term is obtained from a numerical experiment of relaxation dynamics. In particular, we simulate the vortex core dynamics starting from the initial condition where the vortex core is displaced from the center and we compute its dynamics towards equilibrium (center of the nanocontact) monitoring the energy $W(t,I)$. From the knowledge of $W(X,I)$, $X(t)$ is extracted. Since $D^2/G^2 \ll 1$, we can approximately estimate $D \approx G^2|\dot{X}|/(\partial_X W)$. At this point, the knowledge of $W(X,I)$ and $X(t)$ allows us to obtain $D(X,I)$ from the solution of eq. (4.12). In this way, we get two roots, but a simple comparison of their order of magnitude with the one of the approximate value allows one to select the correct one. We remark that the characterization of the damping term coefficient does not involve the spin torque force term. In fig. 4.7, the numerical results for $D(X,I)$ obtained following the procedure described above, are reported.

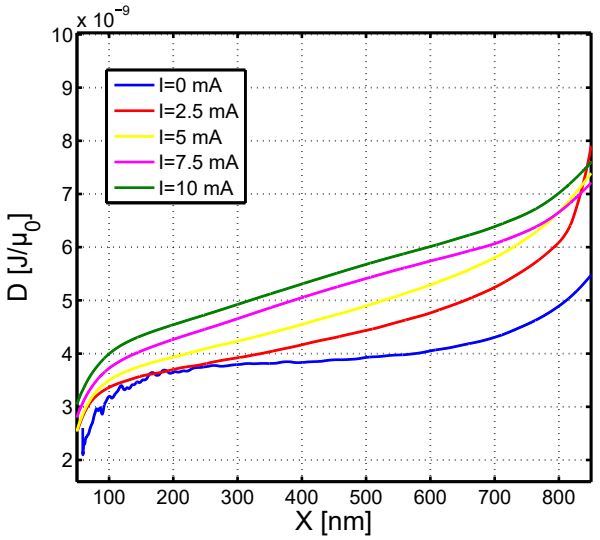

Figure 4.7: Damping D as a function of X for several values of the current I.

We observe that, while for $I = 0$ mA $D(X)$ is approximately constant, the dependence on X becomes more important as the current increases.

For the spin torque force term, one can infer that, for an arbitrary orientation of the polarizer, only the out-of-plane component F_{st}^z can compensate the effect of damping. We adopt for this term the same expression as that provided by the rigid vortex theory [89], namely $F_{st}^z = k_{st} I/X$, where $k_{st} = Ms\sigma L \cos\theta_p$. After the identification of $W(X, I)$ and $D(X, I)$, from the resolution of eqs.(4.6), we get the blue curves in fig.4.8. As can be oserved, they are in very good agreement with full micromagnetic simulations (red symbols).

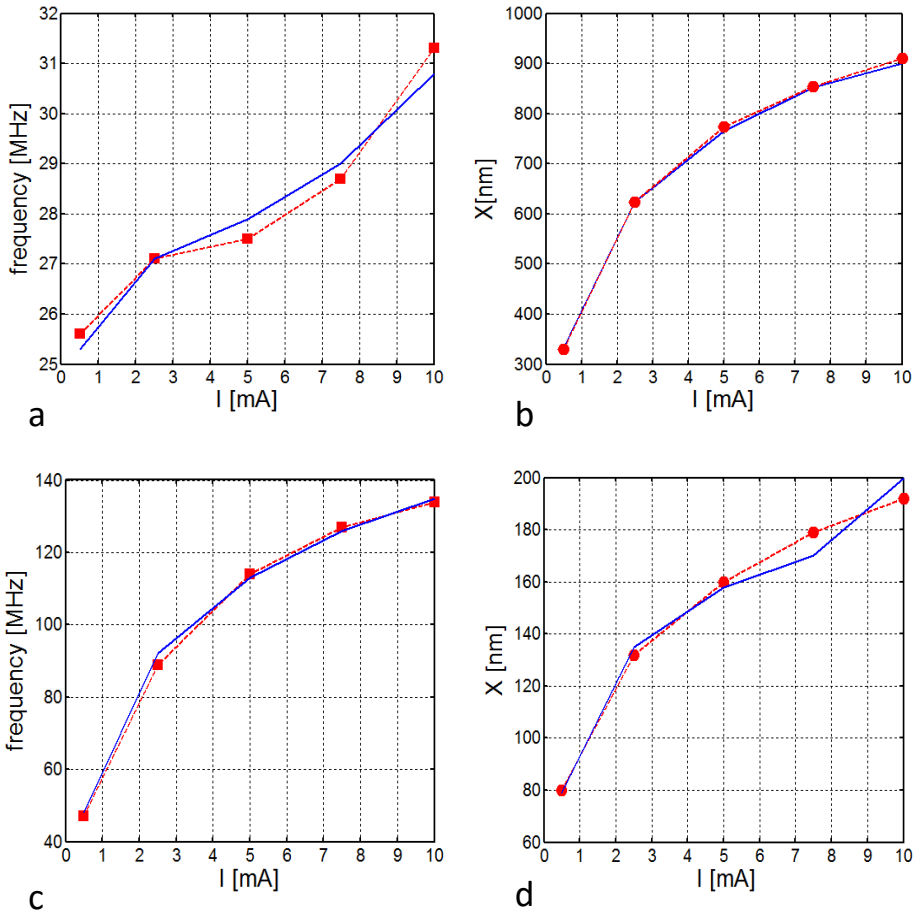

Figure 4.8: Oscillation frequency f and stable orbit radius X as function of the spin-polarized current: (a) $f(I)$, (b) $X(I)$ for $\theta_p = 0$ (out-of-plane polarizer); (c) $f(I)$, (d) $X(I)$ for $\theta_p = 84°$ (in-plane polarizer). Solid lines are obtained from eqs.4.8, whereas lines with symbols refer to the results of full micromagnetic simulations.

4.7 Theory of vortex oscillations synchronization by microwave magnetic field

Up to this point, our model describes a scenario where the only external source exciting the vortex dynamics is the dc spin polarized electric current flowing through the nanocontact. In what follows, we generalize our model in order to include the presence of a microwave magnetic field, instrumental for the synchronization study. We model the interaction between the microwave field and the vortex magnetization state with an additional Zeeman energy contribution. This energy term can be evaluated as:

$$W_{rf} = -\mu_0 L \pi R^2 M_s \boldsymbol{H}_{rf} \cdot < \boldsymbol{m} > , \tag{4.13}$$

where $< \cdot >$ means spatial average and

$$< \boldsymbol{m} > = -\mathcal{C} k_m(I)\, \boldsymbol{e}_z \times \boldsymbol{X} , \tag{4.14}$$

where $\mathcal{C}$ is the chirality of the vortex and the proportionality constant k_m depends on the current I and is evaluated from numerical simulations. This interaction appears in the model through its gradient with respect the vortex core position vector $\boldsymbol{X}$:

$$\boldsymbol{F}_{rf} = -\partial_{\boldsymbol{X}} W_{rf} = \mu_0 k_{rf}\, \boldsymbol{e}_z \times \boldsymbol{H}_{rf} . \tag{4.15}$$

where $k_{rf} = \mathcal{C} M_s L \pi R^2 k_m$.

Thus, the equations which describe the vortex motion become:

$$\begin{aligned} \dot{X} &= \frac{G}{G^2 + D^2} \left[F^z_{st} + F_{rf,\Phi} - D \left(\Omega\, X - \frac{F_{rf,X}}{G} \right) \right] , \\ \dot{\Phi} &= \frac{G}{G^2 + D^2} \left[G\Omega - \frac{F_{rf,X}}{X} + \frac{D\,(F_{rf,\Phi} + F^z_{st})}{G\,X} \right] , \end{aligned} \tag{4.16}$$

where

$$\begin{aligned} F_{rf,\Phi} &= \boldsymbol{F}_{rf} \cdot \hat{\boldsymbol{X}} = \mu_0 k_{W_{rf}} H_{rf} \cos(\Phi - \omega t) , \\ F_{rf,X} &= \boldsymbol{F}_{rf} \cdot \hat{\boldsymbol{e}}_z \times \hat{\boldsymbol{X}} = \mu_0 k_{rf} H_{rf} \sin(\Phi - \omega t) . \end{aligned} \tag{4.17}$$

Here, we use the approach proposed in refs. [76,81–83] where the dynamical equations are rewritten in an appropriate rotating frame leading to an autonomous (i.e. time-independent) two-dimensional dynamical system. As a consequence of that, we can completely characterize the dynamical state by means of bifurcation theory [30–32]. Let us consider a rotating reference frame with angular frequency ω. In this frame, the angular polar coordinate $\Phi = \phi + \omega\, t$ and the rotating field components are given by:

$$\begin{aligned} F_{rf,X} &= \mu_0 k_{W_{rf}} H_{rf} \sin\phi = F_{rf}\ \sin\phi\,, \\ F_{rf,\phi} &= \mu_0 k_{W_{rf}} H_{rf} \cos\phi = F_{rf}\ \cos\phi\,, \end{aligned} \tag{4.18}$$

which, as mentioned before, are time-independent.

Then, if we introduce the normalized quantities $d = D/G$, $x = X/R$, $b = F_{rf}/(G\,R)$, $\omega_0 = F^z_{st}/(D\,X)$ and neglect the $\mathcal{O}(d^2)$ terms , eqs. (4.16) projected in the rotating frame take the following form :

$$\begin{aligned} \dot{x} &= d\,x\,(\omega_0 - \Omega) + b\cos\phi\,, \\ \dot{\phi} &= \Omega - \omega - \frac{b}{x}\sin\phi\,. \end{aligned} \tag{4.19}$$

The latter equations reveal a simple, but neverthless rich mathematical structure, as we will see in the following. In fact, from general arguments of nonlinear dynamical system theory [30–32], it is possible to state that the only steady-state solutions admitted by eqs.(4.19) are either stationary points or limit cycles. As far as the synchronization with the rotating field is concerned, we pay special attention to the equilibrium states. In fact, such equilibria in the rotating reference frame represent synchronized motions of the vortex with the rotating field (P-modes) if we interpret them in the laboratory (non-rotating) reference frame. Conversely, limit cycles in the rotating frame represent unsynchronized quasi-periodic vortex motions (Q-modes) in the lab frame.

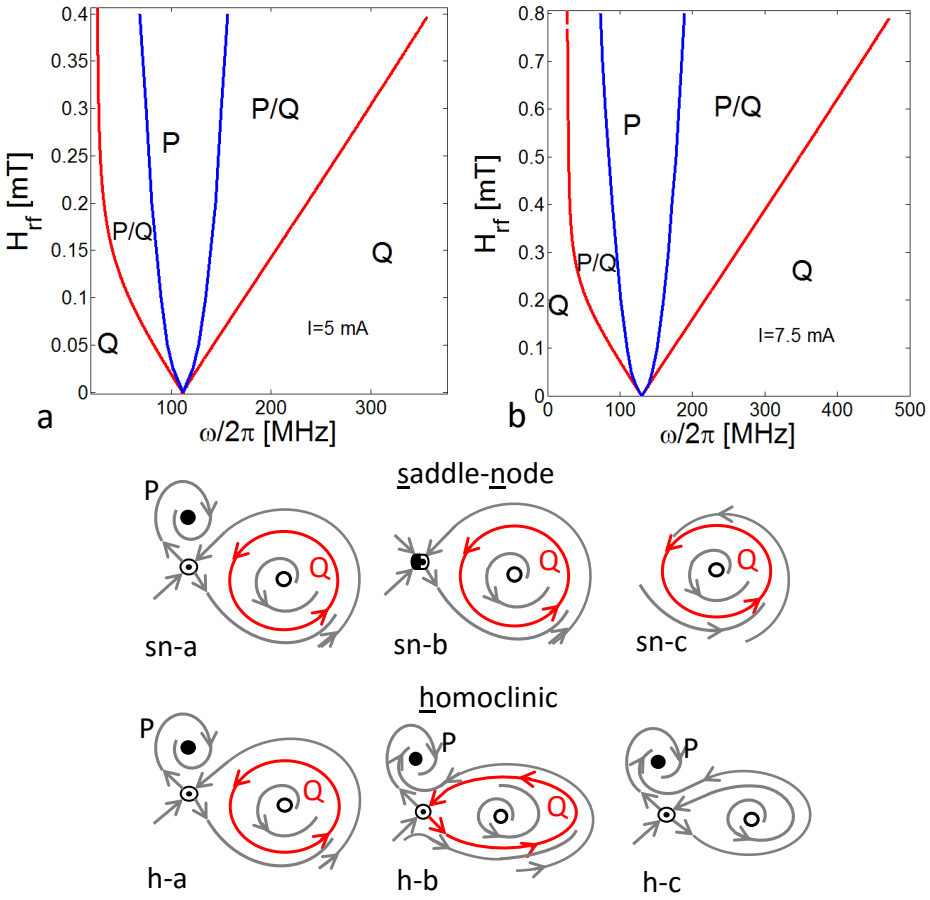

Figure 4.9: Phase locking diagrams in the control plane (ω, H_{rf}) as function of current: (a) $I = 5mA$; (b) $I = 7.5mA$; red lines refer to saddle-node bifucations and blue lines refer to homoclinic bifurcations; (sn) qualitative sketches for saddle-node bifurcations, the sequence a,b,c reproduces the generic transition from region P/Q to region Q; (h) qualitative sketches for homoclinic bifurcations, the sequence a,b,c reproduces the generic transition from region P/Q to region P.

All the possible transitions between P↔Q modes are a consequence of a bifurcation process [20, 30–32]. Among the possible bifurcations for a two-dimensional dynamical system, for the amplitude of current ($2.5mA \leq I \leq 10mA$) and microwave field ($H_{rf} \leq 1$ mT) considered, we find out that, for the dynamical system described by eqs. (4.19), just two of them occur as function of the current: the saddle-node and the homoclinic bifurcation. However this does not exclude the presence of other bifurcations that might occur at higher microwave power.

A sketch of these two bifurcation mechanisms is reported in fig. 4.9(sn,h), where generic transitions from region P/Q to regions Q and P are described. In the former case, an unstable P-mode (saddle point, represented as a striped dot in figure) annihilates with a stable synchronized state (filled dot) leaving just a stable Q-mode (red closed curve) as admissible regime. In the latter case, a stable unsynchronized state (Q-mode) disappears through a saddle connection, leaving just a stable synchronized P-mode as admissible regime. From the description of these bifurcation mechanisms, one can conclude that in the control plane the saddle node bifurcations are responsible for the P→Q transitions, whereas homoclinic bifurcations are responsible for the Q→P ones.

Now we address the quantitative determination of the bifurcation curves from eqs.(4.19). The first step is to express the synchronization conditions:

$$\begin{aligned} &\dot{x} = \dot{\phi} = 0\,, \\ &b = \frac{d\,x}{\cos\phi}(\Omega - \omega_0)\,, \\ &\omega = \Omega - d\tan\phi\,(\Omega - \omega_0)\,, \end{aligned} \tag{4.20}$$

where a correspondence between the synchronized states in the rotating frame (x, ϕ) and the points of the control plane (ω, H_{rf}) is established. The saddle node bifurcation curve can be obtained by considering the linearized form of eqs. (4.19) $\delta\dot{\boldsymbol{x}} = \boldsymbol{J}(x,\phi)\cdot\delta\boldsymbol{x}$, being $\delta\boldsymbol{x} = (\delta x, \delta\phi)$, $\boldsymbol{J}(x,\phi)$ the Jacobian matrix of the right hand side of (4.19), evaluated in the equilibrium point (x, ϕ). In particular, by solving eqs. (4.20) together with $\det\{\boldsymbol{J}(x,\phi)\} = 0$, we obtain the red curves in fig.4.9(a,b). On the other

hand, as far as the homoclinic bifurcation is concerned, there are no general approaches since it is a global bifurcation process. Here we detect the occurrence of such a bifurcation from the analysis of the phase portrait of the dynamical system (4.19) in the plane ($x_1 = x\cos\phi, x_2 = x\sin\phi$). By keeping ω fixed while changing b, we determine the critical value of this parameter related with the onset of the homoclinic bifurcation, as sketched in fig. 4.9(h-a,h-b,h-c), by following a bisection method. By repeating this procedure, we obtain the blue curves enclosing the region P in the phase locking diagram of fig.4.9(a)-(b). The structure of the phase locking diagram is preserved when the current value I changes, as shown in figure 4.9-(a,b). This confirms the general character of the overall picture of the vortex dynamics outlined above in the considered current range. In figure 4.10(a,b), we report the comparison of reduced order model and full micromagnetic simulations results for the phase locking diagram between the current induced vortex oscillations and the external microwave magnetic field. The diagram represents all the possible stable oscillation regimes of the magnetic vortex as function of the control variables (ω, H_{rf}). This diagram can be separated in three regions. Points in the region labelled with P correspond to periodic motions, termed P-modes, and are associated with vortex oscillations synchronized with the microwave magnetic field. On the other hand, points in the region labelled with Q correspond to quasi-periodic motions [100], termed Q-modes, associated with unsynchronized vortex oscillations. In the region P/Q both synchronized (P-modes) and unsynchronized (Q-modes) regimes can exist for the same pair of control variables (ω, H_{rf}). Which one of the two is reached in a particular situation depends on the past history of the vortex dynamical regime. In this respect, the coexistence of multiple stable oscillation regimes implies the occurrence of hysteretic synchronization mechanisms. The critical lines separating the different regions form two curved cones with a common vertex. The larger one bounded by the red curves separates the region where stable P-modes exist from the one where there are only unsynchronized Q-modes. The inner one, instead bounded by the blue curves, encloses the region where the only stable regimes are P-modes. The common vertex on the line $H_{rf} = 0$ mT corresponds to the free-running frequency ω_0 of the nanocontact oscillator,

namely the frequency of oscillations in the absence of microwave field.

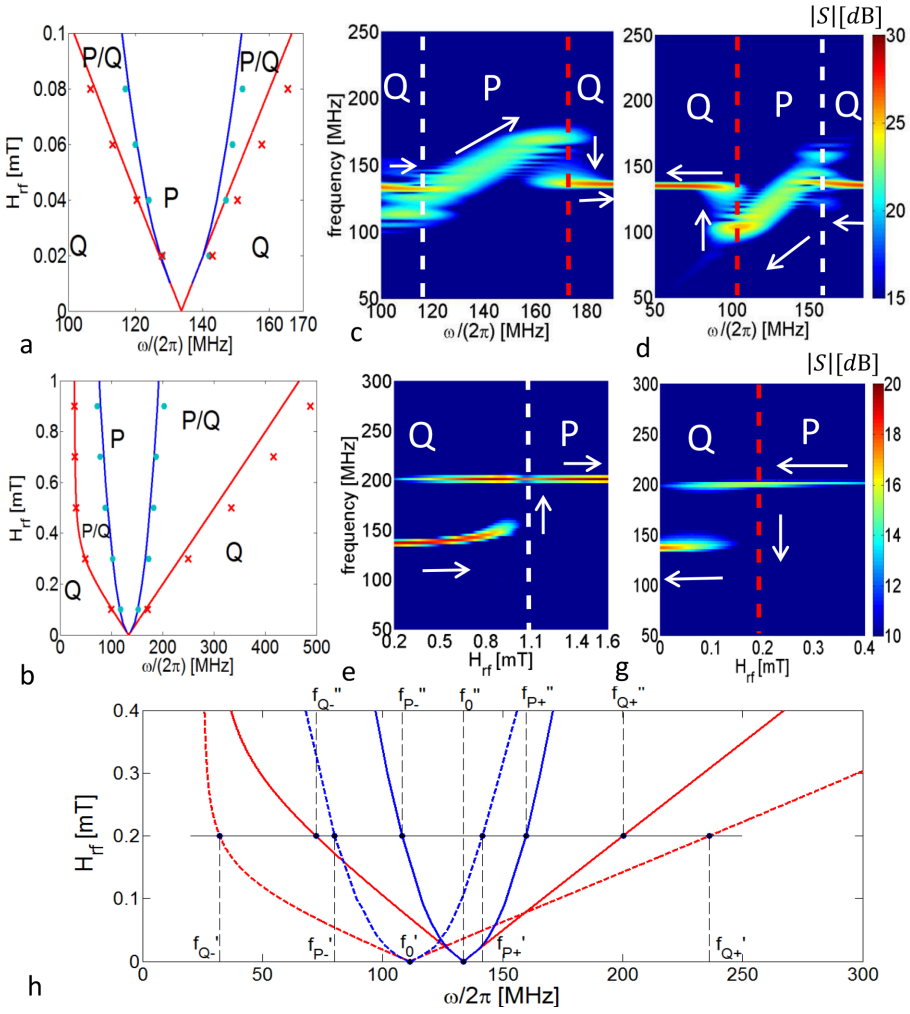

Figure 4.10:

Figure 4.10: (a) phase locking diagram in the control plane (ω, H_{rf}) for a spin-polarized current $I = 10mA$ with $\theta_p = 84°$. Regions P and Q represent synchronized and unsynchronized states, respectively, whereas region P/Q indicates coexistence of both of them. Solid lines refer to reduced order model predictions, symbols to micromagnetic simulations; (b) extended view of the phase locking diagram for $\mu_0 H_{rf} < 0.1mT$; (c),(d) spectrograms of the in-plane magnetization oscillation obtained from micromagnetic simulations of vortex dynamics at microwave field amplitude $\mu_0 H_{rf} = 0.1mT$ and ramping the angular frequency ω up (c) and down (d); (e),(g) spectrograms obtained at $\omega/(2\pi) = 200MHz$ and ramping the field amplitude H_{rf} up (e) and down (g). The color scale refers to the spectrum amplitude expressed in dB; (h) superposition of the phase locking diagrams for different current values $I = 5$ mA (dotted lines) and $I = 10$ mA (solid lines).

To clarify the diagram, let us consider an experimental situation in which a microwave field of a certain amplitude has, initially, a very large frequency. According to the phase diagram in fig.4.10(a), the vortex oscillation regime in this situation will be identified with a point in the right region Q and, therefore, is unsynchronized. Then, let us suppose to slowly decrease the frequency while keeping the field amplitude constant, which means moving the point leftwards along an horizontal line. The system will stay in an unsynchronized regime (Q-mode) until the blue curve separating regions P/Q and P is crossed. At that point, the vortex oscillation will undergo synchronization with the microwave field, since the point (ω, H_{rf}) enters the region P where the only stable regime is a P-mode. By further decreasing the frequency, the vortex oscillations will stay synchronized until the the red line separating the left Q and P/Q regions is crossed. When this occurs, the magnetic vortex will lose the synchronization with the microwave field and will move to a stable quasi-periodic motion. If the microwave field frequency is increased back, we move towards the right in fig.4.10(a) and the synchronization will be restored when the left blue line is crossed. By further increasing the frequency, the loss of synchronization will happen when the right red line is crossed. The hysteretic nature of the synchronization can

be observed in the spectrograms presented in fig.4.10(c) and fig.4.10(d). They have been obtained from micromagnetic simulations by increasing (fig.4.10(c)) and decreasing (fig.4.10(d)) the frequency at constant rate of $100KHz/ns$. The amplitude of the rf field is $0.1mT$ and the injected electric current is $10mA$. The red and white dashed lines indicate the $P \to Q$ and the $Q \to P$ transitions, respectively. It has been checked that smaller value of the frequency change rate does not affect the results.

We observe that the phase locking band, namely the width of region P, increases as a function of H_{rf} (see figs. 4.10(a)-(b)). Moreover, for moderately high microwave field amplitudes, the frequency bands associated with coexistence of P/Q modes also increase and exhibit significant asymmetry, which is the signature of complex nonlinear dynamics. This featue has been already observed experimentally (for a wide range of frequencies) in point contact devices where the magnetization is nearly uniform [84] . Remarkably, we point out that such frequency bands are quite large (several tens of MHz for $\mu_0 H_{rf} \sim 0.1$mT, above 100 MHz for $\mu_0 H_{rf} > 0.5$mT). Thus, it is expected that the hysteretic synchronization might be clearly observable even at room temperature, contrary to what happens for nanopillar STNOs [77, 84].

The hysteretic nature of the synchronization mechanism is also present if the frequency is maintained constant but the amplitude of the rf field is swept at a constant rate, which means moving vertically in the phase diagram of fig.4.10(a). It is observed in fig.4.10(e,f) where we present spectograms of the in-plane magnetization component obtained from micromagnetic simulations at $200\,MHz$ sweeping the field up (e) and down (f) at a rate of $1\,mT/ns$ in both cases. As in the previous case, it has been checked that a smaller rate does not affect the results.

In general, for generic histories of the microwave excitation, represented by closed curves in the control plane (ω, H_{rf}) crossing the aforementioned critical lines, there will be hysteresis in the synchronization process. As outlined above, the different regions in the control plane (ω, H_{rf}) are separated by curves associated with specific transitions of the vortex oscillation regimes. In particular, the blue curves describe transitions from $Q \to P$ (unsynchronized to synchronized regimes), whereas the red curves describe

transitions $P \rightarrow Q$ (synchronized to unsynchronized regimes).

These critical curves, which can be analytically derived from our model, have been checked by means of full micromagnetic simulations. The results are visible in fig.4.10(a,b), where blue circle (red cross) symbols indicate the $Q \rightarrow P$ ($P \rightarrow Q$) transitions observed in the simulations. The good quantitative agreement demonstrates the predictive power of the proposed theoretical model.

The wide range of frequencies around the free-running oscillation frequency in which synchronization is realized is an important requirement for the synchronization of multiple nanocontact vortex oscillators which, as it was pointed out in the introduction, is the solution to increase the power emitted by STNO devices. The study of synchronization of a family of nanocontact vortex oscillators goes beyond the limits of this work, but it is important here to carry out a general discussion about the simultaneous synchronization of multiple oscillators. The main point we want to stress is that, not only the region P, but also the region P/Q where synchronized and unsynchronized regimes coexist, is part of the frequency range in which simultaneous synchronization is possible.

In figure 4.10(h) we present the synchronization cones of two STNOs which differ in the free-running frequency ($f_0'' - f_0' = 22.4$ MHz) and we want to study the frequency range in which simultaneous synchronization occurs. The critical lines of the two STNOs have been computed considering the same STNO subjected to two different injected DC currents ($I = 5\,mA$, $I = 10\,mA$). This is done in order to simulate the situation where point-contacts are connected in parallel and there are differences in the contact resistances due to fabrication tolerances. The intersection points between the horizontal line corresponding to $H_{rf} = 0.2$ mT and the critical lines associated with the two oscillators are denoted with prime and double prime frequencies. Let us now consider again the experiment in which, starting from large enough frequency, we decrease it, i.e. we move from the right to the left on the horizontal line. The oscillator with the larger free-running frequency f_0'' gets synchronized with the external field at the frequency f_{P+}'', while the other one gets synchronized at the lower frequency f_{P+}'. From frequencies below f_{P+}', the oscillators are simultaneously synchronized down to the

frequency f''_{Q-} since $f''_{Q-} > f'_{Q-}$). In this situation, the simultaneous locking frequency range is $f'_{P+} - f''_{Q-} = 71.8$ MHz, more than three times larger than the difference of the free-running frequencies $f''_0 - f'_0$. Remarkably, we observe that, in the absence of hysteresis, the locking range would be simply $f'_{P+} - f''_{P-} = 25.9$MHz, which is less than half of that achievable taking into account hysteresis.

Analogously, if we carry out the experiment by increasing the frequency at given field, by using the same line of reasoning, we find that the frequency range of simultaneous synchronization between the two STNOs goes from f''_{P-} to f''_{Q+} which, according to our computations, is equal to 92.1 MHz. We notice that, in this case, the frequency $f'_{Q+} > f''_{Q+}$ and, thus, the second one determines the upper bound.

In conclusion, the hysteretic synchronization, coupled with an appropriate scheme of variation of the excitation conditions, may lead to considerably large frequency ranges where simultaneous synchronization of nanocontact STNOs is possible.

Conclusions

In this thesis two different spintronic devices of interest for technological applications have been considered. Both devices are constituted by a multilayer structure of magnetic materials separated by a non magnetic spacer which can be an insulator or a conductor. For the purpose of this thesis, a three layers structure is considered. The central layer is a non-magnetic one and it divides the two remaining magnetic layers. Only the magnetization of one of the two magnetic layers is free to change under the action of the external excitations. In the other magnetic layer, the magnetization is fixed and it acts as a spin-polarizer for the electric current flowing perpendicular through the multilayer structure. The magnetization dynamics in the free-layers have been investigated in the framework of micromagnetics, where the external excitations consist in applied magnetic field and spin-polarized-current included in the modelling with the Slonczewski spin-transfer-torque (STT) mechanism.
The first device considered is a magnetic tunnel juction (MTJ), where the free layer is a disk with circular cross section and a fixed thickness. The dimensions of the free layer are such that the magnetization can be considered spatially uniform. Moreover, the chemical composition of the juction free-layer/spacer produces an interfacial perpendicular anisotropy (IPA) effect. It is considered the case where the competition between magnetostatic effect and IPA results in a perpendicular easy axis configuration but where in the energetic expansion of the anysotropy interaction the second order uniaxial perpendicular anisotropy coefficient k_2 is of the same order of magnitude of the effective coefficient of the first order anisotropy k_{1eff}, namely:

($k_{1eff} \sim k_2 \sim 10^4 \div 10^5\, J/m^3$). For this device the several features corresponding to the magnetization statics and dynamics have been explored. First, the magnetization states of equilibrium and their stability when the anisotropy parameters (first and second order) are changed. It is shown that for a given k_2, by tuning k_{1eff} several static configurations can be obtained: easy axis (EA); easy plane (EP); easy cone (EC); and easy axis-plane (EAP). Then, the study of the dynamical phenomena (switching and self-oscillation dynamics) in the EA region is addressed. First, the role of the coefficient k_2 in the determination of the switching current when the spin-polarizer is oriented along the easy axis (out of plane direction) has been investigated. It has been shown that for each value k^*_{1eff} there exists a k^*_2 value where for $k_2 \leq k^*_2$ the switching current value is independent on k_2, while for $k_2 \geq k^*_2$ it increases almost linearly with k_2. From a technological point of view, this fact is relevant to understand the limits of the tuning of k_{1eff} which allows a substantial reduction of the switching current value. Then the study of the self-oscillations regimes when the spin-polarizer is oriented in plane is considered. Fixed the value of k_{1eff} and increasing k_2, the bandwidth, the ratio $\Delta\omega/\Delta J_{MTJ}$ and the interval of current values where the self-oscillations regime is observable considerably increase. In summary, it is shown that the second order anisotropy effect has to be taken into account in the design of STT-MTJ working as a memory or as a nano-oscillator device, where the IPA-magnetostatic compensation effect is important.

The second device considered is a point-contact geometry where the free layer is a thin cylinder hight few nanometers and with a diameter of 2 micron. The spatially uniform magnetization is not the energetically preferred state, in fact the ground state is a magnetic vortex, characterized by an in-plane magnetization pattern curling around the vortex core wherein the magnetization twists up to reach the out of plane direction in its center. By injecting a proper spin-polarized electric current through the metallic nano-contact on the top of the layer, it is possible to excite stable self-oscillations of the vortex core around the nano-contact on a circular orbit of radius X with a frequency value ω_0. A reduced order model based on the collective variables description have been developed, where the collective variables

are the vortex core center coordinates. This model is able to capture the main dynamical aspects of the self-oscillation regime such as the oscillation frequency ω_0 and radius of the oscillations orbit X, corresponding to the distance from the center of the nano-contact to the vortex core center. The fully characterization of that model passes through the identification of two functions, which are the vortex state energy and the damping term of the vortex gyration. In particular, fixed the electric current value, it is proposed an hybrid analytical-numerical procedure to recognize their functional dependencies on X. The model so obtained allowed to overcome the limits of the collective variable description based on the ansatz proposed in literature. In fact, as a general fact such ansatzes, when the radius of the free-layer gets progressively larger, provides a spin-polarized-current independent gyration radius X and a linear dependence on the current of the oscillation frequency ω_0. Such description is not confirmed by the micromagnetic simulations which show a sensible nonlinear current dependence of both terms X and ω_0, which does not disappear when the radius of the free layer gets bigger. At this point the study of the synchronization of the vortex core oscillations with a microwave rotating magnetic field is addressed. The microwave field is introduced in the model as a perturbation. Then, writing the dynamical equation in a rotating frame synchronous with the microwave field, the bifurcation theory has been possible to apply in order to obtain the complete phase diagram of the possible dynamical regimes. When the amplitude of the rotating magnetic field is $\sim 10^{-2}\, mT$, there exists a cone region (Arnold tongue) in the control plane frequency-amplitude of the rotating field (ω, H_{rf}) with vertex in the point $(\omega = \omega_0, H_{rf} = 0)$. For points inside (outside) the cone, the vortex oscillations are synchronized (unsinchronized) with the rotating field. Instead, when the amplitude of the rotating magnetic field is $\sim 10^{-2} \div 10^{-1}\, mT$, a new region where the coexistence of synchronized and unsynchronized oscillations appears. The presence of this region predicts hysteresis in the synchronization process which is confirmed by micromagnetic simulations. A further increment of the rotating field amplitude $\sim 10^{-1} \div 1\, mT$ produces asymmetry of the width of the coexistence regions which indicates asymmetry in the hysteresis bands. This aspect has been confirmed by the micromagnetic simulations

too. Moreover the amplitude of the hysteresis bands becomes in the order of several hundreds of MHz which is the order of magnitude of the vortex gyration frequency when $H_{rf} = 0$.

From a technological point of view, the synchronization of an arbitrary number of independent oscillators driven by a microwave source, represents one of the possible solutions to overcome the physical limit of low output power of the single device. The presence of very large hysteresis bands increases the possibility to achieve the synchronization for an ensemble of devices where the fabrication tolerances produce a difference of parameters among different devices. These differences are reflected in phase diagrams in the control plane of the devices which do not overlap completely on the control plane (ω, H_{rf}) but only for a portion of them. For example, it is considered the case of the study of the synchronization of the vortex oscillations of two different devices. The tolerances defects produce a difference in the electric resistances of the two devices and then in a difference of the electric current values flowing through them. It is obtained that the large hysteresis increases the synchronization band of the two oscillators of a factor which is $\sim 3 \div 4$ respect the case of absence of hysteresis. In conclusion, the design of a grid of vortex based point-contact nano-oscillators working in a synchronized state with a microwave rotating magnetic field, cannot be splitted from the study of the hysteretic effect of the synchronization process because as shown, it plays a key role in the determination of the achievable performances.

Bibliography

[1] E. Fermi, "Termodinamica ", *Bollati Boringhieri*, Torino 1972.

[2] L. Peliti, "Statistical mechanics in a nutshell ", *Princeton University Press*, Princeton 2011.

[3] J. W. Jr. Brown, "Magnetostatic Principles in Ferromagnetism ", *North-Holland Publishing*, Amsterdam 1962.

[4] J. W. Jr. Brown, "Micromagnetics ", *John Wiley and Sons*, New York 1963.

[5] A. Aharoni, "Introduction to the Theory of Ferromagnetism, 2nd ed.", *Oxford Science Publications*, 2000.

[6] G. Bertotti, "Hysteresis in Magnetism ", *ACADEMIC PRESS*, San Diego (CA), 1998.

[7] L. D. Landau, E. Lifshitz"ON THE THEORY OF THE DISPERSION OF MAGNETIC PERMEABILITY IN FERROMAGNETIC BODIES ", *Phys. Zeitsch. der Sow.*,vol. 8, pp. 153-169 (1935) .

[8] ,T. L. Gilbert "Classics in Magnetics ", *IEEE Transaction on Magnetics*, vol. 40, 6, 2004.

[9] F. Gantmacher, "Lectures on Analytical Mechanics ", *MIR PUBLISHERS*, Moscow 1975 .

[10] L. D. Landau and E. M. Lisfic, "Meccanica Classica", *Editori Riuniti Univer. Press*, 2003.

[11] H. Goldstein, C. Poole and J. Safko "Classical Mechanics", *Addison Wesley*, 2000.

[12] X. Liu et al, "Ferromagnetic resonance and damping properties of CoFeB thin films as free layers in MgO-based magnetic tunnel junctions ", *Journal of Applied Physics* 110, 033910 (2011).

[13] T. Devolder et al, "Damping of CoxFe802xB20 ultrathin films with perpendicular magnetic anisotropy ", *APPLIED PHYSICS LETTERS* 102, 022407 (2013).

[14] Y. Zhao et al, "Experimental Investigation of Temperature-Dependent Gilbert Damping in Permalloy Thin Films ", *Sci. Rep.* 6: 22890, 2016.

[15] J. Walowski et al, "Intrinsic and non-local Gilbert damping in polycrystalline nickel studied by Ti: sapphire laser fs spectroscopy ", *Journal of Physics D: Applied Physics*, Volume 41, Number 16, (2008).

[16] J. C. Slonczewski, "Current-driven excitation of magnetic multilayers ", *Journal of Magnetism and Magnetic Materials*, 159 (1996), pp. L1-L7.

[17] J. C. Slonczewski, "Currents and torques in metallic magnetic multilayers ", *Journal of Magnetism and Magnetic Materials*, 247 (2002), pp. 324-338.

[18] J. C. Slonczewski, "Currents, torques, and polarization factors in magnetic tunnel junctions ", *PHYSICAL REVIEW B*, 71, 024411 (2005).

[19] J. C. Slonczewski and J. Z. Sun, "Theory of voltage-driven current and torque in magnetic tunnel junctions ", *Journal of Magnetism and Magnetic Materials* , 310, 169-175, (2007).

[20] G. Bertotti, I. Mayergoyz and C. Serpico, "Nonlinear Magnetization Dynamics in Nanosystems ", *Elsevier*, Oxford, 2009.

[21] N. L. Schryer and L. R. Walker, "The motion of 180Â° domain walls in uniform dc magnetic fields ", *J. Appl. Phys.* 45, 5406 (1974).

[22] J. P. Braselton, et al, "Generalized Walker solutions to the Landau-Lifshitz-Gilbert equations ", *International Journal of Non-Linear Mechanics* 36, 571-579 (2001).

[23] M. d'Aquino et al, "Numerical integration of Landau-Lifshitz-Gilbert equationbased on the midpoint rule ", *JOURNAL OF APPLIED PHYSICS* 97, 10E319 (2005).

[24] A. A. Vansteenkiste, et al, "The design and verification of mumax3 ", *AIP Advances*, volume 4, 107133, (2014).

[25] M.J. Donahue and D.G. Porter, OOMMF User's Guide, Version 1.0, Interagency Report NISTIR 6376, National Institute of Standards and Technology, Gaithersburg, MD (Sept 1999)

[26] J. W. Jr. Brown, "Criterion for Uniform Magnetization ", *Physical Review*, vol. 105 n. 5, 1957.

[27] J. W. Jr. Brown, "THE FUNDAMENTAL THEOREM OF FINE FERROMAGNETIC PARTICLES ", *Annals New York Academy of Sciences*, New York 1969.

[28] J. A. Osborn, "Demagnetizing factors for general ellipsoid ", *Physical Review*, vol: 67, 11-12, 1945.

[29] E. C. Stoner, E. P. Wohlfarth, , "A mechanism of magnetic hysteresis in heterogeneous alloys ", *Philosophical Transactions of the Royal Society A: Physical, Mathematical and Engineering Sciences*, 240 (826),pp 599-642, 1948.

[30] L. Perko, "Differential Equations and Dynamical Systems ", *Springer*, New York, 1996.

[31] S. H. Strogaz, "Nonlinear Dynamics and Chaos ", *Perseus Books*, Cambridge, 1994.

[32] S. Wiggins, "Introduction to Applied Nonlinear Dynamical Systems and Chaos ", *Springer*, New York, 1990.

[33] M. d'Aquino, S. Perna et al, "Analytical solution of precessional switching in nanomagnets driven by hard-axis field pulses ", *Physica B: Condensed Matter*, Vol. 486, pp 126-129, 2016.

.

[34] C. Serpico et al, "Analytical Description of Quasi-Random Magnetization Relaxation to Equilibrium ", *IEEE TRANSACTIONS ON MAGNETICS*, VOL. 45, NO. 11, NOVEMBER 2009.

[35] G. Bertotti, I. Mayergoyz and C. Serpico, "Probabilistic Aspects of Magnetization Relaxation in Single-Domain Nanomagnets ", *Phys. Rev. Lett.*, 110, 147205, 2013.

[36] G. Bertotti et al, "Phase-Flow Interpretation of Magnetization Relaxation in Nanomagnets ", *IEEE Transactions on Magnetics* , Vol. 50, 2014.

[37] M. d'Aquino, S. Perna et al, "Analysis of Reliable Ultrafast Precessional Switching in the Presence of Transverse Applied Magnetic Fields ", *IEEE Transactions on Magnetics*, Vol. 50, 2014.

[38] M. d'Aquino, S. Perna et al, "Analysis of reliable sub-ns spin-torque switching under transverse bias magnetic fields ", *Journal of Applied Physics* , Vol. 117, 17B716, 2015.

[39] J. Akerman, "Toward a Universal Memory", *Science*, vol. 308, p. 508, Apr. 2005.

[40] A. D. Kent and D. C. Worledge, "A new spin on magnetic memories", *Nature Nanotechnology*, vol. 10, pp. 187-191, Mar. 2015.

[41] R. Bishnoi, M. Ebrahimi, F. Oboril and M. B. Tahoori "Improving Write Performance for STT-MRAM", *IEEE Trans. Magn*, vol. 52, p. 3401611, Aug. 2016.

[42] Z. Zeng, G. Finocchio and H. Jiang, "Spin transfer nanooscillators", *Nanoscale*, vol. 5, pp. 2219-2231, Jul. 2013.

[43] K. Yogendra, D. Fan and K. Roy, "Coupled Spin torque Nano Oscillators for Low Power Neural Computation", *IEEE Trans. Magn*, vol. 51, p. 4003909, Oct. 2015.

[44] S. Miwa et al.,"Highly sensitive nanoscale spin torque diode", *Nature Mater.*, vol. 13, pp. 50-56, Oct. 2013.

[45] B. Fang et al.,"Giant spin-torque diode sensitivity in the absemce of bias magnetic field", *Nature Comm.*, vol. 7, p. 11259, Mar. 2016.

[46] S. Ikeda et al., "A perpendicular anisotropy CoFeB-MgO magnetic tunnel junction", *Nature Mater.*, vol. 9, pp. 721-724, Jul. 2010.

[47] P. Khalili et al., "Switching current reducttion using perpendicular anisotropy in CoFeB-MgO magnetic tunnel junctions", *Appl. Phys. Lett.*, vol. 98, p. 112507, Mar. 2011.

[48] Tomasello et al., "Switching properties in magnetic tunnel junctions with interfacial perpendicular anisotropy: Micromagnetic study", *IEEE Trans. Magn*, vol. 50, p. 7100305, Jul. 2014.

[49] E.Liu et al., "[Co/Ni]-CoFeB hybrid free layer stack materials for high density magnetic random access memory applications ", *Appl. Phys. Lett.*, vol. 108, pp. 132405 1-4, Mar. 2016.

[50] J. J. Nowak et al., "Dependence of Voltage and Size on Write Error Rates in Spin-Transfer Torque Magnetic Random-Access Memory ", *IEEE Magn. Lett.*, vol. 7, p. 3102604, Mar. 2016

[51] G. D. Fuchs et al., "Spin-transfer effects in nanoscale magnetic tunnel junctions ", *Appl. Phys. Lett*, vol. 85, pp. 1205-1207, Jun. 2004.

[52] A. V. Nazarov et al., "Spin transfer stimulated microwave emission in MgO magnetic tunnel junctions ", *Appl. Phys. Lett.*, vol. 88, p. 162504, Apr. 2006.

[53] D. Houssamedine et al., "Spin transfer induced coherent microwave emission with large power form nanoscale MgO tunnel junctions ", *Appl. Phys. Lett.*, vol. 93, p. 022505, Jul. 2008

[54] A. M. Deac et al., "Bias-driven high power microwave emission from MgO-based tunnel magnetoresistance devices ", *Nat. Phys.*, vol. 4, pp. 803-809, Aug. 2008.

[55] Z. M. Zeng et al., "High-power coherent microwave emission from magnetic tunnel junction nono-oscillators with perpenmdicular anisotropy ", *ACS Nano*, vol. 6, pp. 6115-6121, Jun. 2012.

[56] Z. Zeng et al., "Ultralow-current density and bias-field-free spin transfer nano-oscillator ", *Sci. Rep.*, vol. 3, p. 1426, Mar. 2013.

[57] J. C. Sankey et al., "Measurement of the spin-transfer-torque vector in magnetic tunnel junctions", *Nat. Phys.*, vol. 4, pp. 67-71, Nov. 2007.

[58] A. Giordano et al., "Semi-implicit integration scheme forr Landau-Lifshitz-Gilbert-Slonczewski equation", *J. Appl. Phys.*, vol. 111, p.07D112, Feb. 2012.

[59] M. Beleggia et al., "Demagnetizing factors for elliptic cylinders", *J. Phys. D: Appl. Phys.*, vol. 38, pp. 3333-3342, Sept. 2005.

[60] C. Serpico et al., "Analytical Approach to current driven self-oscillations in Landau-Lifshitz-Gilbert dynamics ", *J. Magn. Magn. Mater.*, vols 290-291 part I, pp. 502-505, Apr. 2005.

[61] G. Bertotti et al., "Magnetization switching and microwave oscillations in nanomagnet driven by spin polarized currents ", *Phys. Rev. Lett.*, vol. 94, p. 127206, Apr. 2005.

[62] R. Bonin et al., "Analytical study of magnetization dynamics driven by spin-polarized current", *Eur. Phys. Journ. B*, vol. 59, pp. 435-445, Oct. 2007.

[63] G. Bertotti et al., "Geometrical Analysis of Precessional Switching and Relaxation in Uniformly Magnetized Bodies", *IEEE Trans. Magn.*, vol. 39, pp. 2501-2503, Sept. 2003.

[64] G. Bertotti et al., "Current-induced magnetization dynamics in nanomagnets", *J. Magn. Magn. Mater.*, vol. 316, pp. 285-290, Sept. 2007.

[65] C. Serpico et al., "Transient Dynamics Leading to Self-Oscillations in Nanomagnets Driven by Spin-Poolarized Currents", *IEEE Trans. Magn.*, vol. 41, pp. 3100-3102, Oct. 2005.

[66] W. H. Rippard, et al, "Direct-current induced dynamics in Co90Fe10-Ni80Fe20 point contacts", *Physical Rewiew Letters*, vol. 92, 2, (2005).

[67] W. H. Rippard, et al, "Current-driven microwave dynamics in magnetic point contacts as a function of applied field angle", *PRB*, vol. 70, 100406(R), (2004).

[68] D. Ham and A. Hajimiri, "Concepts and Methods in Optimization of Integrated LC VCOs", *IEEE Journal Of Solid-State Circuits*, vol. 36, 6, pp. 896-909 (2001).

[69] W. H. Rippard, M. R. Pufall, S. Kaka, T. J. Silva, and S. E. Russek, J. A. Katine, "Injection Locking and Phase Control of Spin Transfer Nano-oscillators", *Phys. Rev. Lett.* 95, 067203, 2005.

[70] S. Kaka, M.R. Pufall1, W.H. Rippard, T.J. Silva, S.E. Russek, J. A. Katine, "Mutual phase-locking of microwave spin torque nano-oscillators", *Nature* 437, 389, 2005.

[71] F. B. Mancoff, N. D. Rizzo, B. N. Engel, S. Tehrani, "Phase-locking in double-point-contact spin-transfer devices", *Nature* 437 , 393 , 2005.

[72] J. Grollier, V. Cros, A. Fert, "Synchronization of spin-transfer oscillators driven by stimulated microwave currents ", *Phys. Rev. B* 73, 060409(R), 2006.

[73] A. N. Slavin, V. S. Tiberkevich, "Nonlinear self-phase-locking effect in an array of current-driven magnetic nanocontacts ", *Phys. Rev. B* 72, 092407, 2005.

[74] A. N. Slavin and V. S. Tiberkevich, "Theory of mutual phase locking of spin-torque nanosized oscillators ", *Phys. Rev. B* 74, 104401, 2006.

[75] B. Georges et al., "Coupling efficiency for phase locking of a spin transfer nano-oscillator to a microwave current ", *Phys. Rev. Lett.*, 101, 017201, 2008.

[76] R. Bonin, et al, "Analytical treatment of synchronization of spin-torque oscillators by microwave magnetic fields", *European Physical Journal B*, vol. 68, pp. 221-231, (2009).

[77] M. d'Aquino, et al,"Micromagnetic analysis of injection locking in spin-transfer nano-oscillators ", *Physical Review B*, 82, 064415 (2010).

[78] M. d'Aquino, et al, "Micromagnetic study of phase-locking in spin-transfer nano-oscillators driven by currents and ac fields ", *Journal of Applied Physics*, volume 109, 07C914, (2011).

[79] M. d'Aquino, et al, "Stochastic resonance in noise-induced transitions between self-oscillations and equilibria in spin-valve nanomagnets ", *Physical Review B*, volume 84, 214415 (2011).

[80] M. Carpentieri, et al, "Spin-transfer-torque resonant switching and injection locking in the presence of a weak external microwave field for spin valves with perpendicular materials ", *Physical Review B*, volume 82, pages 094434-1,4 (2010).

[81] G. Bertotti, et al, "Magnetization Switching and Microwave Oscillations in Nanomagnets Driven by Spin-Polarized Currents ", *Physical Rewiew Letters*, volume 94, 127206, (2005).

[82] G. Bertotti, et al, "Nonlinear dynamical system approach to microwave assisted magnetization dynamics ", *Journal of Applied Physics*, volume 105, pages 07B712, (2009).

[83] C. Serpico, et al, "Theory of injection locking for large magnetization motion in spin-transfer nano-oscilaltors ", *IEEE Transanctions on Magnetics*, volume 45, pages 3441-3444,(2009).

[84] P. Tabor, et al, "Hysteretic synchronization of nonlinear spin-torque oscillators ", *Physical Review B*, volume 82, pages 020407 1-4, (2010).

[85] S. Urazhdin and P. Tabor, "Fractional Synchronization of Spin-Torque Nano-Oscillators ", *Physical Review Letters*, volume 105, pages 104101-1,4, (2010).

[86] Z. Zeng, et al, "Spin transfer nano-oscillators ", *Nanoscale*, volume 5 (6), pages 2219-2231, (2007).

[87] Q. Mistral, et al, "Current-driven vortex oscillations in metallic nanocontacts ", *Physical Rewiew Letters*, volume 100, 257201, (2008).

[88] M. Manfrini, et al, "Agility of vortex-based nanocontact spin torque oscillators", *Applied Physics Letters*, volume 95, 192507, (2009).

[89] J. V. Kim and T. Devolder, "Theory of the power spectrum of spin-torque nanocontact vortex oscillators ", *arXiv*, 1007.3859v1, (2010).

[90] K. Yamada, et al, "Electrical switching of the vortex core in a magnetic disk ", *Nature Materials*, volume 6, (2007).

[91] K. Guslienko, et al, "Dynamic origin of vortex core switching in soft magnetic nanodots ", *Physical Rewiew Letters*, volume 100, 027203, (2008).

[92] M. R. Pufall, et al, "Low-field current-hysteretic oscillations in spin-transfer nanocontacts ", *Physical Review B*, volume 75, 140404(R)(2007).

[93] S. Erokhin and D. Berkov, "Robust synchronization of an arbitrary number of spin-torque driven vortex nanooscillators ", *Physical Rewiew B*, volume 89, 144421, (2014).

[94] V. Novosad, et al, "Magnetic vortex resonance in patterned ferromagnetic dots ", *Physical Review B*, volume 72, 024455, (2005).

[95] A. Vansteenkiste, et al, "X-ray imaging of the dynamic magnetic vortex core deformation ", *Nature Physics*, volume 5 , pages 332-334, (2009).

[96] O. A. Tretiakov, et al, "Vortex nucleation in spin-torque nanocontact oscillators ", *Physical Review Letters*, volume 100, 127204, (2008).

[97] K. L. Metlov, "Two-Dimensional Topological Solitons in Magnetic Dots ", *Physica status solidi (a)*, volume 189, pages 1015-1018, (2002).

[98] N. A. Usov and S. E. Peschany, "Magnetization curling in a fine cylindrical particle ", *Journal of Magnetism and Magnetic Materials* 118, L 290-294, (1993).

[99] K. Guslienko et al, "Eigenfrequencies of vortex state excitations in magnetic submicron-size disks ", *Journal of Applied Physics* 91, 8037 (2002).

[100] M. d'Aquino, et al, "Quasiperiodic magnetization dynamics in uniformly magnetized particles and films ", *Journal of Applied Physics*, volume 95, pages 7052-7054, (2004).

[101] A. A. Thiele, "Steady state motion of magnetic domain ", *Phys. Rew. Lett.*, volume 30, 6, (1973).